5-2017

Non-contact based structural damage assessment using stochastic subspace identification and finite element model updating.

Li Yang
University of Louisville

NON-CONTACT BASED STRUCTURAL DAMAGE ASSESSMENT USING STOCHASTIC SUBSPACE IDENTIFICATION AND FINITE ELEMENT MODEL UPDATING

By

Li Yang
B.S., Southeast University, 2009
M.S., Nanjing Hydraulic Research Institute, 2012

A Dissertation
Submitted to the Faculty of the
J.B.Speed School of Engineering of the University of Louisville
In Partial Fulfilment of the Requirements
for the Degree of

Doctor of Philosophy
in Civil Engineering

Department of Civil and Environmental Engineering
University of Louisville,
Louisville, Kentucky

May 2017

NON-CONTACT BASED STRUCTURAL DAMAGE ASSESSMENT
USING STOCHASTIC SUBSPACE IDENTIFICATION AND
FINITE ELEMENT MODEL UPDATING

By

Li Yang
B.S., Southeast University, 2009
M.S., Nanjing Hydraulic Research Institute, 2012

A Dissertation Approved on
April 24, 2017
by the Following Committee:

_____
Dr. Young Hoon Kim, Dissertation Director

_____
Dr. J.P Mohsen

_____
Dr. Zhihui Sun

_____
Dr. John Kielkopf

To my family

ACKNOWLEDGEMENTS

First and foremost, I would like to express my most sincere gratitude and appreciation to my mentor and advisor Dr. Young Hoon Kim for his patient guidance, consistent encouragement and support during my research in the University of Louisville. Dr. Kim introduced me to a new and exciting area of research and provided an exciting working environment with many opportunities to explore new ideas. His attitude toward academia has influenced me greatly for the past years and will influence me in my future life.

I sincerely appreciate Dr. Jeffrey Hay with RDI technologies for his technical and experimental support in this research. His insightful knowledge and experience of motion detection have been a great help in my Ph.D. study. Whenever I confront any difficulties, he is always willing to discuss and provide valuable suggestions. Without his precious support, it would not be possible to conduct this research.

I would like to thank my committee members Dr. J.P. Mohsen, Dr. Zhihui Sun and Dr. John Kielkopf for their insightful comments and encouragement, but also for the hard question which incented me to widen my research from various perspectives.

My sincere thanks also goes to Dr. J.P. Mohsen and the Department of Civil and Environmental Engineering at the University of Louisville for the financial support. Also, many thanks to Mr. Bernie Miles who helped me in solving all the problems in the lab.

With a special mention to my master thesis advisor, Dr. Zhinong Hu for his advice and instruction during graduate study. He inspired and encouraged me to pursue my academic interests.

I'm grateful to Dr. Hanying Luo for those supportive she gives me when I am feel overwhelmed. She encouraged me with her experience, and she is always there for my big moments. I would like thank Rebecca Chen and Charles Wang for their friendships and faithful support. They were always there when needed and for that, I am very grateful. My friend Amanda Smart and Allison Siu, they always motivate me working out, and without a healthy body, it would not be possible to finish my Ph.D. study. I would like to thank my friend Jia Grigsby, her hardworking has always been an inspiration and encourage for me.

A very special gratitude goes out to my dog, Moo Moo, who brings so much joy in my life. He is my angel, my sunshine, and I'm so lucky to have him.

I'm grateful to my parents, Rongsheng Yang and Wenxiu Luo for their support to enable me to achieve my academic goals. They raised me with a love of science and engineering and supported me in all my pursuits. I'd like to thank my father-in-law, Donald Harris who sees me as his own daughter. He makes me feel like home when I am thousands of miles away from my hometown.

Last but not the least, I would like to thank my loving and patient husband Nathaniel Williams for his faithful supportive, understanding and encouragement through my research and in my life. Thank you.

ABSTRACT

NON-CONTACT BASED STRUCTURAL DAMAGE ASSESSMENT
USING STOCHASTIC SUBSPACE IDENTIFICATION AND
FINITE ELEMENT MODEL UPDATING

Li Yang

April 24th 2017

This research proposed and verified an innovative method to identify and locate structural damage using only the response of operational vibration, that is the displacement acquired by a non-contact optical method.

The most efficient and economical way to detect damage within the structure is to monitor its structural health while in operation. However, the uncertainties and the randomness of ambient vibrations due to the operation and environments cause a challenge in conducting the operational analysis. Current technology limits the ability to collect data on the properties of the structure without the interruption of operation. Frequencies and mode shapes have been widely used in structural damage detection, but they are not sensitive enough and cannot provide sufficient information for identifying damage locations and their quantification. Therefore, the goal of this research is to design and verify a method to detect the damage, as well as its location and severity, of structures in operation without any physical contacts for data acquisition (i.e., non-contact based structural health monitoring (SHM)).

Three algorithms are integrated into this SHM process. The first algorithm is the determination of structural characteristics (frequencies and mode shapes) of a vibrating structure from output-only data. Stochastic Subspace Identification (SSI) method is applied to measured displacements over time to extract the structural characteristics. The second algorithm is to estimate the scaling factor. The mode shapes obtained from the output-only model analysis are unscaled due to the absence of the information of input excitation forces. Mass Change Modal Scale (McMS) algorithm is used to estimate the modal scaling factors and determine the scaled mode shapes. The third algorithm is to estimate the structural system matrices (i.e., mass and stiffness matrices) and assess the damages. A Finite Element Model Updating (FEMU) is applied and the system matrices are updated from frequencies and scaled mode shapes. The damage within the structure can then be detected by analysing changes in mass and stiffness matrices. All three phases are verified by numerical simulation and laboratory experiments with deflections acquired by non-contact optical methods through video system. At last, to achieve the non-contact based SHM, a modal scaling method based on temperature change is proposed and verified by numerical simulation. Experimental program reveals that the proposed algorithm using McMS method is applicable to detect damage locations and their mass losses. With proposed non-contacted based SHM, the limitations of contact based sensor can be addressed, and the structural damage can be assessed without any interruption of structure operation.

TABLE OF CONTENTS

LIST OF FIGURES

LIST OF TABLES

CHAPTER 1

INTRODUCTION

When the civil infrastructure, such as bridges, buildings, dams, pipelines, etc., are built, the deterioration started and maintenance of the infrastructures are desired. Damage assessment and failure prediction is important to the safety and well-being of the society. The knowledge and analysis on the effects of infrequent by high force such as overloading, major earthquake, hurricane or tornadoes on structures are essential for preventing failure. Including the extreme events, there are five main sources to cause the structural failure (Wood 1992).

1) Statically under-designed;
2) Erected using substandard constructional techniques;
3) Subject to cyclic effects: (structural fatigue);
4) Subject to changes at the structure boundary conditions;
5) Subject to insufficient maintenance procedures.

In practice, a structure will be subject to the effects of all the above to some degree. The collapse of I-35 west Mississippi River bridge on August 1st, 2007 is an example. The collapse of the bridge is shown in Figure 1.

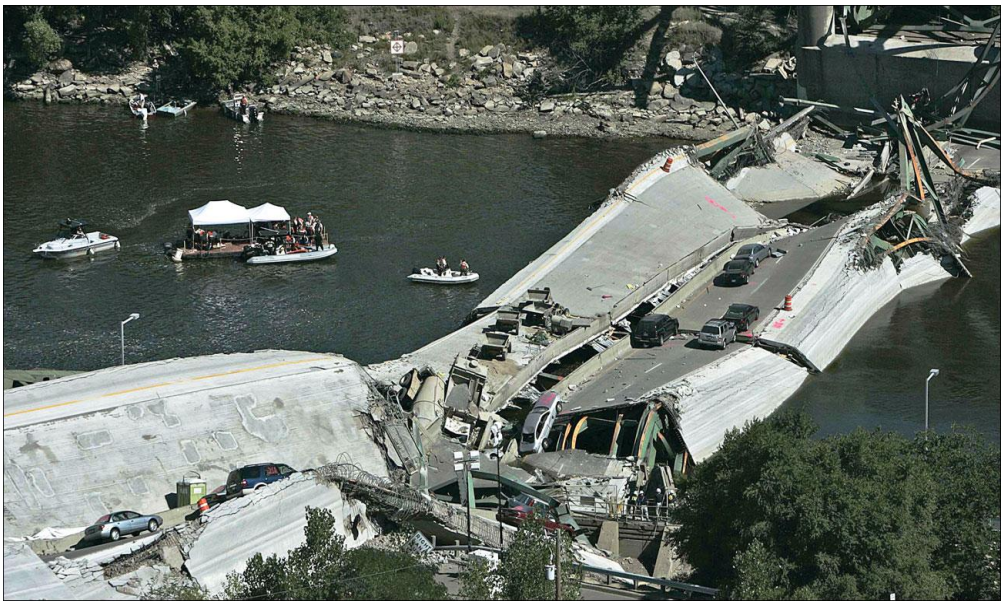

Figure 1.1. I-35W Bridge Collapse (Google.com)

The central span of the bridge failed and brought the bridge down in Mississippi River during rush hour, 13 people were killed and 145 others were injured (Stachura 2007). The National Transportation Safety Board (NTSB) reported that the primary causes of the collapse were 1) the undersized gusset plates from design or construction error; 2) the addition of concrete layers over years, and 3) overloading (Holt and Hartmann 2008). This is clearly the combination of several causes that Wood (1992) presented out.

1.1 Structural Health Monitoring (SHM)

The structural condition of aging infrastructure is drawing great concern in recent years. American Society of Civil Engineering (ASCE) (2017) reported that 20% of the nation's highways; 32% of urban roads and 14% of rural roads had poor pavement condition in 2014. Large amount of highway bridges in the United States were built decades ago so that they are now under the risks of structural deficiency (Chase and Laman

2000). Billions of dollars are spent from state and local governments for the operation and maintenance of highway each year. To maintain the safety and reduce the costs, structural health should be inspected and monitored frequently. Moss and Matthews (1995) and Mita (1999) identified the cases where the structural monitoring may be required and here listed some primary cases:

1) Modification of an existing structure;
2) Monitoring of structures affected by external forces;
3) Monitoring during destruction;
4) Structures subject to long-term movement or degradation of materials;
5) Fatigue assessment;
6) Assessment of post-earthquake structural integrity.

In the past years, visual inspection is still the primary tool for structural health inspection which largely relies on inspector's experiences. A survey of Federal Highway Administration showed that such inspection is limited on accuracy and efficiency (Washer 2001). Visual inspection can only determine whether damage is present in the entire structure. Such methods are referred to as "global health monitoring" methods (Chang et al. 2003). However, after the visual inspection, further examination of the structure to locate and quantify the damage must be taken. Many non-destructive evaluation (NDE) methods are used to find the damage, those methods are so called "local health monitoring" methods. NDE techniques are often time-consuming and expensive, and the access of inspectors and equipment are not always possible. The health monitoring of civil infrastructure consists of determining, by measured parameters, the location and severity of damage in buildings or bridges (Chang et al. 2003). Structure Health Monitoring (SHM)

started to be a dominant method to analyze structures serviceability, reliability and durability (Sikorsky et al. 1999). The process of implementing a damage detection strategy for aerospace, civil and mechanical engineering infrastructure is referred to as Structural Health Monitoring (SHM) (Sohn et al. 2003). Farrar et al. (2001) defined SHM process in terms of a four-step statistical process which is widely used in SHM:

1) Operational evaluation: this step contains life-safety evaluation and economic justification for performing SHM, the operational and environmental condition investigation, damage definition and priority mission
2) Data acquisition and normalisation: this step involves selecting the excitation method, the sensor types, number and location of response needed
3) Feature extraction: this step includes the selection, extraction of feature as well as data condensation
4) Model development for health diagnosis: This step develops statistical models for discrimination between features from undamaged and damaged structures

There are two main features of SHM: system identification and damage detection. Herein, the system identification (SI) defined as the quantification of structural parameters to determine structural performance and serviceability. Therefore, SI is the essential step for identifying any available damages and their locations. After the multiple SI processes with different time of measurements, the change of modal parameter can indicate the damage of structures and their location along with severity. Herein, it is defined as damage detection (DD).

1.2 Problem Statement and Motivation

Early detection of structural deterioration provides information for effectively structural maintenance, minimises the repair cost, and prevents a catastrophic collapse of those structures. Vibration based SHM method has drawn significant attention in recent years, that is vibration based approach to compare values of natural frequencies and mode shapes measured at different time (e.g., baseline (non-damaged) versus damaged condition). These modal parameters can be analyzed over different time span. Different sensors are adopted to collect the vibration response. Number and location of sensors are the main limitation of contact base sensors (e.g., accelerometers, strain gages, etc.). In addition, the installation of contact base sensor is typically time-consuming and the operation of structure needs to be interrupted. Another limitation of contact base sensor is the possible damage when deployed in the field. Non-contact based sensor (herein, optical sensors) on the other hand does not require the installation. And any location of the dynamic response can be acquired simultaneously as long as the sensor can obtain the outputs of vibration objects.

Most global health monitoring methods are to evaluate shifts of frequencies or changes in mode shapes from dynamic responses of the structures that has limitations such as:

(1) The environmental, such as temperature, moisture etc., changes could also cause changes in those dynamic characteristics. The ambient noise leads to increase uncertainties of the measurements. Therefore, the changes of those parameters due to damage must be significantly greater than the changes due to

ambient noise. Otherwise, ambient noise can dominantly change the dynamic parameters regardless the changes of structural damages.

(2) Even though the damage appears on the element, it would not affect the fundamental frequency or mode shape (Friswell and Penny 1997). When there is only low level of vibration, some of the damage cannot affect the frequency.

To detect the location and severity of damage using frequencies and mode shapes, higher modes need to be extracted and large amount of data is needed. Alternative index for SHM is a potential solution for this.

In many civil infrastructures, the global frequency changes already indicate the significant damages existence, at that moment, the local health monitoring is not necessary. However, unforeseen cracks or damage not correlated to the low modes cannot be identified using global SHM. There is a need to develop a new method to combine the global and local health monitoring simultaneously with one single sensor. To overcome current limitations of SHM, the following two problem statements and motivation are stated:

(1) Current SHMs have two individual paths to evaluate structures using more than one method. Two paths are global and local health monitoring. They require large amounts of contact based sensors for identifying the locating and severities of damages. This requires the development of many sensors and labors for monitoring the large-scale structures.

(2) Generally, existing SHMs are requiring the input forces and system properties for identification. However, it is impractical to measure the input or generate

external excitation force especially for large-scale structures such as building and bridges. In many cases, the exact system properties (e.g., mass and damping properties) are rarely known. The estimation of system properties without the input is required to address problems stated above.

(3) Non-contact SHM can address the requirements to combine global and local SHM. Especially, indicial pixels of visual images over time can provide infinite numbers of equivalent sensors to replace contact based sensors.

Additional algorithms are needed to identify the systems without any information of inputs such as existing system properties. This research ultimately eliminates any contact based requirements for global and local SHM.

As discussed in previous studies, the current practices of SHM are contacted base and local SHM or vibration based global SHM. To overcome the difficulties of the integration of two approaches, a structural system identification and damage detection method are identified and validated using the non-contact based sensor. It is motivated by the need of non-contacted based damage assessment of structures with uncertainties of ambient vibration. With the development of non-contact based sensor such as high-speed camera, there are potentials that both local and global damage can be identified.

1.3 Goal and Objectives

The goal of this research is to establish the strategies to identify and estimate structural damages using structural vibrational responses acquired by non-contact based

sensors. In addition, new modal scaling method using temperature variations are proposed for system identification and damage estimation.

To achieve the goal, the following research objectives are established.

(1) Develop the damage assessment algorithm:

To achieve this, types of input and output for the algorithm are analyzed. Displacements of the structure during vibration are chosen to be served as the only input for the algorithm. Different system identification algorithms have been navigated and three algorithms are integrated in this study: 1) Stochastic Subspace Identification (SSI); 2) Modal scaling; 3) Finite Element Model Updating (FEMU). The Proposed algorithm can identify the damage location and severities using vibration responses acquired by the non-contact based sensor.

(2) Propose the non-contact based modal scaling method using superficial temperature changes:

Optical sensor provides the ability for the motion capture of the structure at any location simultaneously. The proposed algorithm can extract dynamic characteristics. However, the output-only identification method only gives the unscaled mode shapes. Traditional modes scaling method is a contact based approach to change mass or/and stiffness. In this study, a non-contact base modal scaling method are proposed based on temperature changes. With the scaled modes, FEMU can estimate the mass and stiffness matrices.

(3) Examine the application of system identification algorithms and damage detection through numerical simulation:

The proposed algorithms are applied to numerical simulation models (case 1: 4-story building [4 degrees of freedom], case 2: truss bridge [12 degrees of freedom]). To address the ability of the method under uncertainties resulting from the ambient environment, artificial noise is added in numerical simulation as well. The proposed algorithms can identify the locations of damages and the severity in the quantitate manner.

(4) Verify the algorithms in experimental test program:

Experimental testing is carried out to verify the proposed algorithm. Displacements of the structure during vibration are recorded by the optical sensor (high-speed camera) system. The algorithms have then been applied for damage assessment.

1.4 Research Significance

The proposed method overcomes the uncertainties of ambient excitation and addresses the limitations of contact based types of sensor. It also can identify the system without any information of input forces. The ambient noise and unknown forces can be neglected in the process of the algorithm. With the advantage of the optical sensor, the time cost for assessing damages in large infrastructure would be reduced. This research focuses on the realization of a non-contacted based SHM method that can detect, localise and quantify the damage. Damage assessment algorithm has been developed and validated with numerical simulation and experimental testing using the data acquired from the optical sensor system.

The outcomes of this research can impact the current practices of structural health monitoring of civil engineering. First, the proposed algorithm can be used to monitor structural health in operation in conjunction with optical sensor (high-speed camera) system. This can be used to identify the critical elements in a distance before investigating the locations further (i.e., contact based NDT). Therefore, the inspectors time and labors can be reduced significantly using the algorithms and non-contact based sensors. Instead of using contact based sensors. Furthermore, the disturbance of the structural operation is not required for the owner and operators. Second, The outcomes of this algorithm can be potentially combined the dynamic condensation or static condensation techniques to minimize the complexity of the entire system. Therefore, the analysis can promptly assess the structural health without prior information of structure's system (i.e., mass and stiffness)

1.5 Outlines of the Dissertation

Chapter 1 presents the necessity for damage assessment and the advantages of the non-contact based approach. The limitations of current SHM method are stated. To overcome the limitations, the goal and objectives of this research are presented.

Chapter 2 provides a literature review on the non-contact based sensor. This chapter also reviews the development and application of commonly used contact based sensors. With the desire and advantage of the non-contact based sensor, recent non-contact based sensors system and its application are discussed.

Chapter 3 provides a comprehensive literature review on SHM algorithms, with special attention on Operational Model Analysis (OMA) method. The development and application of those algorithms are presented.

Chapter 4 proposes an innovative method to identify and locate structural damage encompassing the uncertainties of modal and ambient excitations. A non-contact based modal scaling method: temperature change based modal scaling is proposed. The formula of modal scaling factor is derived mathematically. The unique feature of this algorithm is that system matrices are used as damage indicator. Displacements are served as the only input of this method.

Chapter 5 presents two numerical simulations that illustrate the proposed algorithms (4 story building and a truss bridge). The capability and accuracy of system identification and damage detection algorithms. The accuracy of the proposed temperature change modal scaling method is validated.

Chapter 6 presents an experimental program and results that validated the proposed method. Displacements acquired by a high-speed camera is used as the input for system identification. Damage are localised and quantified by analysing changes in system matrices using algorithms.

Chapter 7 summarizes the findings and results in this dissertation. The innovative contribution made in this research are highlighted. Future works of this field of research are discussed.

CHAPTER 2

LITERATURE REVIEW ON SHM

Damage in civil structures may come from structural aging, environmental and weather impact, operational loads or external loads such as earthquakes, explosions, floods and winds, etc. Generally, damage can be defined as changes in a system that adversely affects its current or future performance. In SHM, damage means changes to the material and/or geometric properties of the structural systems, including changes in the boundary conditions and joints (Farrar and Worden 2007). To improve the safety and performance of structures, a deep understanding of structural responses to the ambient condition is required. There are four classifications for structure health monitoring schemes (Rytter 1993):

Table 2.1Classification Levels for SHM Schemes

Classification Level	Scheme Capability
Level I	Identify damage
Level II	Identify damage, determine damage location
Level III	Identify damage, determine damage location, estimate severity
Level IV	Identify damage, determine damage location, estimate severity, estimate the durability of the structure

The higher the level reaches the more sophisticated the scheme is. Most global health monitoring methods can achieve Level I scheme. They can only determine whether there is damage occurring or not. Local health monitoring methods can achieve Level II. The location of the damage can be determined, and some of them can indicate the severity of the damage. But the local health monitoring methods are always costly and require the interruption of the operation. Modal analysis methods have been developed dramatically in the past to achieve up to level IV scheme.

Section 2.1 introduces the concept of vibration-based SHM schemes. Different parameters are used as indicators for damage detection. Damage detection based on frequencies, mode shapes, and system matrices are reviewed in this section. Section 2.2 introduces two main types of modal analysis: Experimental Modal Analysis (EMA) and Operational Modal Analysis (OMA). Various of OMA algorithms are introduced and compared. Section 2.3 explains different types of sensor used in the acquisition of structure vibration response. The feature of the non-contact based sensor is described in this section.

2.1 Vibration based SHM: Damage Detection

Typical structural health assessment is accomplished through on-site visual inspections. The accuracy of such methods are based on inspectors' experiences, knowledge and accessibility, however, damages might take place inside the structures and been covered by walls or facades and leave no major visible damages (Caicedo et al. 2004). Research shows that visual inspection of structures in the U.S after 1994 Northridge Earthquake did not detect the beam-column joints damage until removing fire-protection coating (Mita 1999). This case prompted to the application of non-destructive damage

detection methods. Therefore, NDT has been carried out for further inspection. NDT is a labour intensive and time-consuming process which often requires traffic closure and minimising operational disturbance. The limitation of such methods motivated the development of vibration-based SHM. In addition, the development of related technologies such as the advance in vibration detection sensors, cost-effective computer memory and speed also contribute to the increase in research activities regarding vibration-based SHM (Doebling et al. 1998).

2.1.1 Damage Detection Based on Frequencies Change

Recently, vibration-based SHM has drawn significant attention using modal analysis (Grouve et al. 2008; Liu et al. 2008; Ooijevaar et al. 2010; Parloo et al. 2002). Generally, four steps are associated in SHM using modal analysis: Operational evaluation, data acquisition, dynamic characteristic extraction and damage detection. Modal analysis damage detection is based on changes in structure properties such as stiffness, mass and damping due to global and/or local damage, boundary condition changes will affect the vibration response of the structure. Structural dynamic properties such as frequencies and mode shapes extracted from vibration responses of structures are commonly used to diagnose any damage. Frequency shift from measurements of two different states is a well-established method to detect structural damages. It is always defining one of the states as "initial condition" that the other states will be compared with (Kawchuk et al. 2009; Patil and Maiti 2005; Salawu 1997). Mirza et al. (1990) report a decrease in the fundamental natural frequency with progressive damage. Support failure, cracks in structures, joints disconnection and overloading can cause the change of frequencies (Ågårdh 1991; Salane

and Baldwin Jr 1990). However, previous research also indicates that at damaged regions of low stresses frequency measurements are unreliable to be an indicator for damage detection (Halling et al. 2001; Kirkegaard and Rytter 1995). Other factors such as change in temperature can also cause frequency shifts (Farrar et al. 1997). Bradford et al. (2004) found that other environmental condition such as heavy rain and strong wind can change structural natural frequency by up to 3 percent. Therefore, only frequency shift cannot be a single method to detect damage of structures as a reliable indicator.

2.1.2 Damage Detection Based on Mode Shape Change

To overcome the limitations of SHM based on frequency shifts in damage detection, mode shape and modal assurance criteria (MAC) were introduced in the early 1990s (Cobb and Liebst 1997; Fox 1992; Mayes 1992). MAC (Pastor et al. 2012) is used to evaluate the correlation between two mode shapes. The MAC between two measured modes $\varphi_{m1}$and φ_{m2} are defined as:

$$MAC = \frac{|\varphi_{m1}^T \varphi_{m2}|^2}{(\varphi_{m2}^T \varphi_{m2})(\varphi_{m1}^T \varphi_{m1})} \tag{2.1}$$

where φ_{m1} is the measured mode at t_1, and φ_{m2} is measured mode at t_2. MAC value ranges between zero and one, the value of 1 indicates that the measured mode shape is highly correlated with comparable mode shape. And a value of 0 indicates that there is no correlation between the two modes. The value of 0.95 or higher of the MAC value is acceptable to conclude that two modes are highly correlated (Friswell and Mottershead 1995). Fox (1992) found that fundamental mode shape changes are insensitive to damage

in a beam system. This indicates that large amounts of data are needed in the damage detection using mode shape changes in higher modes.

2.1.3 Damage Detection Based on System Matrices

Using system matrices, stiffness and mass estimations of structures become alternative indicators for damage detection, location and severity. The different between updated system matrices and the original correlated matrices can be used to quantify the location and the extent of damage of structures (Doebling et al. 1998). The system matrices can be updated from frequencies and mode shape extracted from structural vibration responses. Mass and stiffness matrices can possibly be the quantified indicators to detect damage and estimate damage in the Level IV of SHM Scheme.

2.2 Modal Analysis

To perform damage detection, modal analysis methods have been widely used in studying the dynamic properties of a structure under vibrational excitation. Using modal analysis, the modal parameters of a structure can be extracted. There are two types of modal analysis that can be performed: Experimental Modal Analysis (EMA) and Operational Modal Analysis (OMA).

2.2.1 Experimental Modal Analysis

EMA is a convenient method to analyze the modal characteristics of structures from the relationship between input excitation (i.e. impact force) and the structural responses (i.e. acceleration, strain or displacement). EMA is a method that the excitation force and

the response has to be measured, simultaneously (Ewins 2000). EMA can produce data that have very high signal to noise ratios. Typical EMA process is shown in Figure 2.1:

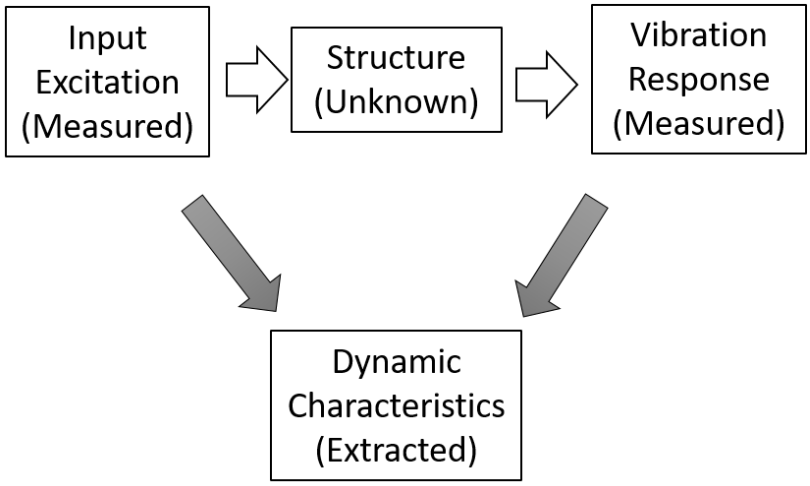

Figure 2.1. EMA Scheme

As an input-output method, EMA requires the knowledge of input excitation along with output responses OF measurement. Impact hammer, shaker and dropping weights are normally used. EMA has been wide used and numerous modal identification algorithms such as Single-Input/Single-Output (SISO). Single-Input/Multi-Output (SIMO) to Multi-Input/Multi-Output (MOMI) techniques has been developed both in Time Domain (TD), and Frequency Domain (FD) (Zhang and Brincker 2005). In most EMA, artificial excitations are normally conducted, however, it is impractical for large structures. Using ambient excitation such as the wind, traffic, etc. as input for EMA is impractical as well due to the impossibility of measuring the ambient forces.

2.2.2 Operational Modal Analysis (OMA)

In the EMA method, the input excitation and output response are measured simultaneously. The modal properties extracted from this input-output modal are usually mass scaled. However, sometimes it is impractical to excite a structure with controllable force especially for large civil structures without damage on the structure or causing nonlinear behavior of the structures (Hanson 2006) and it is challenging to measure the excitation without interrupting the operation of structures. Additionally, the ambient condition can easily cause noises to the excitation force and resulting in the errors of analysis. On the other hand, Operational Modal Analysis (OMA) is an output-only modal analysis method that only measures the response excited by ambient forces. Thus, OMA methods has received more attention (Brownjohn et al. 2010; Cury et al. 2012; Devriendt et al. 2014; Rainieri and Fabbrocino 2014; Ramos et al. 2011; Yan and Ren 2012). The vibration responses are used as the only input for system identification. Typical OMA process is shown in Figure 2.2:

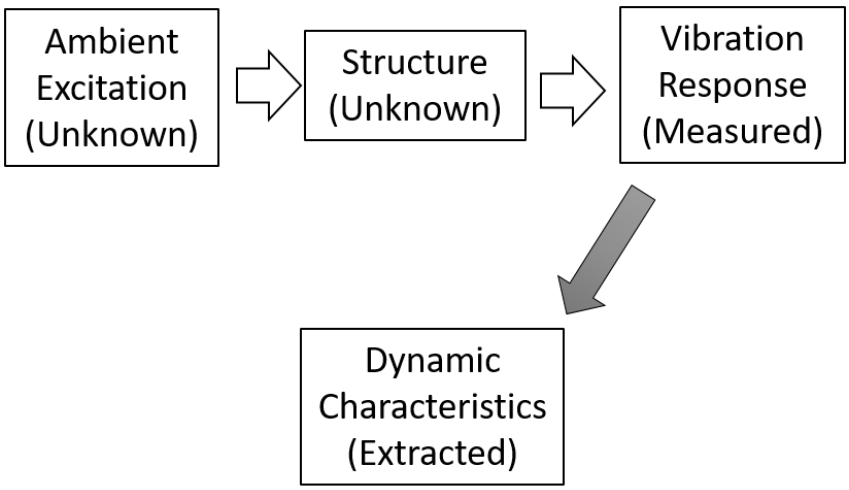

Figure 2.2. OMA Scheme

System identification using OMA method is emphasised on extracting modal parameters of structures using only outputs measurements. All OMA methods have the same assumptions (Rainieri and Fabbrocino 2014) such that:

(1) Linearity: The response of the system to the given combination of inputs is equal to the same combination of the corresponding outputs;
(2) Stationary: The dynamic characteristics of the structure do not change over time, so the coefficients of the differential equations governing the dynamic response of the structure are independent of time;
(3) Observability: The sensor layout has been properly designed to observe the modes of interest.

2.2.3 Overview of OMA Methods

Variety of OMA methods has been proposed and applied on structural system identification. The simplest OMA method is Basic Frequency Domain (BFD) method which is also known as Peak-Picking method. BFD assumes that only one modal is dominant around a resonance. The frequencies are identified by pick the value of power spectral density plot peaks (Ojeda 2012). As a simple and fast system identification method, BFD estimates the mode shapes accurately when only one mode is dominant at the considered frequencies. However, it is very difficult to distinguish frequencies which are very close to each other. This method is effective only when damping is low and modes are well separated (Rainieri and Fabbrocino 2014). Some OMA method requires knowledge of undamaged normal condition such as Novelty detection. In this method,

damage classification is based on data from the undamaged system. An internal representation of the system's undamaged condition is set up; this is called as the baseline representing undamaged condition. When the measured data after the events are significantly different from the baseline, this indicates the damaged condition (Farrar and Worden 2007). However, it is hard to describe the undamaged condition accurately due to effects of ambient changes. In addition, only first level damage detection can be achieved through this method.

Siringoringo and Fujino (2008) applied random decrement (RD) method in SHM. This method assumes that dynamic response of a structure under ambient excitation at a time instance can be divided into two deterministic part of responses due to initial displacement and velocity and one random part due to random excitation during the time instance (Mahmoud et al. 2001). Adopting Ibrahim Time Domain (ITD) method, RD selects an appropriate initial value of the response and then extracts equally spaced segments of time histories. By averaging the value of each segment, the random parts are even out. Modal parameters are estimated directly from the free-decay response which overcomes the fact that the information of input excitation may not be available. However, with RD and ITD, only the first few modes of low frequency can be identified with high accuracy (Siringoringo and Fujino 2008).

Natural Excitation Techniques (NExT) method considers the ambient excitation as a random noise signal such as white noise excitation (Farrar and James III 1997). NExT adopts to Eigensystem Realization Algorithm (ERA) in data normalisation process (James III et al. 1993). As a curve-fitting algorithm, ERA associate with NExT can be applied on

cross-correlation function through which the resonant frequencies and modal damping can be obtained. This method is effective for identification of lightly damped structures and can be applied to complex structures. However, when all the modes are desired, a frequency range needs to be estimated first (Alvin et al. 2003; Siringoringo and Fujino 2008).

Auto Regression (AR) along with Auto-associative neural network are also well-known OMA methods. Through data normalisation in AR, some significant ambient effects in frequencies such as moisture and temperature variations are filtered out (Peeters and De Roeck 2001). With two methods conjunction with each other, ambient variation is modelled as a linear, time-invariant structure vibration model is estimated. The main disadvantage of these methods is the excessive computational time. A database must be built up and trained in the neural network. Parameters of the time prediction model will be computed and fed to the trained neural network. In addition, a wide range of operational and environmental variations must be captured, that increases the amount of computational work. Furthermore, a large set of extracted features and measured environmental variables needs to be available for the process of these two methods (Sohn et al. 2002), in most of the cases, this prerequisite cannot be satisfied.

Au (2011) proposed a Bayesian method for extracting dynamic characteristics as well as their uncertainties operating in the frequency domain. However, this method is applicable only to single mode. To deal with structures with different operational conditions, Shih et al. (1988) proposed to use Singular Value Decomposition (SVD) based on the assumption that the singular vectors are orthogonal. However, the mode shapes obtained by SVD may be biased because of the assumption (Ruotolo and Surace 1999;

Sohn 2007). Pintelon et al. (1994) proposed Least Squares Complex Frequency domain (LSCF) to extract mode shapes and frequencies from correlation functions using a curve-fitting algorithm. The LSCF can obtain only global estimates of mode shapes combining with other system identification methods.

Akaike (1975) proposed the theory of Stochastic Subspace Identification (SSI) to solved the stochastic realization problem based on canonical correlation analysis. Overschee and Moor (1996) improved the SSI that can identify the state-space matrices by using QR-factorization, Singular Value Decomposition (SVD) and Least Squares (LS). QR-factorization is used to reduce the data size, SVD is used to cancel out the noise in output data (Chang and Loh 2015; Elsner and Tsonis 2013; Qin et al. 2016; Zhang et al. 2012). SSI is considered as one of the most robust and accurate system identification algorithm for OMA since it has been successfully applied to several types of structures (Boonyapinyo and Janesupasaeree 2010; Fan et al. 2007; Gontier 2005; Hermans and Van der Auweraer 1999; Reynders et al. 2008; Zhang et al. 2012). SSI can be applied to the complex structures under high uncertainties of ambient vibrations. In this research, SSI has been chosen as system identification algorithm to extract structural dynamic characteristics obtained from the displacements using the non-contact based sensor.

2.3 SHM Sensor System

Structural dynamic characteristics are extracted from vibration response. To obtain the time history of structural response (i.e. acceleration, strain, velocity and displacement etc), several types of sensor have been applied in vibration-based SHM that includes contact based wire sensor, contact based wireless sensor and non-contact based sensor.

This section will discuss the overview of state-of-the-art sensors for SHM related to this research.

2.3.1 Contact based SHM Sensor System

Contact based sensors such as accelerometers have been widely used for structural vibration tests (Farrar and James III 1997; Halling et al. 2001; Khatibi et al. 2012; Magalhães et al. 2009). Contact based sensor system has three main components: sensor, Data Acquisition (DAQ) system and receiver. Figure 2.3 shows a typical acceleration acquisition system.

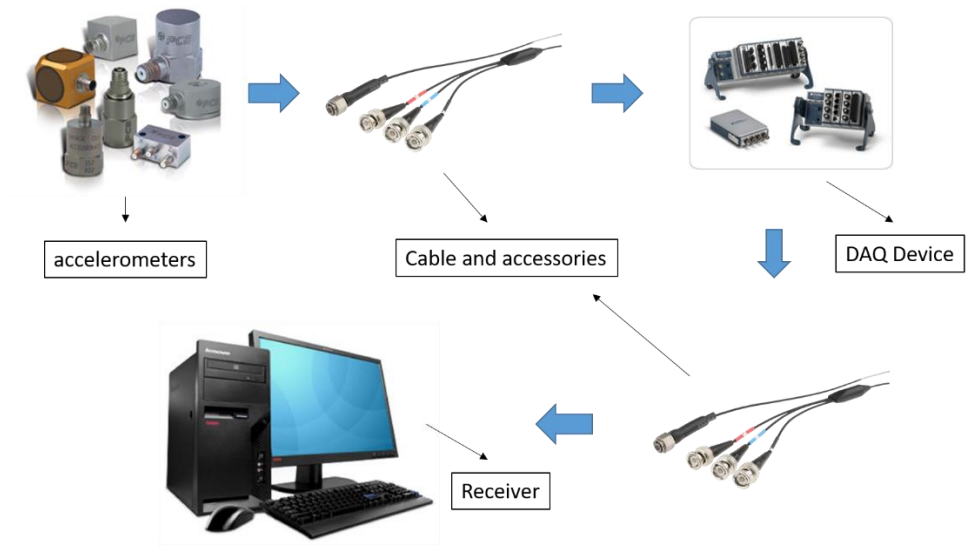

Figure 2.3. Typical Acceleration Acquisition System

Accelerometer is one of the most common sensors due used for SHM due to high sensitivity. Acceleration responses can be measured readily; velocity and displacement response can be obtained through numerical integration from measured accelerations.

Accelerometers are generally used for large specimens having a mass much greater than the accelerometer itself. Therefore, the mass of accelerometer can be negligible for overall vibration. Alternatively, strain is also a response that can be measured by sensors such as strain gauges and fiber-optic sensor. They have light self-weight and small size and immunity to electromagnetic fields (Kiesel et al. 2007; López-Higuera 2002). The power supply and maintenance are remaining challenges in long-term SHM.

As contact based sensor, installation and maintenance normally needs the interrupt or disturbance of structural operation. The distance between sensor and DAQ device and data process device are limited by the length and availability of cable and accessories. Installation of the sensors and hardwiring them to data acquisition system requires extensive time consumption. Electric power is required for all the devices throughout the SHM process. To overcome those limitations, wireless sensor network (WSN) has been widely used. WSN in SHM is a set of integrated devices to measure structural vibration response and transmit the measured data to the receiver. Wireless sensor interface, data processing subsystem, wireless transceiver and power supplier need to be encompassed to achieve wireless data acquisition (Dorvash 2013). Different wireless techniques have been used in structural health monitoring (Buckner et al. 2008; Grosse and Krüger 2006; Mascarenas et al. 2010). A typical wireless sensor network is shown in Figure 2.4.

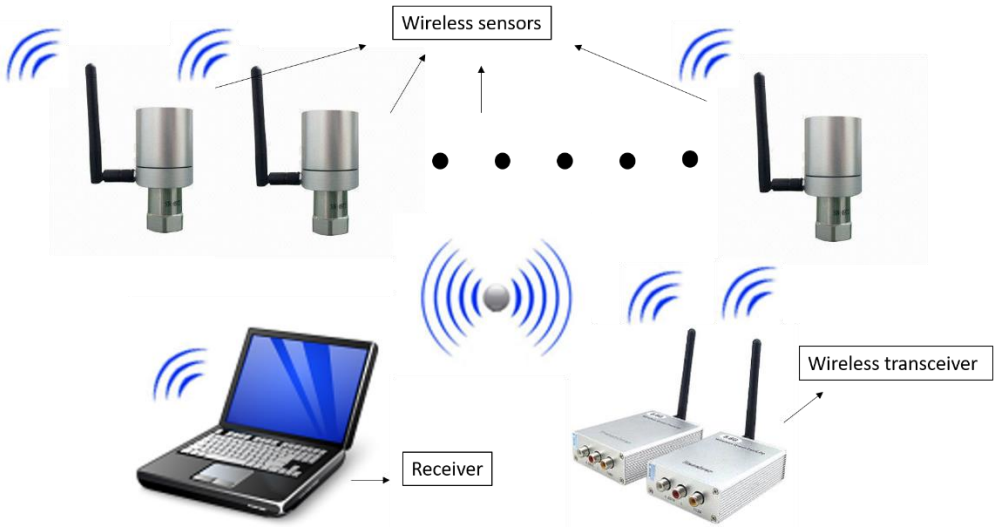

Figure 2.4. Typical Wireless Sensor Network

The installation and placement of sensors are still a key factor for the accurate assessment of SHM. SHM normally requires the measurements of several locations of the structure. A larger number of points requires a more rigorous calibration of the numerical model of the structure for the precise identification of the locations of damages (Antunes et al. 2012). Even though WSN overcome the limitation of device distance, the sensor is still required to be contacted with structures. Civil structures are typically large and complex, response collected from a limited number of sensors is inadequate to accurately assess the structural condition. Furthermore, in small-scale structures, such contact base sensor may potentially change the structure characteristics resulting from the mass of the sensor attached to the structures.

2.3.2 Non-contact Based SHM Sensor System

When limited sensors and/or data acquisition channel are available in the field, DAQ process has to be repeated with different locations of sensors (i.e., rearrangement of

sensor distribution). However, data merge may not be feasible when the response process is not stationary from different set-ups. To overcome those limitations of contact based SHM sensors, the development and application of non-contact based sensor are necessary.

Laser-based technique has been developed. For example, Laser Doppler Vibrometer (LDV) can sensitively measure the velocity of structural response. However, LDV is a short range sensor, it cannot analyze the entire structure simultaneously when the structural is large and the detection are strictly localised (Monkman and Connolly 2005). Radar-based sensor has recently been used as a non-contact based health monitoring for large structures. Farrar and Cone (1994) described and applied microwaves in measuring the vibration response of I-40 bridge. However, the detection of damages using this method is not accurate enough to identify the damage locations. Gentile and Bernardini (2008) improved the technique of the application of microwaves to measure the deflection of several points on a large structure, simultaneously.

Camera based starts to be drawing significant attention in SHM due to the large range of detection. Image processing techniques are used to quantify the motion in structures. Wadhwa et al. (2013) introduced a technique to manipulate small movements in videos based on the analysis of motion in complex-valued image pyramids. As discussed previously, velocity and displacement can be obtained by numerical integration from measured acceleration, however, challenges remain in practice. Significant error is unavoidable when these velocity and displacement responses were obtained via the integration of acceleration. The presence of measurement noise affects the accuracy of integrated displacement from acceleration data (Li 2011; Smyth and Wu 2007). Accurate

displacement extracted from motion magnification has then been used in structural damage detection by serving as input for dynamic characteristics extraction. Chen et al. (2014) identified modal of a cantilever beam using motion magnification captured through high-speed camera video. Temporal filtering is applied to separate the different modal motions in order to compute the mode shapes (Chen et al. 2015). However, their approach is not validated to detect and quantify the damages of the structure.

Kielkopf and Hay (2014) developed a non-contact based sensor system. Since the optical sensor is a non-contact based instrument, there is no need for the installation on the structure that avoids the operational interruption of structures (Kielkopf and Hay 2014). The system was used to identify the dynamic characteristics of bridges using the measured displacement (Hay 2011; Hay et al. 2012). High-speed camera as an optical sensor can detect very small intensity changes caused by motions in large structures when stimulated by ambient excitation. A system of hardware and software has been built that enables the rapid non-contact assessment of the structural characteristics of structures using ambient light from a distance (Hay 2011). This optical sensor and correlated technique are easy to adopt to different types of structures with a small amount of time-consuming and the reduction in cost are significant. Figure 2.5 shows the application of this technique in capturing displacements of highway bridge vibration due to traffic.

Figure 2.5. Application of High-speed Camera on Highway Bridge Vibration

The displacement of the bridge can be acquired with ambient traffic vibration. Yang et al. (2017) successfully applied this technique in a lab validation for system identification using stochastic subspace identification and modal scaling methods.

In this study, the non-contact high-speed camera is used to obtain the displacements to serve as input for SSI. Also, without contacting sensor on structures, the properties (mass and stiffness) of a structure will not be changed due to sensor's self-weight and cable potential changes on the stiffness. This study focuses on the feasibility and applicability of the proposed algorithms using the non-contact based sensor. Further, the camera-based sensor can acquire as much as responses simply by measuring different locations in the image as opposed to the complexity and high cost of adding a contact base sensor.

CHAPTER 3

LITERATURE REVIEW ON ALGORITHMS

Damage detection methods based on frequency shifts or mode shape changes depend on data from "undamaged condition". It is also very hard to locate and detect the severity of damages in the structure using mode shape. With lower modes' dynamic characteristics, only Level I damage detection can be achieved. To achieve higher level detection (e.g. Level IV SHM Scheme), higher modes is needed which requires more sensor locations. Non-contact sensor is not limited by the availability of sensor, instead, the response of the entire structure is recorded and information of any points can be extracted. Besides frequencies and mode shapes, stiffness and mass matrices of structure can provide more information about existence, location and severity of damages in structure. It is difficult to obtain system matrices (i.e., mass and stiffness) from structural vibration response directly. However, modal parameters (i.e., frequencies and mode shapes) can be extracted form responses using OMA method. With response acquired from the non-contact sensor as the only input to obtain mass and stiffness matrices, an algorithm needs to be developed.

Stochastic Subspace Identification (SSI) is one of output only method that can identify the system from vibration response of the structure. With finite element model updating (FEMU), the system matrices can be updated from frequencies and mode shapes extracted from SSI. However, there is one gap between those two methods. From SSI, only the unscaled mode shapes are obtained. To update system matrices, the scaled mode shapes are required. To detect damage using mass and stiffness obtaining from vibration response, a modal scaling method is needed. Mass change modal scaling (McMS) is an efficient method to scale mode shapes obtained from SSI. In this study, three algorithms are used to evaluate structural damage location and quantification. Sections 3.1-3.3 explain each of the algorithms in this research.

3.1 Stochastic Subspace Identification (SSI)

SSI is considered to be the most powerful technique for output-only modal analysis. This algorithm was proposed by Overschee and Moor (1996). SSI identifies the state space matrices by using QR-factorization, Singular Value Decomposition (SVD) and least squares.

3.1.1 The Discrete Time Formulation

The stochastic response from a system is a function of time represented by a linear matrix as follows:

$$y(t) = \begin{Bmatrix} y_1(t) \\ y_2(t) \\ \vdots \\ y_m(t) \end{Bmatrix} \tag{3.1}$$

In the classical formulation, the system is considered as a multiple-degree-of-freedom (MDOF) structural system as follows:

$$\boldsymbol{M}\ddot{y}(t) + \boldsymbol{D}\dot{y}(t) + \boldsymbol{K}y(t) = f(t) \tag{3.2}$$

where $\boldsymbol{M}$ is the mass matrix, $\boldsymbol{D}$ is the damping matrix, $\boldsymbol{K}$ is the stiffness matrix, and $f(t)$ is the loading force vector. A state space transformation must be introduced in Eq. 3.2 to take the response from a continuous time formulation to a discrete time domain.

$$x(t) = \begin{Bmatrix} y(t) \\ \dot{y}(t) \end{Bmatrix} \tag{3.3}$$

Introducing the state space formulation transforms the original second order system equation, represented by Eq. 3.1, into a first order equation.

$$\begin{aligned} \dot{x}(t) &= \boldsymbol{A}x(t) + \boldsymbol{B}f(t) \\ y(t) &= \boldsymbol{C}x(t) \end{aligned} \tag{3.4}$$

where $\boldsymbol{A}$ is the system matrix, and the load matrix $\boldsymbol{B}$ in continuous time. After discretization in time, the discrete-time state-space model of the structure is obtained as:

$$x_{k+1} = \boldsymbol{A}x_k + \boldsymbol{B}f_k \tag{3.5}$$

$$y_k = \boldsymbol{C}x_k + \boldsymbol{D}f_k \tag{3.6}$$

The input of f_k is unknown and there is some measurement noise on the measured outputs that cannot be neglected. To solve the problem without information of input force, Eq. 3.5 and 3.6 can be rewritten into:

$$x_{k+1} = \boldsymbol{A}x_k + w_k \tag{3.7}$$

$$y_k = \boldsymbol{C}x_k + v_k \tag{3.8}$$

where

$$w_k = \boldsymbol{B}f_k \text{ and } v_k = \boldsymbol{D}f_k + n_{y,k} \tag{3.9}$$

where w_k is the input noise, v_k and $n_{y,k}$ are the output measurement noise. $n_{y,k}$ is unknown but are assumed to have a discrete zero-mean white noise features (Zhang et al. 2012). They have covariance matrices as:

$$E\left[\begin{pmatrix} w_p \\ v_p \end{pmatrix}\begin{pmatrix} w_p^T & v_q^T \end{pmatrix}\right] = \begin{pmatrix} \boldsymbol{Q} & \boldsymbol{S} \\ \boldsymbol{S^T} & \boldsymbol{R} \end{pmatrix}\delta_{pq} \tag{3.10}$$

where δ_{pq} is the Kronecker delta and E(.) is the expected value operator. ***Q, R, S*** are the covariance and cross-covariance matrices of the measurement and process noise, respectively.

3.1.2 The Block Hankel Matrix and Projection

With only the measured outputs, y_k, are available, and the system matrices *A*, and *C* have to be identified. First, a Block Hankel matrix of output, $y(t)$, is formulated:

$$Y_{0|2i-1} \overset{\text{def}}{=} \begin{array}{l} \left.\begin{array}{l} \\ i \\ \\ \end{array}\right\} \\ \left.\begin{array}{l} \\ i \\ \\ \end{array}\right\} \end{array} \left[\begin{array}{cccc} y_0 & y_1 & \cdots & y_{j-1} \\ \cdots & \cdots & \cdots & \cdots \\ y_{i-2} & y_{i-1} & \cdots & y_{i+j-3} \\ y_{i-1} & y_i & \cdots & y_{i+j-2} \\ \hline y_i & y_{i+1} & \cdots & y_{i+j-1} \\ y_{i+1} & y_{i+2} & \cdots & y_{i+j} \\ \cdots & \cdots & \cdots & \cdots \\ y_{2i-1} & y_{2i} & \cdots & y_{2i+j-2} \end{array}\right] \begin{array}{l} \left.\begin{array}{l} \\ \\ \text{“past”} \\ \\ \end{array}\right\} \\ \left.\begin{array}{l} \\ \\ \text{“future”} \\ \\ \end{array}\right\} \end{array} \overset{\text{def}}{=} \left(\frac{Y_{0|i-1}}{Y_{i|2i-1}}\right) \overset{\text{def}}{=} \left(\frac{Y_p}{Y_f}\right) \tag{3.11}$$

where $Y_{i|j}$ means row i to row j of Block Hankel matrix. Y_p and Y_f are defied as “past” and “future” Block Hankel Matrix respectively. Subspace identification algorithms make extensive use of observability matrix, Γ_i , and projection matrix, $\mathcal{O}_i$, and of their structure (Overschee and Moor 1996). The observability matrix, Γ_i , is defined as:

$$\Gamma_i \stackrel{\text{def}}{=} \begin{pmatrix} C \\ CA \\ CA^2 \\ \cdots \\ CA^{i-1} \end{pmatrix} \tag{3.12}$$

Define matrix $\mathcal{O}_i$ as:

$$\mathcal{O}_i \stackrel{\text{def}}{=} Y_f / Y_p \tag{3.13}$$

and

$$\mathcal{O}_i = \Gamma_i \cdot \hat{X}_i \tag{3.14}$$

the matrix Γ_i is unknown, so SVD is used on $\mathcal{O}_i$ to estimate the states:

$$\mathcal{O}_i = USV^T \tag{3.15}$$

and

$$\Gamma_i = US^{1/2} \tag{3.16}$$

$$\hat{X}_i = S^{1/2}V^T \tag{3.17}$$

define

$$\Gamma_{i-1} = \underline{\Gamma_i} \tag{3.18}$$

$\underline{\Gamma_i}$ denotes the matrix Γ_i without the last ith row. And state matrices $\hat{X}_i$ and $\hat{X}_{i+1}$ can be determined as:

$$\hat{X}_i = \Gamma_i^{\dagger}.\mathcal{O}_i \quad \text{and} \quad \hat{X}_{i+1} = \Gamma_{i-1}^{\dagger}.\mathcal{O}_{i-1} \tag{3.19}$$

where † is the pseudo inverse operation.

3.1.3 System Matrices Estimation

At this point, $\hat{X}_i$ and $\hat{X}_{i+1}$ can be calculated using output data only. Following relationship can be obtained:

$$\begin{pmatrix} \hat{X}_{i+1} \\ Y_{i|i} \end{pmatrix} = \begin{pmatrix} \boldsymbol{A} \\ \boldsymbol{C} \end{pmatrix} (\hat{X}_i) + \begin{pmatrix} \rho_W \\ \rho_V \end{pmatrix} \tag{3.20}$$

where $Y_{i|i}$ only one row outputs of Block Hankel matrix, and system matrices, $\boldsymbol{A}$ and $\boldsymbol{C}$, can be solved through least square sense. ρ_W and ρ_V are Kalman filter residuals that are not correlated with $\hat{X}_i$. Then the dynamic system matrices, $\boldsymbol{A}$ and $\boldsymbol{C}$, can be determined as follows:

$$\begin{pmatrix} \boldsymbol{A} \\ \boldsymbol{C} \end{pmatrix} = \begin{pmatrix} \hat{X}_{i+1} \\ Y_{i|i} \end{pmatrix} (\hat{X}_i)^{\dagger} \tag{3.21}$$

An eigenvalue decomposition of A leads to the diagonal matrix A $\in R^{n \times n}$ of discrete-time system poles, λ_i, and corresponding eigenvectors, ψ_i, as

$$\boldsymbol{A} = \varphi \Lambda \varphi^{-1}, \ \boldsymbol{A}\varphi_i = \lambda_i \varphi_i \tag{3.22}$$

the frequencies, f_i , can be calculated as

$$f_i = \frac{|f_s ln\lambda_i|}{2\pi} \tag{3.23}$$

and the damping ratio, ξ_i, would be

$$\xi_i = \frac{(ln\lambda_i)^R}{|ln\lambda_i|} \tag{3.24}$$

where f_s is the sampling frequency. The eigenvector of **A** leads to the experimental mode shapes, ψ_i:

$$\psi_i = \boldsymbol{C}\varphi_i \tag{3.25}$$

SSI is recognized as an effective algorithm for the modal estimation of a system

with only the information of output response as an input data and treats excitation force as noise (Ghasemi et al. 2006). When handling a large amount of input data, SSI is a suiTable choice due to the robust technique to estimate dynamic characteristics.

3.2 Modal Scaling

As discussed in Chapter 2, OMA is an output-only modal analysis method that only measures the response excited by ambient forces. The vibration responses are used as the input for system identification. With the advantage of not using excitation force or measurement of ambient input OMA has been widely used (Brincker et al. 2000; Brincker et al. 2003; Magalhães et al. 2009). Since the input forces are unknown, the mode shapes cannot be normalised thus only unscaled mode shapes can be obtained that is considered as the major disadvantage of OMA (Coppotelli 2009; Parloo et al. 2003). However, to achieve the high level of SHM schemes, normalised mode shapes are required (Fang et al. 2008; Gentile and Gallino 2008). To estimate the scaling factor several approaches have been proposed such as mass-change (López Aenlle et al. 2005), stiffness-change (Ewins 2000) and mass-stiffness-change (Khatibi et al. 2009) based modal scaling methods. The scaled mode shape, $\{\phi\}$, and unscaled mode shape, $\{\psi\}$, are related as:

$$\{\phi\} = \frac{\{\psi\}}{\sqrt{\{\psi\}^T \cdot \boldsymbol{M} \cdot \{\psi\}}} \tag{3.26}$$

so the scaling factor, α, is expressed as:

$$\alpha = \frac{1}{\sqrt{\{\psi\}^T \cdot \boldsymbol{M} \cdot \{\psi\}}} \tag{3.27}$$

where $\{\phi\}$ is the scaled mode shape, $\{\psi\}$ is unscaled mode shape, $[m]$ is the mass matrix and α is the modal scaling factor. Then the relation between unscaled mode shape, $\{\psi\}$, and scaled mode shape $\{\phi\}$, can be expressed as:

$$\{\phi\} = \alpha\{\psi\} \tag{3.28}$$

The following sections present three scaling methods.

3.2.1 Mass-change Modal Scaling (McMS)

Mass-change scaling method (McMS) was validated by experiments in the lab and in field tests (Brincker et al. 2004; López Aenlle et al. 2005; Parloo et al. 2003). This method is based on adding small change of mass to the point of the structure where the mode shapes are known. López-Aenlle et al. (2012) suggested that mass change around 5% of the total mass of the structure can accurately obtain the scaling factor. The scheme of this method is shown in Figure 3.1 below (López Aenlle et al. 2005):

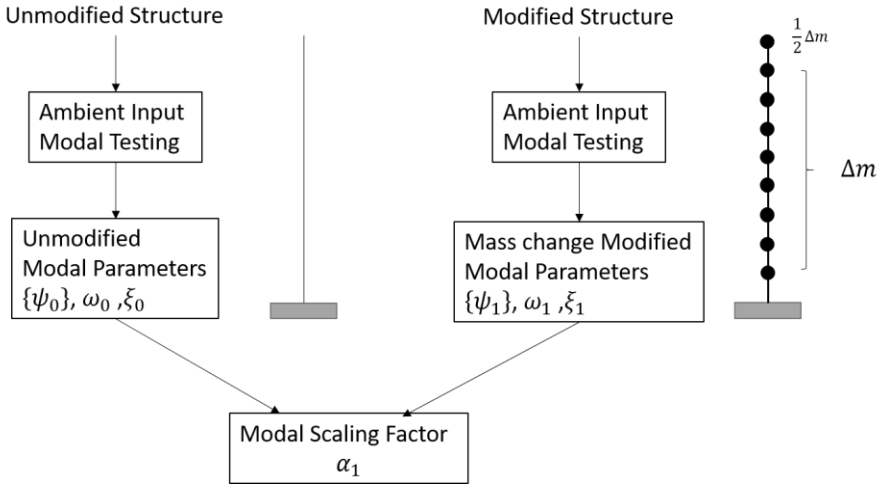

Figure 3.1. Mass-change Modal Scaling Scheme (McMS)

The method can be derived from the eigenvalue equations of the unmodified and the modified (mass added) structure (Brincker and Andersen 2003). In the case of no damping or proportional damping the eigenvalue equation can be expressed as:

$$\boldsymbol{M}\{\phi_0\}\omega_0^2 = \boldsymbol{K}\{\phi_0\} \tag{3.29}$$

where $\{\phi_0\}$ is the scaled mode shape before modification, ω_0 is the natural frequency, $\boldsymbol{M}$ the mass matrix, and $\boldsymbol{K}$ is the stiffness matrix. The addition of mass to the points where the structure modes should be known, the new eigenvalue equation with added mass in the system can be expressed as:

$$(\boldsymbol{M} + [\Delta m])\{\phi_1\}\omega_1^2 = \boldsymbol{K}\{\phi_1\} \tag{3.30}$$

where $\{\phi_1\}$ is the scaled mode shapes after modification, ω_1 is the frequencies after mass modification, and $[\Delta m]$ is the mass change matrix. Subtracting Eq. 3.29 from Eq. 3.30, and we can obtain:

$$\boldsymbol{M}(\{\phi_1\}\omega_1^2 - \{\phi_0\}\omega_0^2) - [\Delta m]\{\phi_1\}\omega_1 = 0 \tag{3.31}$$

Given the assumption that the mass change is so small that the mode shape does not change significantly, where $\{\phi_0\} \cong \{\phi_1\} \cong \{\phi\}$ and we can obtain:

$$\boldsymbol{M}\{\phi\}(\omega_1^2 - \omega_0^2) - [\Delta m]\{\phi\}\omega_1 = 0 \tag{3.32}$$

apply the orthogonality condition, we can obtain that

$$(\omega_1^2 - \omega_0^2) = \{\phi\}^T([\Delta m]\omega_1^2)\{\phi\} \tag{3.33}$$

With the relation given by Eq. 3.26 and the assumption $\{\psi_0\} \cong \{\psi_1\} \cong \{\psi\}$ the scaling factor based on mass-change, α_1, can be expressed as:

$$\alpha_1 = \sqrt{\frac{(\omega_1^2 - \omega_0^2)}{\{\psi\}^T[\Delta m]\omega_1^2\{\psi\}}} \tag{3.34}$$

The factor of α_1 can be used in Eq. 3.28 for obtaining scaled mode shape $\{\phi\}$.

3.2.2 Stiffness-change Modal Scaling (ScMS)

Ewins (2000) found that the mass change has less effect on the low natural frequencies compared to the higher natural frequencies. Therefore, stiffness-change modal scaling method (ScMS) has the higher sensitivity to the first natural frequency compared to the mass-change method when higher modes are not available (Coppotelli 2009). ScMS would be more accuracy towards modal scaling. ScMS changes the stiffness of structure by attaching springs, or other devices such as cables or bars, at certain points of the structure where the mode shapes are known. The scheme of ScMS is shown in Figure 3.2.

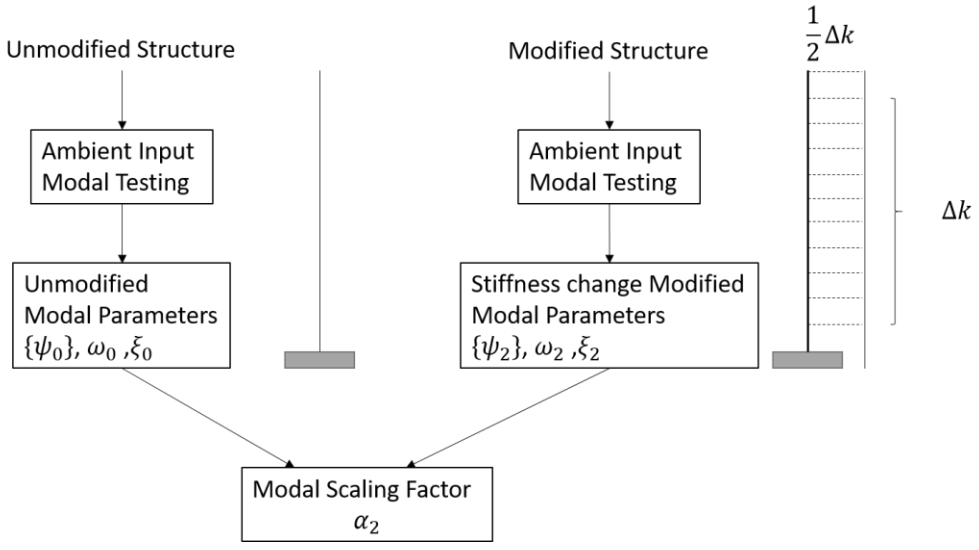

Figure 3.2. Stiffness-change Modal Scaling Scheme (ScMS)

ScMS method can also be derived from Eq. 3.29. The addition of stiffness to the points where the structure modes are known. Then the new eigenvalue equation with the change of stiffness can be expressed as:

$$\boldsymbol{M}\{\phi_2\}\omega_2^2 = (\boldsymbol{K} + [\Delta k])\{\phi_2\} \tag{3.35}$$

where $\{\phi_2\}$ is the scaled mode shapes after stiffness modification, ω_2 is the frequencies after modification, and $[\Delta k]$ is the stiffness change matrix. Subtracting Eq. 3.29 from Eq. 3.35, and we obtain:

$$\boldsymbol{M}(\{\phi_2\}\omega_1^2 - \{\phi_0\}\omega_0^2) = \boldsymbol{K}\{\phi_2\} - \boldsymbol{K}\{\phi\} + [\Delta k]\{\phi_2\} \tag{3.36}$$

Given the assumption that the stiffness change is so small that the mode shape does not change significantly, where $\{\phi_0\} \cong \{\phi_2\} \cong \{\phi\}$ and we can obtain:

$$\boldsymbol{M}\{\phi\}(\omega_2^2 - \omega_0^2) = [\Delta k]\{\phi\} \tag{3.37}$$

apply the orthogonality condition, we can obtain:

$$(\omega_2^2 - \omega_0^2) = \{\phi\}^T[\Delta k]\{\phi\} \tag{3.38}$$

With the relation given by Eq. 3.26 and the assumption, $\{\psi_0\} \cong \{\psi_2\} \cong \{\psi\}$ the scaling factor based on stiffness-change can be expressed as:

$$\alpha_2 = \sqrt{\frac{(\omega_2^2 - \omega_0^2)}{\{\psi\}^T[\Delta k]\{\psi\}}} \tag{3.39}$$

The factor of α_2 can then be used in Eq. 3.28 for obtaining scaled mode shape, $\{\phi\}$.

3.2.3 Mass-Stiffness-Change Modal Scaling (MScMS)

Khatibi et al. (2012) suggested a way to scale mode shapes based on mass-stiffness change by the addition of mass and stiffness. The scheme of MScMS is shown in Figure 3.3.

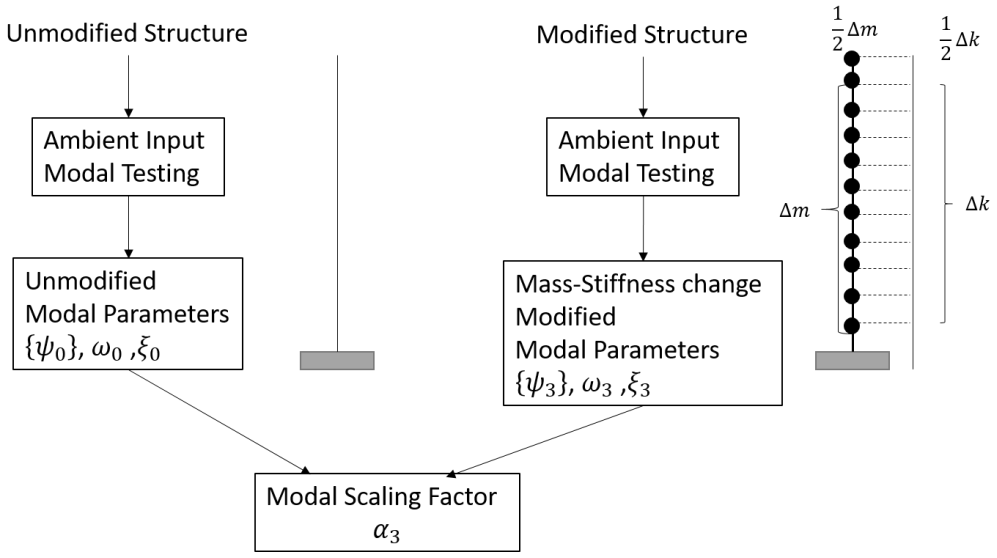

Figure 3.3. Mass-Stiffness-change Modal Scaling Scheme (MScMS)

MScMS method is also derived from Eq. 3.29. the addition of mass and stiffness to the points where the structure modes are known, the new eigenvalue equation with added stiffness can be expressed as:

$$(\boldsymbol{M} + [\Delta m])\{\phi_3\}\omega_3^2 = (\boldsymbol{K} + [\Delta k])\{\phi_3\} \tag{3.40}$$

where $\{\phi_3\}$ is the scaled mode shapes after mass and stiffness modification, ω_3 is the frequencies after modification. Subtracting Eq. 3.29 from Eq. 3.40, and we obtain:

$$\boldsymbol{M}(\{\phi_3\}\omega_3^2 - \{\phi_0\}\omega_0^2) - [\Delta m]\{\phi_3\}\omega_3 = \boldsymbol{K}\{\phi_3\} - \boldsymbol{K}\{\phi_0\} + [\Delta k]\{\phi_3\} \tag{3.41}$$

Given the assumption that the mass-stiffness change is so small that the mode shape does not change significantly, where $\{\phi_0\} \cong \{\phi_3\} \cong \{\phi\}$ and we can obtain:

$$\boldsymbol{M}\{\phi\}(\omega_2^2 - \omega_0^2) + [\Delta m]\{\phi\}\omega_3^2 = [\Delta k]\{\phi\} \tag{3.42}$$

apply the orthogonality condition, we can obtain that

$$(\omega_3^2 - \omega_0^2) = \{\phi\}^T([\Delta k] - [\Delta m]\omega_3^2)\{\phi\} \tag{3.43}$$

With the relation given by Eq. 3.26 and the assumption $\{\psi_0\} \cong \{\psi_3\} \cong \{\psi\}$ the scaling factor based on stiffness-change can be expressed as:

$$\alpha_3 = \sqrt{\frac{(\omega_3^2 - \omega_0^2)}{\{\psi\}^T([\Delta k] - [\Delta m]\omega_3^2)\{\psi\}}} \tag{3.44}$$

The factor of α_3 can then be used in Eq. 3.28 for obtaining scaled mode shape, $\{\phi\}$.

A major disadvantage of OMA is that the mode shapes extracted cannot be normalised and only the unscaled mode shapes are estimated. Modal scaling methods applied to overcome this. The accuracy of obtaining scaling factor using methods we presented above depends on the accuracy of OMA algorithm as well as the amount of mass and/or stiffness change.

3.3 Finite Element Model Updating (FEMU)

SHM methods that based on dynamic characteristics (frequencies and mode shapes) have limited capability for early detection of damage and are not able to diagnose the sources of damage (Fritzen et al. 1998). To assess the location and extent of structural

damage from vibration test data, SHM based on FEMU has developed rapidly in the past decades (Friswell and Mottershead 1995; Reynders et al. 2010). FEMU can be used to identify unknown properties of an FE model and the structural damages are represented by the change in stiffness and mass of the individual elements (Teughels and De Roeck 2005).

3.3.1 Overview of FEMU

Model updating methods can be classified into direct methods and iterative methods. The direct methods are also called model-based methods and directly update the structural parameters such as stiffness and mass (Caesar and Peter 1987; Carvalho et al. 2007). The iterative methods update structural parameters by the optimization process. However, the sensitivity analysis used in the iterative model updating methods might have large error due to the discrepancy between the initial FE model and the actual structure under test (Carvalho et al. 2007).

Various of FEMU method has been developed. The difference between those algorithms is the objective function that to be minimized and the constraints during the updating. Different algorithms can be implemented in the optimisation. Doebling et al. (1996) summarised that common model updating algorithms are: 1) optimal matrix update methods; 2) sensitivity-based methods; 3) eigenstructure assignment method, and 4) hybrid methods.

Olsson and Nelson (1975) proposed a Nelder-Mead FEMU method. The method does not require the objective function. It is efficient and relatively simple. However, it is only accurate in the early stages of the simulations.

Zimmerman and Kaouk (1992) proposed an FE updating algorithm that determines the perturbation matrices to the original FE model. And the damage was expected to exhibit in the updated perturbation FE model. It was found that this method has low resistant under high noise. Zimmerman and Kaouk (1994) then improved the algorithm using an original finite element model and a subset of measured eigenvalues and eigenvectors to overcome noise effect on the previous method. Although this method provides location and extension of damage successfully. However, the original FE model is not always available, especially for old or large structures.

Liu (1995) proposed to use the error norm of the eigenequation as the objective function to be minimized in the optimisation process. The discretized eigenvalues are then derived to detected damage.

Alvin (1997) proposed an FEMU method based on the minimization of dynamic residuals. Bayesian estimation is implemented in this method. This method has the assumption that the optimisation process is linear. The dynamic residual was arising from the errors in the mass and stiffness when evaluating the model parameters. This method relies on experimental analysis that requires the knowledge of input excitation force. Lam et al. (2004) also used model updating method based on the Bayesian modal identification and his approach doesn't require knowledge of the input excitation. However, the extent of damage was found to be overestimated due to the modelling error.

Cobb and Liebst (1997) proposed a method based on eigenvector sensitivity analysis of structure FE model. Damages are detected by the updated model and measured modal data (i.e., frequencies). However, this method is applicable only when there are small limited degrees of freedom.

Lam et al. (1998) proposed an FEMU method based on approximate parameter change technique and the damage signature matching technique. The damage location is determined by calculating the approximate change of system parameters based on two set of modal data. The parameter prior to the damage needs to be obtained first to use this approach.

Capecchi and Vestroni (1999) proposed to use the different between analytical and experimental frequencies as the objective function to be minimized. Jang et al. (2002) improved this method by adding a regularisation function to the primary error function. However, error remained in this method due to the discrepancy between analytical frequencies and the actual frequencies.

Based on the first-order Taylor series expansion of eigenvalues, Zhang et al. (2000) proposed an FEMU approach based on eigenvalue sensitivity. The changes in the updated eigenvalues are used as an indicator for damage detection. Another sensitivity based updating algorithm was proposed by Wahab (2001). Modal curvatures are served as modal parameters for updating.

Xia et al. (2002) developed a method to calculate the mean and standard deviation of the updated stiffness parameters in damaged configurations with perturbation method and Monte Carlo simulation. The possibility of damage existence is prohibited by the probability of damage existence. Frequencies and mode shapes before and after damage are compared to identify structural damage. Pothisiri and Hjelmstad (2003) also used the Monte Carlo methods to calculate the probabilities based on the statistical distributions of the parameters for the damaged and undamaged structures. This method can identify damage successfully when the noise level is low.

Teughels and De Roeck (2005) minimized the discrepancies in the frequencies and unscaled mode shape obtained from ambient vibration to update the FE model. It became more robust by the implementation of Gauss-Newton method.

Most of the indirect method is to update the discrepancy between analytical model and tested model or between undamaged model and damaged model. However, the analytical modal cannot represent the true structure model. And the undamaged model sometimes cannot be obtained. When the scaled mode shape and frequencies are available, direct FEMU can obtain the mass and stiffness directly. Two Lagrange multiplier based methods as known as direct methods are considered in this study.

3.3.2 Berman and Nagy (1983) FEMU

The first method is proposed by Berman and Nagy (1983). In the method, the mass matrix of FE model, $\boldsymbol{M}$, was updated to be $\boldsymbol{M_u}$ subjected to the orthogonality constraint. The stiffness matrix, $\boldsymbol{K}$, is updated to be $\boldsymbol{K_u}$ using updated mass matrix, $\boldsymbol{M_u}$, to get $\boldsymbol{K_u}$. "Updated" means that the matrix reflects the real condition of structure. The updated mass matrix $[M_u]$ is found to minimize the objective function J:

$$J = \frac{1}{2}\left\| \boldsymbol{M}^{-\frac{1}{2}}(\boldsymbol{M_u} - \boldsymbol{M})\boldsymbol{M}^{-\frac{1}{2}} \right\| \tag{3.45}$$

and the measured eigenvector matrix $\boldsymbol{V_e}$ and $\boldsymbol{M_u}$ are subject to the orthogonality constraint:

$$V_e^T \boldsymbol{M_u} V_e = \boldsymbol{I} \tag{3.46}$$

where $\boldsymbol{V_e}$ is the scaled mode shapes. The constrained minimization function is converted into an equivalent unconstrained minimization problem using Lagrange multipliers to input equality constraints, the updated mass matrix can be obtained as follows:

$$\boldsymbol{M_u} = \boldsymbol{M} + \boldsymbol{M}V_e\bar{\boldsymbol{M}}^{-1}(\boldsymbol{I} - \bar{\boldsymbol{M}}^{-1})\bar{\boldsymbol{M}}^{-1}V_e^T\boldsymbol{M} \tag{3.47}$$

where

$$\bar{\boldsymbol{M}}^{-1} = V_e^T\boldsymbol{M}V_e \tag{3.48}$$

Now the stiffness matrix can be updated by the updated mass matrix [$\boldsymbol{M_u}$] by minimizing the objective function J as follow:

$$J = \frac{1}{2}\left\|\boldsymbol{M_u}^{-\frac{1}{2}}(\boldsymbol{K_u} - \boldsymbol{K})\boldsymbol{M_u}^{-\frac{1}{2}}\right\| \tag{3.49}$$

Subject to the constraints as

$$\boldsymbol{K_u}V_e = \boldsymbol{M_u}V_eL_e \tag{3.50}$$

$$\boldsymbol{K_u} = \boldsymbol{K_u^T} \tag{3.51}$$

where L_e is a diagonal matrix of the measured eigenvalues. The equation for the updated stiffness matrix can be written as follows:

$$\begin{aligned}\boldsymbol{K_u} = \boldsymbol{K} - \boldsymbol{K}V_e{V_e}^T\boldsymbol{M_u} - \boldsymbol{M_u}V_e{V_e}^T\boldsymbol{K} + \boldsymbol{M_u}V_e{V_e}^T\boldsymbol{K}V_e{V_e}^T\boldsymbol{M_u} \\ + \boldsymbol{M_u}V_eL_eV_e^T\boldsymbol{M_u}\end{aligned} \tag{3.52}$$

3.3.3 Baruch (1978) FEMU

The first direct FEMU method is updating mass and stiffness matrix by updating $\boldsymbol{M}$ and $\boldsymbol{K}$, directly, while Baruch (1978) has proposed another way to update stiffness matrix using the eigenvector, V_e. The objective function, J can be expressed as follows:

$$J = \left\| \boldsymbol{M}^{-\frac{1}{2}}(V_{eu} - V_e) \right\| \tag{3.53}$$

where the orthogonality constraint applied as:

$$V_{eu}{}^T \boldsymbol{M} V_{eu} = \boldsymbol{I} \tag{3.54}$$

By minimising the value of J and the Lagrange multiplier method, updated eigenvector matrix, V_u ,can be obtained as

$$V_{eu} = V_e / (V_e^T \boldsymbol{M} V_e)^{1/2} \tag{3.55}$$

Baruch (1978) presented that the updated stiffness matrix K_u can be obtained by minimize the objective function, J as follows:

$$\boldsymbol{J} = \frac{1}{2} \left\| \boldsymbol{M}^{-\frac{1}{2}}(\boldsymbol{K_u} - \boldsymbol{K}) \boldsymbol{M}^{-\frac{1}{2}} \right\| \tag{3.56}$$

and subjected to two constraints:

$$\boldsymbol{K_u} V = \boldsymbol{M} V L \tag{3.57}$$

$$\boldsymbol{K_u} = \boldsymbol{K_u^T} \tag{3.58}$$

By using the Lagrange Multiplier methods, the updated stiffness matrix can be calculated as follows:

$$\boldsymbol{K_u} = \boldsymbol{K} - \boldsymbol{K}V_u{V_u}^T\boldsymbol{M} - \boldsymbol{M}V_u{V_u}^T + \boldsymbol{M}V_u{V_u}^T\boldsymbol{K}V_u{V_u}^T\boldsymbol{M} + \boldsymbol{M}V_uL_u{V_u}^T\boldsymbol{M} \quad (3.59)$$

Using the Baruch (1978) method, the stiffness matrix is updated based on first updating. The method proposed method is to combine both FEMU methods ((Berman and Nagy 1983) and (Baruch 1978)), using the updated mass, stiffness and eigenvectors of the first method as the initial value to perform the second updating and obtain the mass and stiffness matrices. information is explained in the following Chapter 4.

CHAPTER 4

ALGORITHM DEVELOPMENT

In this chapter, a framework of damage assessment algorithm is developed. To determine the presence of damage, the general steps are: 1) recognize the modal parameters 2) update system matrices, and 3) compare with health structure system matrices or previous matrices. To extract dynamic characteristics, displacements of structure element at multiple nodes under ambient vibration will serve as the only input without any information about excitation forces. SSI is implemented for recognising the structural dynamic characteristics. With the frequencies and mode shape vectors extracted from SSI, a McMS method is used to obtain the scaling factor for identifying true mode shapes (herein, scaled mode shapes). The scaled dynamic characteristics are used in FEMU to update mass and stiffness matrices. Different from using frequencies and mode shapes change as an indicator for damage detection, in this research, mass and stiffness matrices are updated and used to detect damages. With this approach, damage's location and severity can be reflected in values of matrices. In addition, a non-contact based modal scaling method that is based on temperature change over the structure is proposed.

4.1 Damage Indicators (DIs)

Vibration based SHM is based on changes in the dynamic behavior of structure due to damages. The change of dynamic characteristics can serve as a damage indicator (DI) for the identification of damages. Several DIs have been proposed and applied to structural damage assessment.

4.1.1 Frequencies as DI

As discussed in Chapter 3, frequency shift measured from structural vibration a well-established method to determine the existence of structural damages (Kawchuk et al. 2009). However, research has shown that the frequency shifts are not sensitive enough to detect damage. Also, frequencies are a global property of the structure and damages are typically local phenomena. The local damages can lead to change the global behavior, but it is not always true. Some local damage doesn't lead to change global frequencies. It is not clear that shifts in frequencies can be used to locate the damage (Doebling et al. 1998). Alampalli et al. (1992) also concluded that it is insufficient to locate the damage when natural frequencies are used alone as DI. Generally, this method is combined with other approaches. Random error sources can also cause undesirable and significant frequency shifts (Farrar et al. 1997). Typically, the presence of damage will cause a decrease in the natural frequencies. However, Sommer and Thoft-Christensen (1990) found increases in frequencies when the damage occurred in prestressed concrete beams. Later, the increase of elastic modulus of the concrete was discovered as the cause of the increase in frequencies. This indicates that damage might not reveal on frequencies changes in some situations.

4.1.2 Mode Shapes as DI

To overcome the limitations of SHM based on frequency shifts in damage detection, mode shape and modal assurance criteria (MAC) were used as DI in the early 1990s (Cobb and Liebst 1997; Fox 1992; Mayes 1992). The modal assurance criterion (MAC) (Pastor et al. 2012) is used to evaluate the correlation between two mode shapes. However, when using mode shape as DI, large amounts of data from multiple locations of structures are needed and only Level I SHM scheme can be achieved with high accuracy.

4.1.3 Damping as DI

Damping coefficient is proposed to be used as the DI due to the sensitivity on damages. When damping coefficient is used in a controlled environment and with homogenous material, it can precisely identify the damages. However, Hearn and Testa (1991) found that the modal damping ratio is extremely sensitive to small cracks in the steel structure. However, Rytter (1993) concluded that several factors are highly correlated to changes in damping such as structural material, boundary condition, environment conditions (the wind, soil, temperature, moisture, air, etc.). Thus, it is impossible to separate the damping from related to different sources (Alampalli et al. 1992). Complexities of damping measurement and analysis is another reason that damping as DI has not been comprehensively used. Thus, damping-based damage identification is still not well understood (Cao et al. 2016).

4.1.4 Stiffness and Mass Matrices as DI

To achieve a high level of damage detection, neither frequencies, mode shapes nor damping can be used as a single DI. For those reasons, stiffness and mass matrices of structures become alternative indicators for damage detection, location, and severity. The difference between updated system matrices (mass and stiffness matrices) and the original matrices can be used to quantify the location and the extent of damage (Doebling et al. 1998). The system matrices can provide more detailed information about the state of the system than the dynamic characteristics alone. Updated matrices can be enough for the identification of damaged elements. Therefore, the system matrices can be updated from modal characteristics (i.e. frequencies and mode shapes).

4.2 FEMU Integration

In the process of finite element modal updating, two direct updating methods are used together Berman and Nagy (1983) and Baruch (1978). Mass matrix is obtained after first updating and stiffness matrix is updated twice with both methods. The framework for integrating two methods are shown in Figure 4.1.

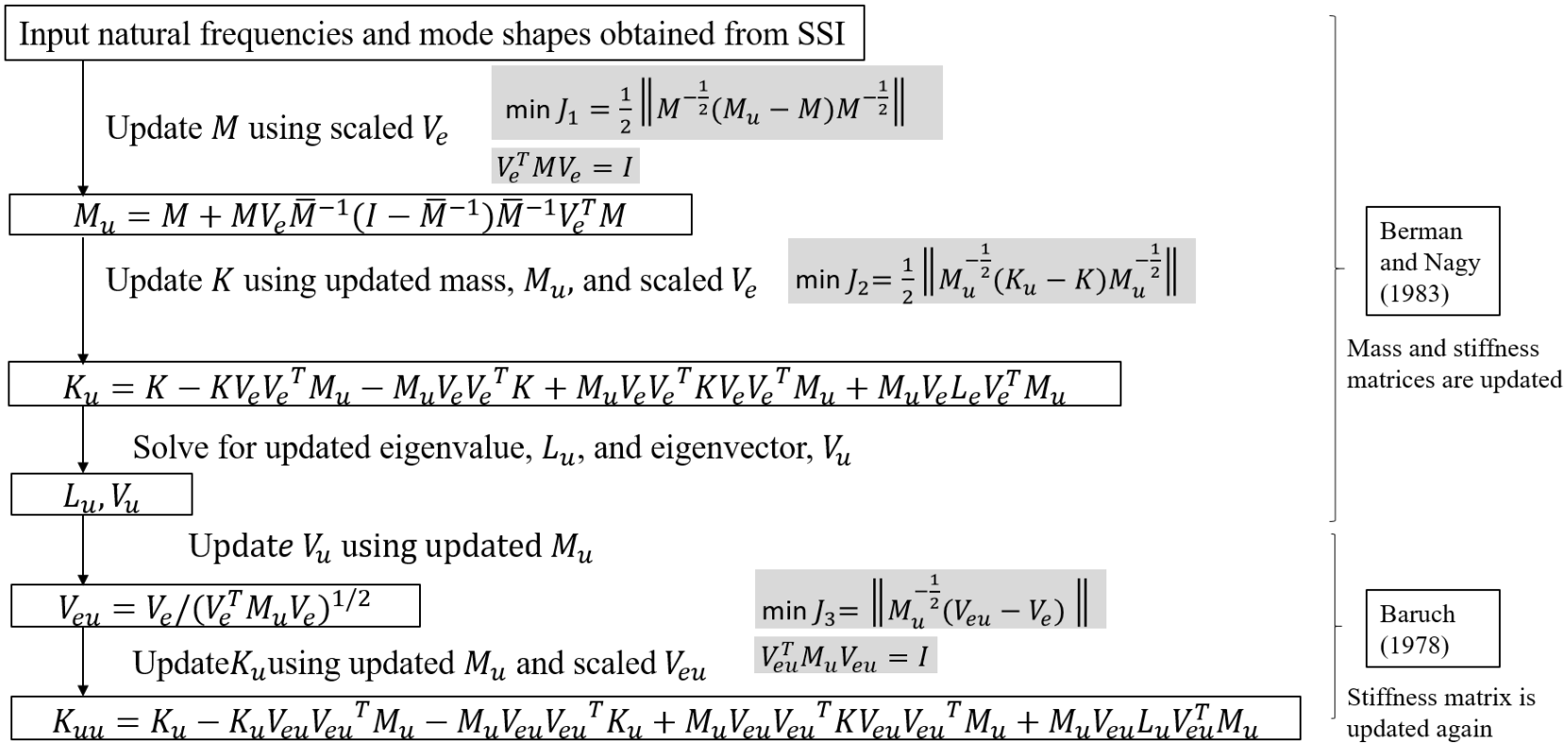

Figure 4.1. The Proposed Combined FEMU

The application of this algorithm has following steps: 1) assign mass and stiffness matrices and the dimensions that are determined by the modes extracted from OMA method; 2) update assigned mass matrix with first FEMU method with the orthogonal relationship and minimise the objective function, J_1 (see Figure 4.1); 3) update stiffness matrix with the minimization of the second objective function, J_2 (see Figure 4.1); 4) obtain updated eigenvector using updated mass matrix; 5) update stiffness matrix one more time using updated mass matrix and updated eigenvalue under the constrain of orthogonal and minimize of the objective function, J_3 (see Figure 4.1). The advantage of this method is that there is no requirement of the original matrices as long as the assigned matrices has the corresponding size with number of modes analyzed. In addition, in the second updating, the stiffness matrix is additionally updated using updated mass and eigenvector that were updated in the first updating method.

4.3 Procedure of Algorithm Applications

When updating the stiffness matrix twice, the accuracy of FEMU has been improved. The improvement will be discussed in Chapter 5. The unique feature of this algorithm is that system matrices are used as DI. To obtain mass and stiffness matrices, the vibration response of structures needs to be acquired. Typically, SHM uses the acceleration of structural vibrations, as it is the simple property to measure. However, displacement provides more information on the dynamic behaviors of the structure (Cha et al. 2015). And as discussed previously, velocity and displacement can be obtained by the integration from measured acceleration, however, the error is cannot be avoided during the mathematic

calculation. An optical sensor, however, can directly measure the deflections of the structures under operational conditions without any attachment of sensors to the structure.

To use the displacements, $y(t)$, acquired by non-contact optical sensor as the only input for damage detection, a process is proposed with the scope shown in Figure 4.2.

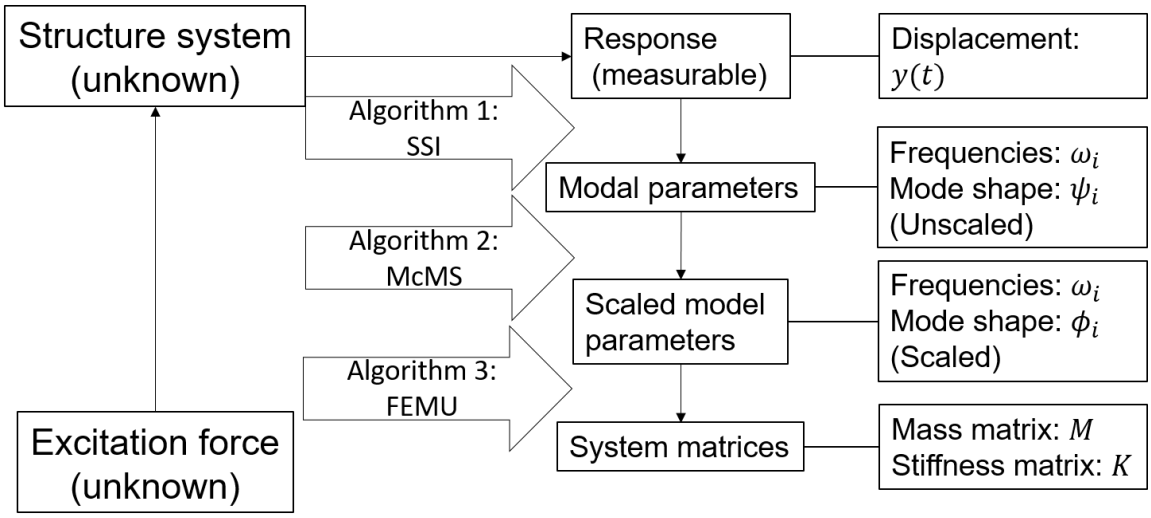

Figure 4.2. Scope of Damage Detection Algorithm

As shown in Figure 4.2, The algorithm can obtain the mass and stiffness matrices of structure using displacements, $y(t)$, of multiple points as the input for SSI to extract dynamic characteristics, ω_i and φ_i. McMS is used to scale the mode shape extracted from SSI to obtain the scaled mode shape, ϕ_i. With scaled mode shape, ϕ_i, and frequencies, ω_i, mass matrix, M and stiffness matrix, K of structure are the updated. Damage within the structure can be presented by the changes in those matrices.

4.4 Temperature Change Modal Scaling (TcMS)

This section presents a new approach to scale modes using temperature variations. The derivation of the proposed method is presented.

Mass and/or stiffness changes were used for modal scaling. They have been proposed and validated in several research (Aenlle and Brincker 2013; Bernal 2004; Brincker and Andersen 2003; Brincker et al. 2004; Coppotelli 2009; Ewins 2000; Khatibi et al. 2009; Khatibi et al. 2012; López Aenlle et al. 2005; Parloo et al. 2003). The addition mass and/or stiffness is impractical in large structures. The main assumption of this proposed method is that material properties change would affect dynamic characteristics due to temperature changes. The measured temperature change at different times can be theoretically used to estimate mass and stiffness changes for modal scaling. This should be measured with identifying thermal coefficient of materials. Practically, the temperature on the structure can be varied by the daily solar radiation or seasonally climate change. The major advantage of this method is that it doesn't require contacts to increase or decrease mass and stiffness.

4.4.1 Structural Properties and Geometric Changes due to Temperature Variations

The shift in natural frequencies of the structure is related to material and geometries changes due to temperature change. For example, the undamped vibration frequency of order, n is expressed as follows (Blevins and Plunkett 1980):

$$f_n = \frac{\lambda_n^2}{2\pi l^2}\sqrt{\frac{EI}{\mu}} \tag{4.1}$$

where λ_n is a dimensionless parameter as a function of the boundary conditions, l is the length of beam, μ the mass per unit length, E the elastic modulus and I the moment of inertia of the cross-sectional area. It is assumed that the boundary condition has not been affected by small variation of temperature. The relationship between natural frequencies and the geometry and the material properties change due to temperature variation can be expressed as (Xia et al. 2012):

$$\frac{\Delta f_n}{f_n} = -2\frac{\Delta l}{l} + \frac{1}{2}\frac{\Delta E}{E} + \frac{1}{2}\frac{\Delta I}{I} - \frac{1}{2}\frac{\Delta \mu}{\mu} \tag{4.2}$$

where Δ represents an increase or decrease in the corresponding parameters.

With the thermal coefficient of linear expansion of the material, θ_T, and the thermal coefficient of modulus, θ_E, then the relationship can be written below:

$$\frac{\Delta l}{l} = \theta_T \Delta T \tag{4.3}$$

$$\frac{\Delta E}{E} = \theta_E \Delta T \tag{4.4}$$

$$\frac{\Delta I}{I} = 4\theta_T \Delta T \tag{4.5}$$

$$\frac{\Delta \mu}{\mu} = -\theta_T \Delta T \tag{4.6}$$

The linear thermal expansion coefficient, θ_T, and the modulus thermal coefficient, θ_E, of steel (Brockenbrough and Merritt 1999) are $1.1\times10^{-5}/°\text{C}$ and $-3.6\times10^{-4}/°\text{C}$,

respectively. Concrete (MC90 1993) are $1.0\times10^{-5}/℃$ and $-3.0\times10^{-3}/℃$ for θ_T and , θ_E, respectively.

4.4.2 Modal Scaling Factor based on Temperature Variations

When the stiffness of a cantilever beam with the fixed support is considered, the stiffness coefficient, k, in beam element stiffness is:

$$k = \frac{EI}{l^3} \tag{4.7}$$

when there is temperature change, elastic modulus, E and moment of inertial, I will change accordingly. The following equation can be expressed to temperature changes:

$$\frac{\Delta k}{k} = -3\frac{\Delta l}{l} + \frac{\Delta E}{E} + \frac{\Delta I}{I} = (\theta_E + \theta_T)\Delta T \tag{4.8}$$

When the mass of a beam is considered,

$$m = \mu\times l \tag{4.9}$$

The following relationship can be obtained:

$$\frac{\Delta m}{m} = \frac{\Delta l}{l} + \frac{\Delta \mu}{\mu} = 0 \tag{4.10}$$

As seen in Eq. 4.10, the increase in the length and decrease in the unit weight can even out the change of mass due to the change of temperature. Therefore, only stiffness change due to temperature change should be considered. Eq. 4.8 can be written as:

$$\frac{\Delta k}{k} = \theta_k \Delta T \tag{4.11}$$

where $\theta_k = (\theta_E + \theta_T)$ defines as thermal coefficient of stiffness. For steel the value of θ_k can be calculated to have a value of $-3.49\times10^{-4}/℃$ and for concrete the thermal coefficient of stiffness has a value of $-2.99\times10^{-3}/℃$. Eq. 3.29 provided the modal scaling factor based on stiffness change as follows:

$$\alpha_4 = \sqrt{\frac{(\omega_4^2 - \omega_0^2)}{\{\psi\}^T[\Delta k]\{\psi\}}} \tag{4.12}$$

where ω_4 is the frequency of temperature modified structure. Plugging the Eq. 4.11 into Eq. 4.12, the equation can be rewritten as:

$$\alpha_4 = \sqrt{\frac{(\omega_4^2 - \omega_0^2)}{\{\psi\}^T \boldsymbol{K}\theta_k \Delta T\{\psi\}}} \tag{4.13}$$

Using the relationship between $\boldsymbol{K}$ and $\boldsymbol{M}$**:**

$$\boldsymbol{M} = \frac{\boldsymbol{K}}{\omega_0^2} \tag{4.14}$$

The equation can be expressed as:

$$\alpha_4 = \sqrt{\frac{(\omega_4^2 - \omega_0^2)}{\{\psi\}^T \omega_0^2 \boldsymbol{M}\theta_k \Delta T\{\psi\}}} \tag{4.15}$$

considering orthogonality of mode shapes,

$$\alpha_4 = \sqrt{\frac{(\omega_4^2 - \omega_0^2)}{\omega_0^2 \theta_k \Delta T}} \tag{4.16}$$

or

$$\alpha_4 = \sqrt{\frac{(\omega_4^2 - \omega_0^2)}{\omega_0^2(\theta_E + \theta_T)\Delta T}} \tag{4.17}$$

The proposed method provides a non-contact approach for modal scaling. No additional mass or stiffness is needed to attach to structures. When temperature distribution is monitored, the temperature change at any location can be used to calculate scaling factor. In addition, dynamic characteristic change due to temperature change has already been considered in modal scaling process, that false damage detection based on dynamic characteristics change due to temperature variation can be avoided. Numerical simulation and verification of this method are presented in the following Chapters. The process of the algorithms is similar to them presented in Figure 4.2, only the McMS is replaced by TcMS as shown in Figure 4.3.

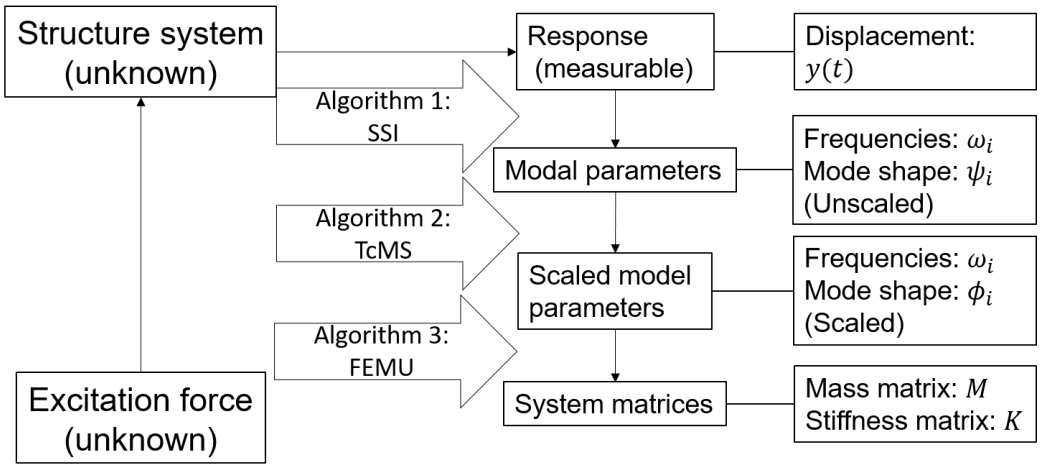

Figure 4.3. Scope of Damage Detection Method with TcMS

TcMS is used to obtain the scaled mode shapes. Then, mass and stiffness updated form FEMU are used as damage indicator. The detail simulation to show the applicability of the proposed method is presented in Chapter 5.

CHAPTER 5

NUMERICAL SIMULATION

In this Chapter, numerical simulation are provided to: 1) verify the proposed damage identification algorithm proposed on beam structure, 2) validate the proposed TcMS method, 3) verify the proposed damage identification algorithm integrate with TcMS in truss structure.

Numerical models are used to verify the feasibility and applicability of the proposed algorithm and damage identification method. Finite element method was used to obtain the discrete-time deflection as the input of the damage identification algorithm. The frequencies and their corresponding mode shapes were used to verify the extracted frequencies and mode shapes from proposed algorithms. Two cases are considered in this study. In the first case, a four-story steel frame structure is used as a model to verify the proposed damage identification algorithm. In this case, the effects of different loading types and noise levels in the response are evaluated for verifying the applicability of the proposed algorithms (SSI, McMS, and FEMU). In the second case, a truss structure is used to verify the algorithm with TcMS method. The application of TcMS method is examined with varies temperatures. In this process, the non-contact concept is developed in the whole process of damage assessment.

5.1 Numerical Simulation (Case 1)

A numerical simulation is presented in this section for the verification of proposed algorithm that used to determine mass and stiffness matrices to identify damages. A theoretical model of a four-story steel frame structure system is used and is shown in Figure 5.1.

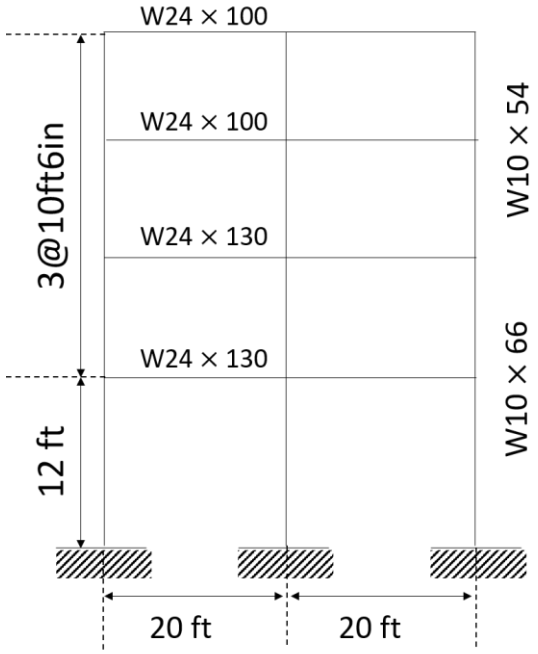

Figure 5.1. Numerical Simulation Example (Naeim 1989)

The horizontal displacement of each story is used as the input of the algorithm, Thus, this four-story frame can be treated as an equivalent spring-mass-damper system as shown in Figure 5.2.

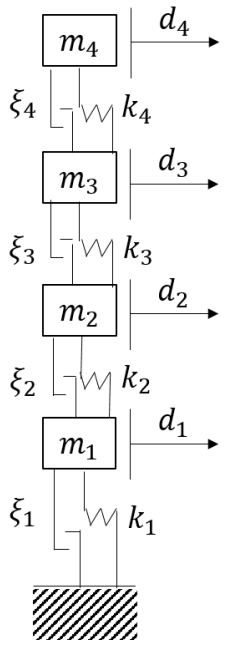

Figure 5.2. Equivalent Spring-Mass-Damper System

Each story is lumped into mass, m_i, stiffness, k_i, and damping ratio ξ_i. And d_i is the horizontal displacement of each story. The steel frame structure can be modeled using multi-degree of freedom system (4 degrees of freedoms [4DOFS]).

To verify the applicability of the proposed damage identification algorithms using only information of output responses, three aims are established: 1) to analyze the effects of different types of excitation, 2) to analyze the sensitivity of this method under different levels of noises of the responses, 3) to analyze damage detection capability to identify different levels of change in mass and/or stiffness. Both damped and undamped system were considered in this study.

5.1.1 Simulation Considerations

In the case of the 4-story frame, the simulation considerations are as follows:

(1) Effects of different loading types: In this phase, both damped and undamped system are analyzed with different loading types. The accuracy of SSI in various of loading types are validated.

(2) Effects of noise levels: Different level of noise is added on the displacement to analyze the influence of noise to dynamic characteristics extraction.

(3) Application of McMS method: After the validation of SSI under different loading types and noise levels, constant forced loading type with 5% of noise level added on displacement is used for modal scaling. McMS is used to obtain the scaled mode shapes.

(4) Application of FEMU method: Different levels of changes in mass and stiffness are simulated in this step to validate the capability of proposed damage detection method for identifying locations and levels of damage.

5.1.1.1 Effects of Different Loading Type

Different types of loading have been used to generate the displacements of each node over time. Both undamped and damped systems under different loading types are considered. Different types of loading are shown in Table 5.1.

Table 5.1. Loading Types for Numerical Simulation

System	Loading Type		
Undamped	Free Vibration	Constant Force	Short Duration of Air Blast
Damped	Constant Force	Triangular Impulse	Sine Wave

For the undamped system, the structure has the free vibration with the initial displacement ($t = 0$) of 9, 7, 5, and 5 in. At each story from roof level (d_4 in Figure 5.2) to the floor level (d_1 in Figure 5.2). Second and third scenarios are: (a) constant force and (b) air blast as shown in Figure 5.3 (a) and (b).

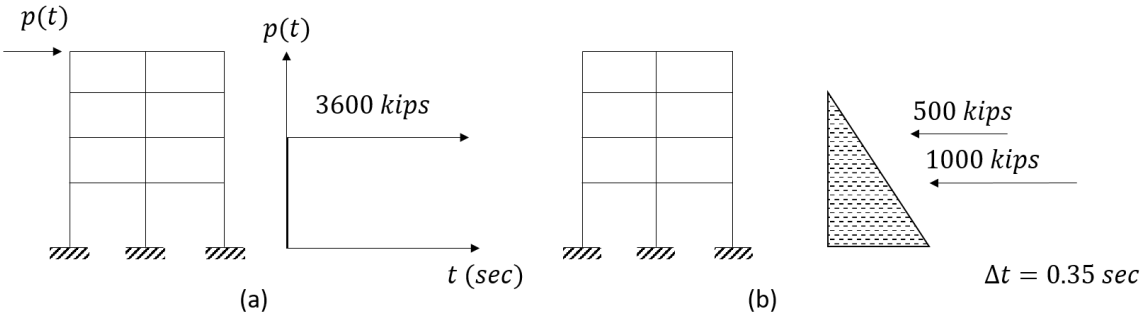

Figure 5.3. Different Loading Type: Undamped System
(a) Forced vibration; (b) Air blast

In Figure 5.3 (a) the roof level has the constant force, $p(t)$. In Figure 5.3 (b), the structure is subjected to the air blast load for 0.35 seconds.

Different loading types for damped systems are shown in Figure 5.4 (a), (b) and (c).

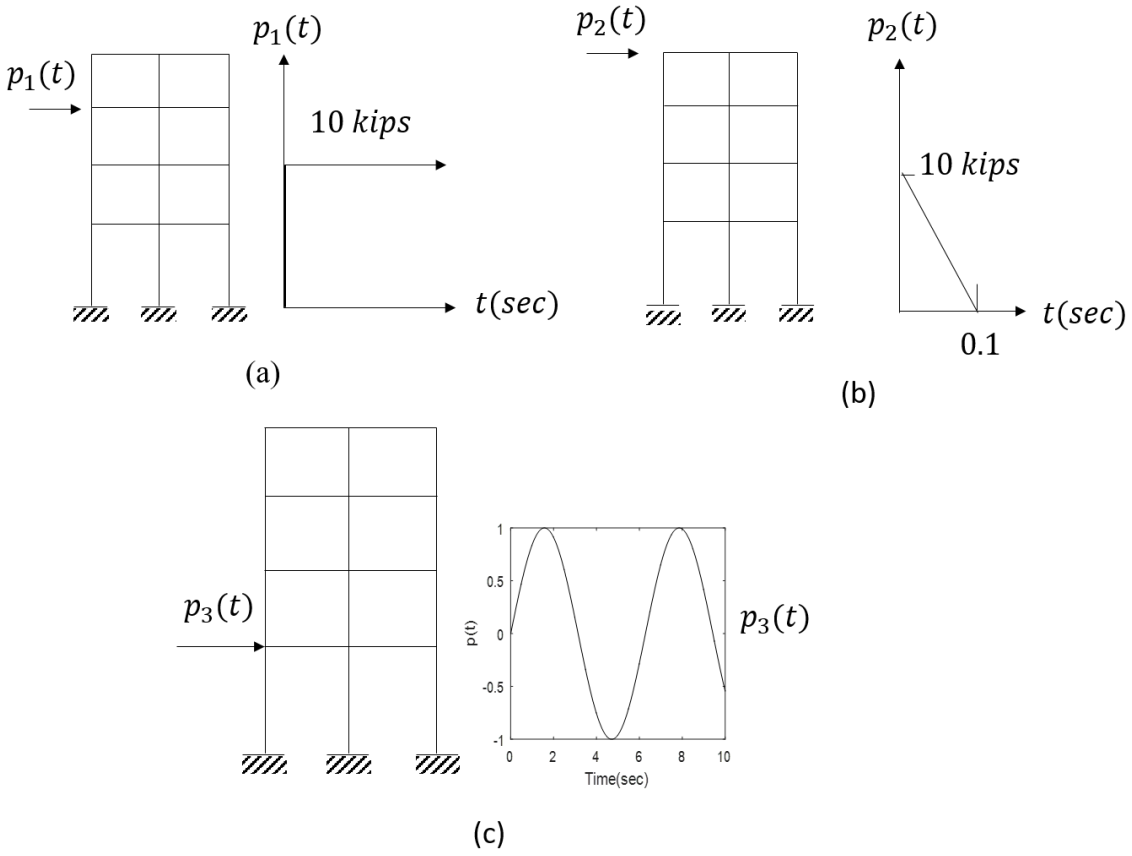

Figure 5.4. Different Loading Types: Damped System:
(a) Constant force; (b) Triangular impulse; (c) Sine wave

Figure 5.4 (a) shows a constant force, $p_1(t)$, that is applied at the third story (d_3), Figure 5.4 (b) shows that the roof story (d_4), that is subjected to a horizontal triangular impulsive force, $p_2(t)$. Figure 5.4 (c) shows the application of sine wave, $p_3(t)$ on the first story (d_4). In multi-degrees of freedom (MDOF) system, the proportional damping is assumed in the mode as:

$$\boldsymbol{C} = \alpha \boldsymbol{M} + \beta \boldsymbol{K} \tag{5.1}$$

where α and β are constants. In this simulation, α is assigned to be 0 and β is assigned as 0.01. Then the assumed damping ratio of each story is obtained as shown in Table 5.2.

Table 5.2. Damping Ratio of Each Story

Damping Ratio				
Story	1	2	3	5
ξ value	0.0045	0.0125	0.0199	0.0244

Figures 5.5 shows the time history of displacements of all the loading scenarios for the undamped system. Sampling frequencies for each scenario are the same as 100 Hz.

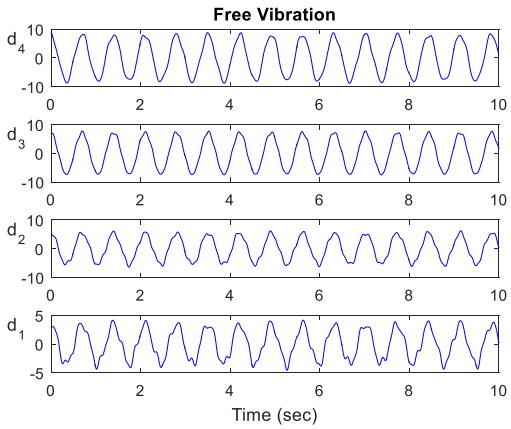

(a) Free Vibration

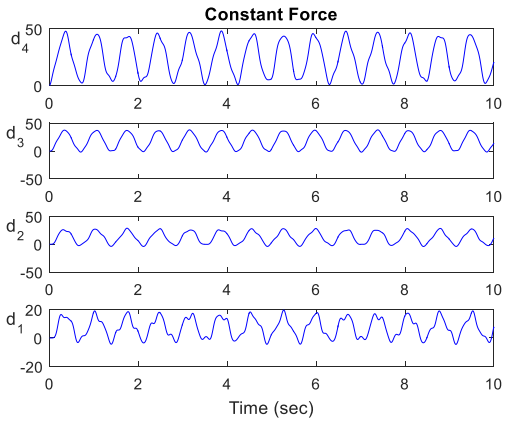

(b) Constant Force

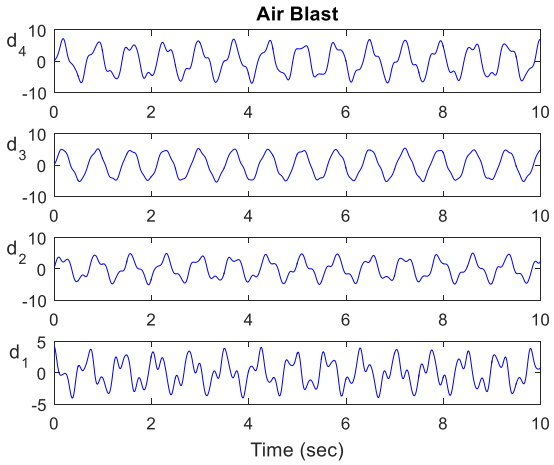

(c) Air Blast

Figure 5.5. Displacements of Undamped System (unit: *in.*)

Figures 5.6 shows the time history of displacements of all the loading scenarios for the damped systems. Sampling frequencies for each scenario are the same as 100 Hz. Duration

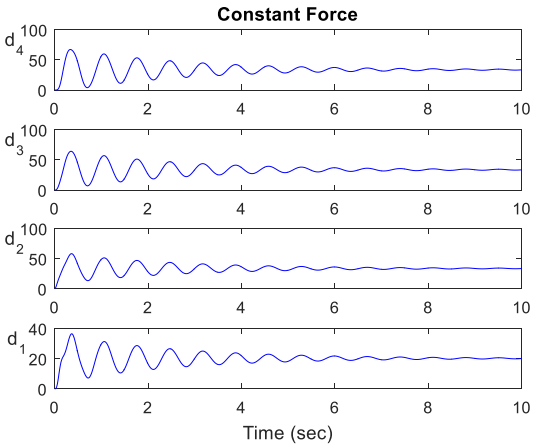

(a) Constant Force

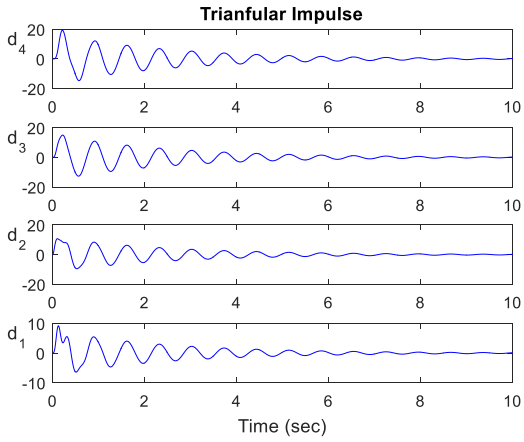

(b) Triangular Force

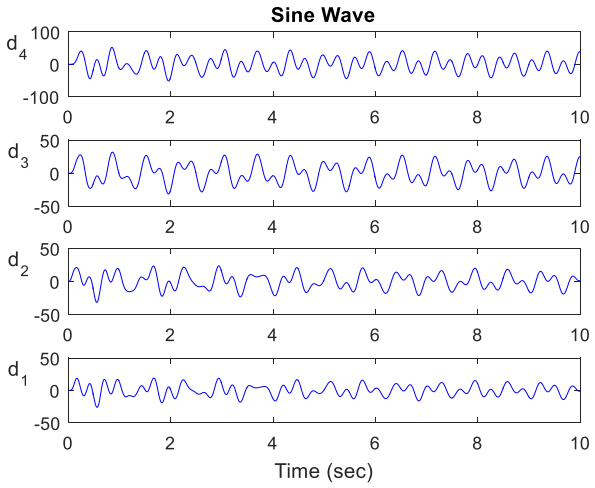

(c) Sine Wave

Figure 5.6. Displacement of Damped System (unit: *in.*)

5.1.1.2 Effects of Noise Level on SSI Accuracy

Generally, the source of noise is random and usually unknown. To analyze the effect of random noise on the extracting dynamic characteristics, different levels of noise are artificially added in the response of the structure under constant loading to simulate the ambient noises. The noise range is from 5% to 125% of the max amplitude of responses (see Table 5.3).

Table 5.3. Noise Level Added on Vibration Response

Levels of Noise on Response (Maximum Amplitude)					
5%	25%	50%	75%	100%	125%

Figure 5.7 shows the noise level of 5% of the maximum amplitude of responses is added to the displacements of each story. Figure 5.8 shows the displacement d_1 with 5% noise addition.

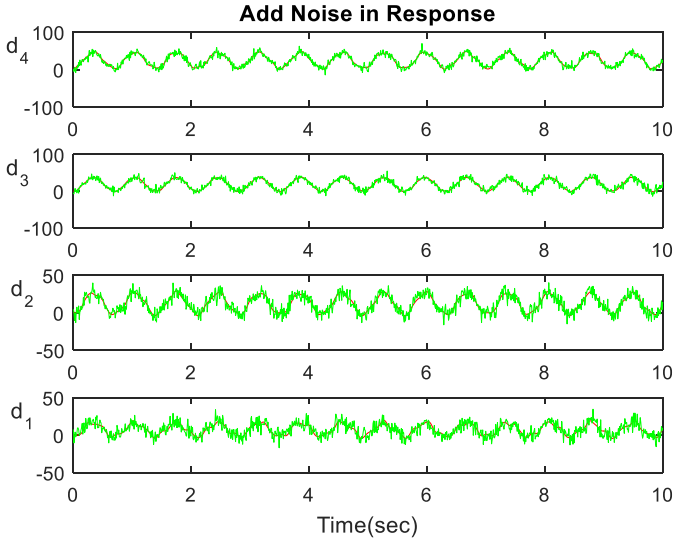

Figure 5.7. Add 5% Noise in Response for All Stories (unit: *in.*)

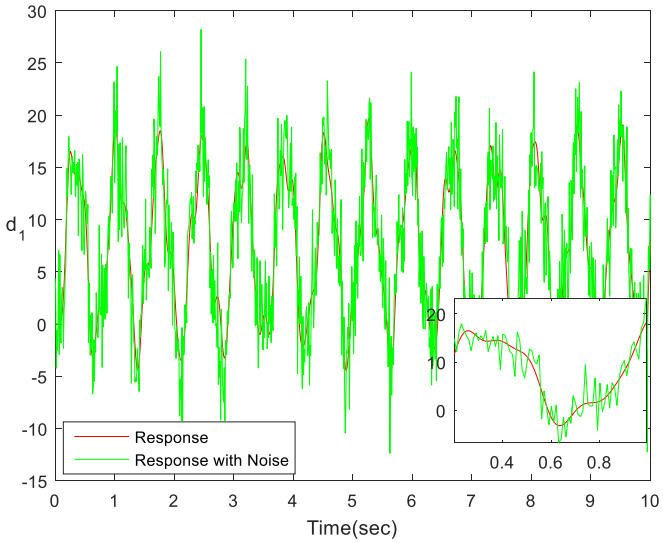

Figure 5.8. Add 5% Noise in Response on Floor Story (unit: *in.*)

5.1.1.3 Damage Scenario Simulation

When damages were existing in structure, the magnitude of mass and stiffness changed from original mass and stiffness (baseline). Figure 5.9 shows the location of damage in mass and stiffness of the element. Table 5.4 shows the levels of change ranging from 5 to 20% of original mass, m_3. Similarly, the change of stiffness was varied from 5 to 20% of the original stiffness, k_4.

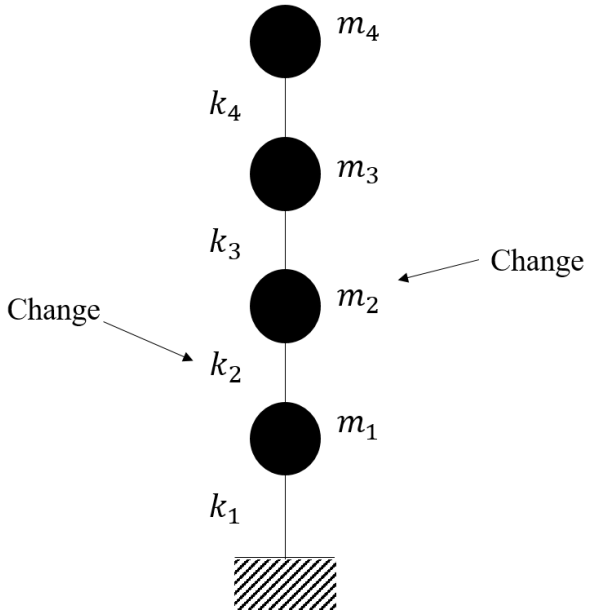

Figure 5.9. Damage Location of Element

Table 5.4. Different Levels of Damages of m_3 and k_4

Damage Levels and Types					
Reduction of Mass			Reduction of Stiffness		
20%	10%	5%	20%	10%	5%

The results of the damage detection are presented in the following section.

5.1.2 Simulation Result (Case 1)

In this section, simulation results are presented:

1) Dynamic characteristics of both damped and undamped system under different loading types are extracted from SSI;
2) Results of SSI extracted dynamic characteristics with different levels of noise added on displacements;
3) Applicability of McMS method;
4) Applicability of FEMU in different damage scenarios.

5.1.2.1 Effects of Different Loading Types

Using displacements acquired from FEA estimation, SSI algorithm is used to extract dynamic characteristics (i.e., frequencies, mode shapes and damping ratios). The frequencies for the undamped systems extracted from the time history of displacements using SSI are shown in Table 5.5.

Table 5.5. SSI Extracted Frequencies (Undamped System) (unit: Hz)

Modes	FEA	Loading Types		
		Free Vibration	Constant Force	Air Blast
1	8.94	8.94	8.94	8.94
2	25.03	25.03	25.03	25.03
3	39.93	39.93	39.93	39.93
4	48.75	48.75	48.75	48.75

Note: FEA value is calculated by Finite Element Model Analysis and is not related to SSI.

Table 5.5 shows the same results with those from the FEA estimation. Equation 5.1 shows the ratio of the difference between each frequency and that of the FEA estimation.

$$DR_{\omega i} = \frac{\omega_{i\_FEA} - \omega_{i\_SSI}}{\omega_{i\_FEA}} \tag{5.1}$$

where ω_{i_FEA} is frequency of ith mode calculated from FEA, ω_{i_SSI} is frequency of ith mode extracted from SSI. The difference ratio of each method for each mode is shown in Figure 5.10.

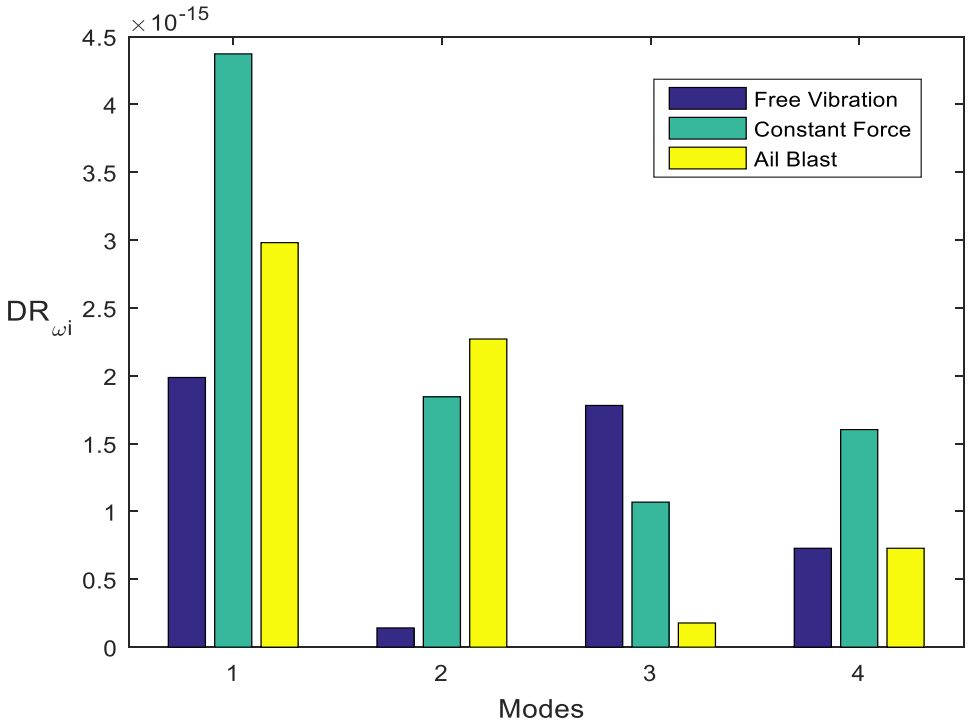

Figure 5.10. $DR_{\omega i}$ of SSI Extracted Frequencies (Undamped System)

Figure 5.10 shows an unobvious pattern of frequencies regarding the modes or types of loading. Because the difference ratio is smaller than 10^{-14}, they are negligible and

meaningless. The results indicate that SSI can accurately extract the frequencies of the undamped system under different excitation scenarios.

Mode shapes are extracted using SSI as well. MAC values between extracted mode shapes and FEA are listed in Table 5.6.

Table 5.6. MAC Value from SSI (Undamped System)

Modes	Loading Types		
	Free Vibration	Constant Force	Air Blast
1	1	1	0.9765
2	1	1	0.8701
3	0.9998	1	0.8254
4	0.9990	1	0.9834

Both frequencies and MAC indicate that SSI can accurately extract the dynamic characteristics with the output response only. However, the 2nd and 3rd modes of air blast yield lower than the acceptable range of MAC value which is a minimum threshold value of 0.95. The frequencies of damped system extracted from displacements using SSI are shown in Table 5.7.

Table 5.7. SSI Extracted Frequencies (Damped System)

Modes	FEA	Loading Type		
		Constant Force	Triangular Force	Sine Wave
1	8.94	8.94	8.94	8.94
2	25.03	25.04	25.04	25.04
3	39.89	39.89	39.89	39.89
4	48.75	48.77	48.75	48.76

Note: FEA value is calculated by Finite Element Model Analysis and is not related to SSI.

It is shown that higher discrepancy in damped system frequencies than in undamped system. Eq. 5.1 is used to calculate the difference ratio between SSI extracted frequencies and FEA calculated frequencies for the damped system. The results are shown in Figure 5.11.

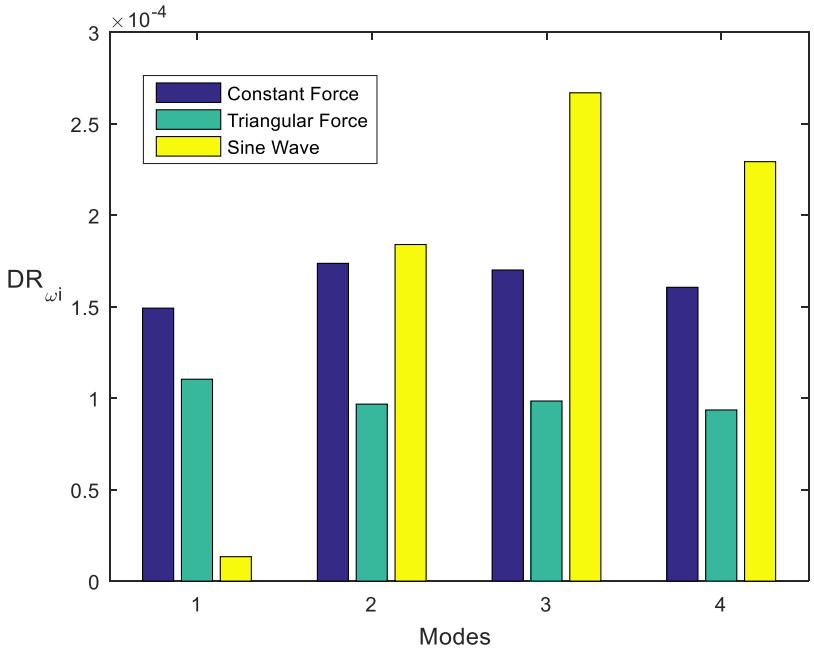

Figure 5.11. $DR_{\omega i}$ of Frequencies (Damped System)

Even through the $DR_{\omega i}$ from damped system is higher than undamped system, the errors are still small enough to be neglected. The results indicate that SSI can accurately extract the frequencies of the damped system under different excitation scenarios. Mode shapes are extracted using SSI as well. MAC value between extracted mode shapes and that of FEA estimation are listed in Table 5.8.

Table 5.8. MAC Value from SSI (Damped System)

Modes	Loading Types		
	Constant Force	Triangular Force	Sine Wave
1	1	1	1
2	1	1	1
3	0.9925	0.9997	0.9948
4	0.9941	0.9998	0.9973

Results indicate that SSI algorithm can accurately extract the frequencies and mode shapes. The MAC values are all above 0.95. This indicates that the mode shapes obtained from SSI are highly correlated with mode shapes estimated from FEA.

In the damped system, damping ratio is another dynamic characteristic that can be extracted using SSI. Table 5.9 shows the damping ratios extracted from SSI.

Table 5.9. Damping Ratio Extracted from SSI

Modes	FEA	Loading Types		
		Constant Force	Triangular Force	Sine Wave
1	0.0045	0.0045	0.0045	0.0045
2	0.0125	0.0126	0.0126	0.0126
3	0.0199	0.0200	0.0200	0.0200
4	0.0244	0.0244	0.0244	0.0243

Note: FEA value is calculated by Finite Element Model Analysis and is not related to SSI

Table 5.9 shows that damping ratio extracted from SSI is very close to the value calculated from FEA. The ratio of difference in damping ratios between SSI estimation and FEA estimation, DR_{ξ_i} , is calculated from Eq. 5.2.

$$DR_{\xi_i} = \frac{\xi_{i\_FEA} - \xi_{i\_SSI}}{\xi_{i\_FEA}} \tag{5.2}$$

where ξ_{i_FEA} is damping ratio of ith mode calculated form FEA and ξ_{i_ssi} is damping ratio of ith mode extracted form SSI. Figure 5.12 shows $DR\xi_i$ for four modes under different force types.

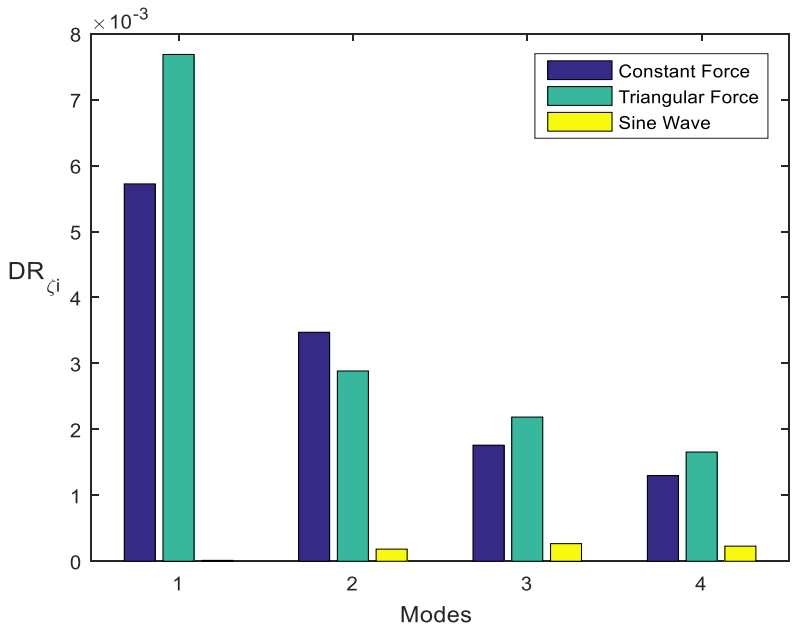

Figure 5.12. $DR_{\xi i}$ of Damping Ratio

It can be observed that the constant force and triangular force excitation had the reduction of the error of damping ratio extracted from SSI as the mode increases. For the sine wave scenario, the error of damping ratio is relatively small. For different scenarios, the error of extracted damping ratio is small enough to be neglected.

5.1.2.2 Effects of Noise Level on SSI

Frequencies of each scenario with different levels of noise added on responses are extracted from SSI. The values of $DR_{\omega i}$ of frequencies extracted from SSI are calculated using Eq. 5.1 (see Figure 5.13).

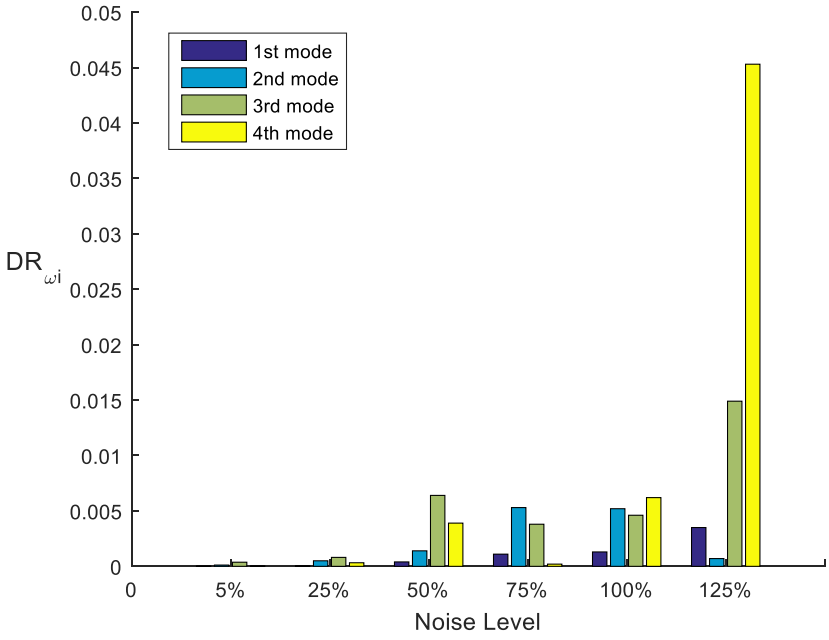

Figure 5.13. $DR_{\omega i}$ with Different Level of Noise Added

Figure 5.13 shows that the higher level of noise leads to increase the error in natural frequencies. When noise level is below 100%, the changes in frequencies is less than 1% (0.01 in $DR_{\omega i}$). However, the noise reaches at 125%, the $DR_{\omega i}$ value of 3rd mode exceeds 1% (0.01 in $DR_{\omega i}$), Furthmore, the value of $DR_{\omega i}$ of 4th mode exceeds 4% (0.04 in $DR_{\omega i}$). A level of noise below 100% of the max amplitude of response still yielded with a high accuracy in frequencies extracted from SSI.

MAC values between FEA and SSI extracted for each mode with varying noise levels are presented in Figure 5.14.

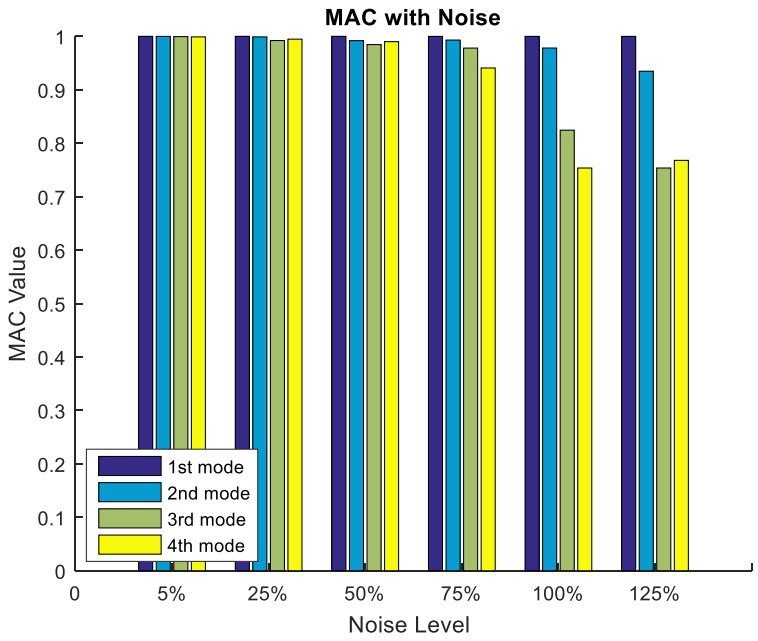

Figure 5.14. MAC Value between FEA and SSI with Varied Noise Levels

When the noise levels increase, the higher mode shapes decrease in MAC value (See Figure 5.14). The lower modes are not affected by the noise as much as higher modes. The results of mode shapes extracted from SSI is acceptable when the noise level is below 75% of the max amplitude of the response.

5.1.2.3 Applicability of McMS Method

As an output-only modal analysis method, SSI only extracts the unscaled mode shape. For the higher level of SHM scheme, the scaled mode shape is required. McMS is used to demonstrate the applicability of modal scaling. Figure 5.15 shows the unscaled mode shapes of undamped system extracted from SSI with different types of loading. In each case, the noise of 5% is added on the response.

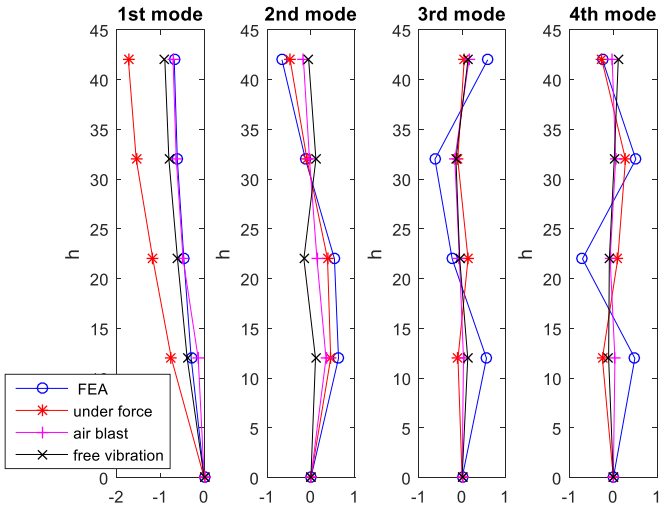

Figure 5.15. Unscaled Mode Shapes (h in ft)

The scaled mode shapes are presented in Figure 5.16.

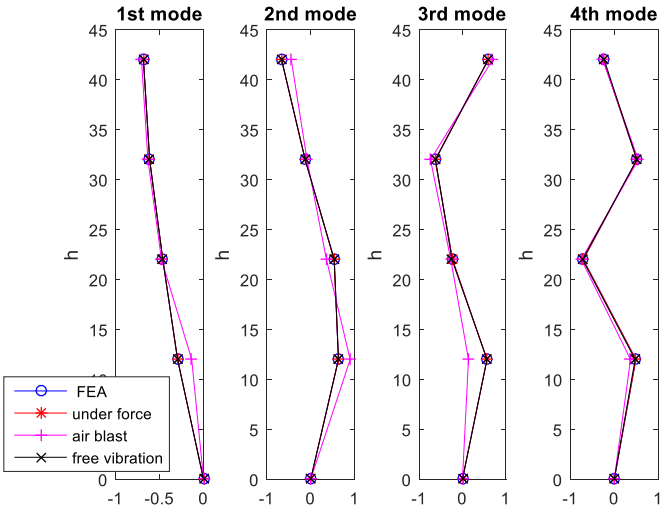

Figure 5.16. Scaled Mode Shape (h in ft)

Figure 5.16 shows the comparison of scaled mode shapes with FEA estimation for different loading cases. The case of air blast has higher discrepancy than free vibration and constant forced vibration, which is consistent with their MAC value (see Table 5.6). Figure

5.17 is the comparison between unscaled and scaled mode shapes of the undamped system under constant force with 5% noise level added in the response.

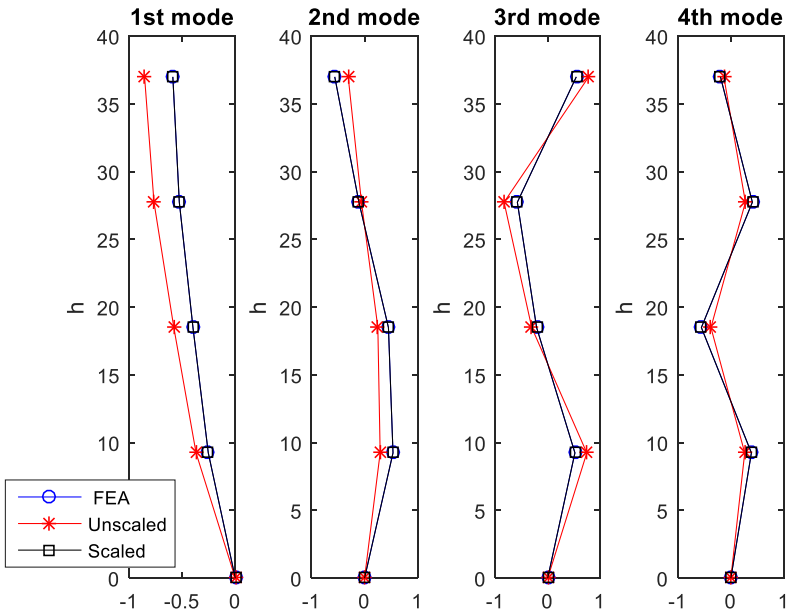

Figure 5.17. Comparison between Unscaled and Scaled Mode Shapes (h in ft)

Figure 5.17 shows unscaled and scaled mode shapes along with FEA mode shape. When the scaled mode is compared with the mode shape obtained from FEA, the scaled mode shape is almost identical to mode shapes of FEA. Therefore, McMS method is an efficient tool for modal scaling.

5.1.2.4 Damage Scenario Simulation (Applicability of FEMU Method)

In the 4 degrees of freedom system, the lumped mass and stiffness matrices are formed with element mass and stiffness as follows:

$$M = \begin{bmatrix} m_1 & & & \\ & m_2 & & \\ & & m_3 & \\ & & & m_4 \end{bmatrix} \text{ and } K = \begin{bmatrix} k_1 & -k_1 & & \\ -k_1 & k_1+k_2 & -k_2 & \\ & -k_2 & k_2+k_3 & -k_3 \\ & & -k_3 & k_3+k_4 \end{bmatrix}$$

Note: Voids in matrices are zeros.

The mass and stiffness matrices used in the numerical FEA model are:

$$M_{FEA} = \begin{bmatrix} 0.761 & & & \\ & 0.952 & & \\ & & 0.952 & \\ & & & 0.958 \end{bmatrix}$$

and

$$K_{FEA} = 10^{-3}\times \begin{bmatrix} 587.5 & -587.5 & & \\ -587.5 & 1175.5 & -587.5 & \\ & -587.5 & 1321.5 & -733.5 \\ & & -733.5 & 1225.5 \end{bmatrix}$$

Element mass and stiffness can be evaluated from the matrices.

With free vibration and 5% noise in the responses, the FEMU method updated the mass and stiffness of undamaged system as:

$$M_{FEMU\_HELATH} = \begin{bmatrix} 0.761 & & & \\ & 0.952 & & \\ & & 0.952 & \\ & & & 0.958 \end{bmatrix}$$

and

$$K_{FEMU\_HEALTH} = 10^{-3}\times \begin{bmatrix} 587.5 & -587.5 & & \\ -587.5 & 1175.5 & -587.5 & \\ & -587.5 & 1321.5 & -733.5 \\ & & -733.5 & 1225.5 \end{bmatrix}$$

The error of updated mass matrix is calculated as:

$$Error_m = \frac{M_{FEA} - M_{FEMU\_HELATH}}{M_{FEA}} \tag{5.3}$$

Since the values of matrix elements are identical in Eqs. 5.2 and 5.3, the difference between M_{FEA} and M_{FEMU_HELATH} can be only observed at the level of 10^{-14}. Figure 5.18 shows the error of updated mass of the baseline (i.e. healthy condition) campare with FEA mass matrix.

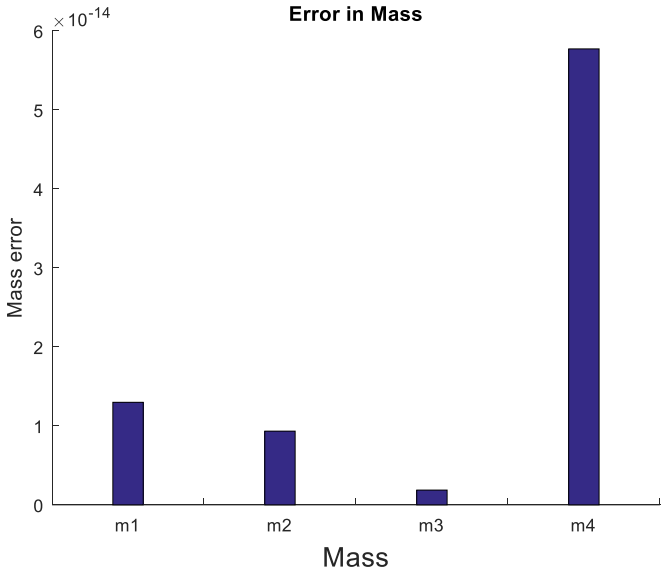

Figure 5.18. Mass Error of FEMU

As seen in Figure 5.18, errors of mass elements are too small to be neglected.

The proposed FEMU is to combine two methods: Berman and Nagy (1983) and Baruch (1978). The proposed method is to update stiffness and mass matrices using Berman and Nagy (1983) method and update stiffness using Baruch (1978). Thus, the stiffness is updated twice.

$$Error_k(FEMU1) = \frac{K_{FEA} - K_{FEMU1\_HELATH}}{K_{FEA}} \tag{5.4}$$

$$Error_k(FEMU2) = \frac{K_{FEA} - K_{FEMU2\_HELATH}}{K_{FEA}} \tag{5.5}$$

where K_{FEMU1_HELATH} is the updated stiffness matrix using Berman and Nagy (1983) method only and K_{FEMU2_HELATH} is the updated stiffness matrix using proposed method (combination of Berman and Nagy (1983) and Baruch (1978)). Figure 5.19 shows the error of the updated stiffness with FEMU1 (only Berman and Nagy (1983)) and FEMU2 (proposed method).

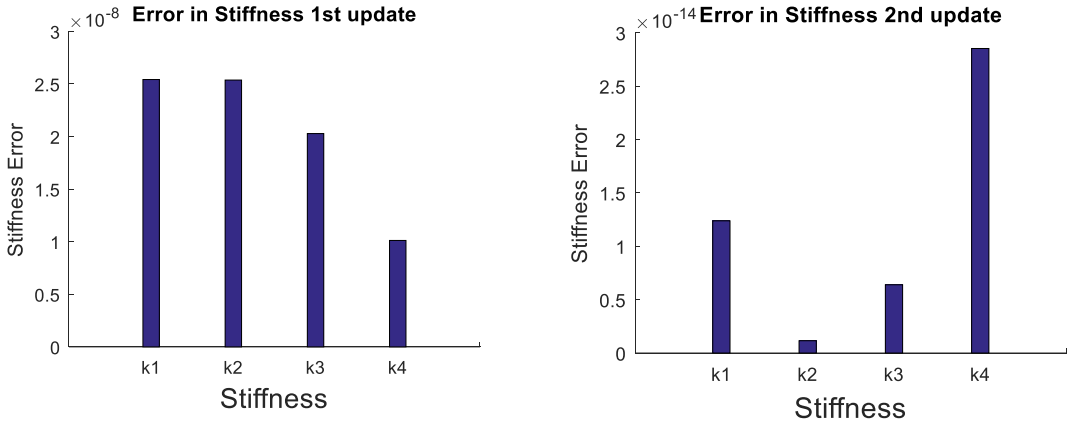

(a) Error of K_{FEMU1} (b) Error of K_{FEMU2}

Figure 5.19. Stiffness Error of FEMU

Because there is no damage in elements, the estimation leads to almost zero of error as shown in Figure 5.19. The stiffness error obtained from FEMU and the FEA estimation are small enough to be neglected for both methods. However, the proposed methods have substantial improvements in the accuracy. For example, the element k_1 has the error of

2.5×10^{-8} using FEMU1, while the same element has the error of 1.7×10^{-14} using FEMU2.

When there is different level of the reduction of m_4, displacement of damaged structure can be obtained from FEA and SSI can extract the dynamic characteristics. After scaling the mode shapes, the mass and stiffness of the damaged structure can be analyzed using FEMU2. The change ratio of mass (CR_m) can be calulcated using Eq. 5.6:

$$CR_m = \frac{M_{FEMU2\_HELATH} - M_{FEMU2\_DAMAGED}}{M_{FEMU2\_HEALTH}} \tag{5.6}$$

where M_{FEMU2_HELATH} is the updated mass matrix of baseline (undamaded structure) and $M_{FEMU2\_DAMAGED}$ is the updated mass matrix of damaged structre. When m_4 has reduction of 20%, 10% and 5%, the reduction of FEMU mass mattices are shown in Figure 5.20.

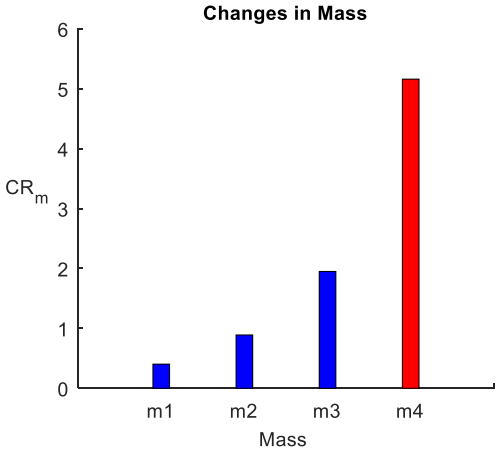

(a) Reduction of 5% in m_4

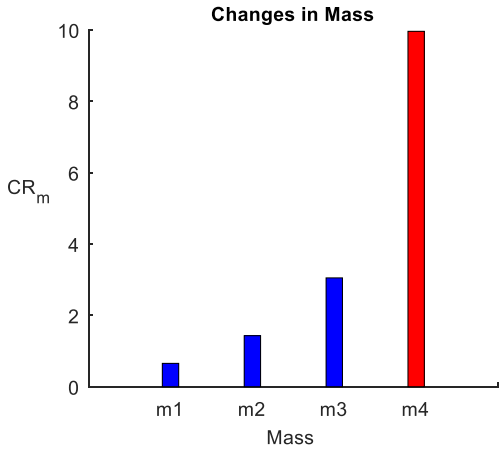

(b) Reduction of 10% in m_4

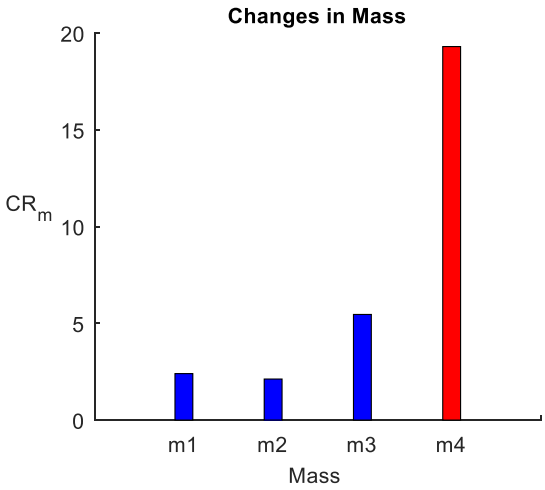

(c) Reduction of 20% in m_4

Figure 5.20. FEMU Estimation of the Reduction of Mass

Figure 5.20 shows that the proposed damage detection method can locate the damages element with quantifying the magnitude of mass change.

When k_2 has the reduction of 20%, 10% and 5%, the estimation of FEMU to quantify the reduction of stiffness are shown in Figure 5.21.

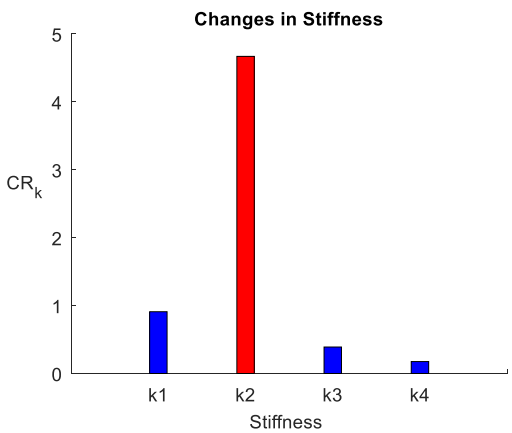

(a) Reduction of 5% in k_2

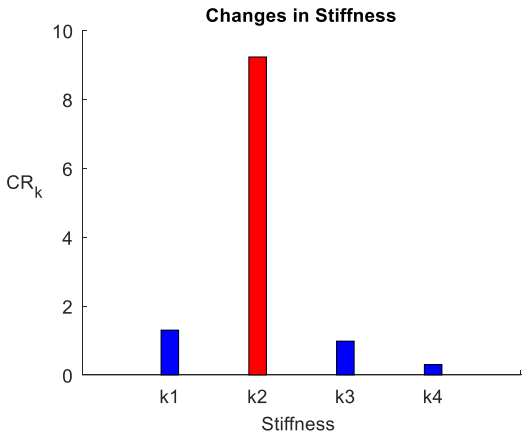

(b) Reduction of 10% in k_2

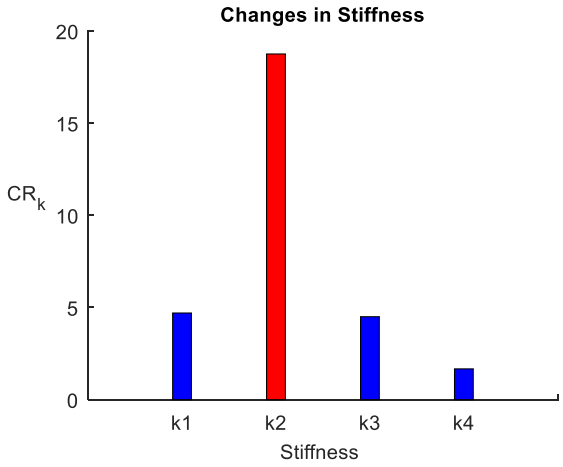

(c) Reduction of 20% in k_2

Figure 5.21. FEMU Estimation of the Reduction of Stiffness

Table 5.10 shows the comparison of the quantified damage levels (% reduction) in mass and stiffness using FEMU method and the target estimation.

Table 5.10. FEMU Results for Estimating Damages

Targets	Reduction of Mass (Δm_3)			Reduction of Stiffness (Δk_4)		
In model	20%	10%	5%	20%	10%	5%
FEMU	18.35%	9.96%	5.16%	18.75%	9.23%	4.67%

Generally, the prediction accuracy is within 2% of both mass and stiffness. When there are both mass and stiffness changes occurred in the structure at different locations, the proposed method can detect the damage location and severity. Figure 5.21 shows the prediction of mass and stiffness reduction of all elements when there is the reduction of 10% in m_3 and the reduction of 20% in k_4.

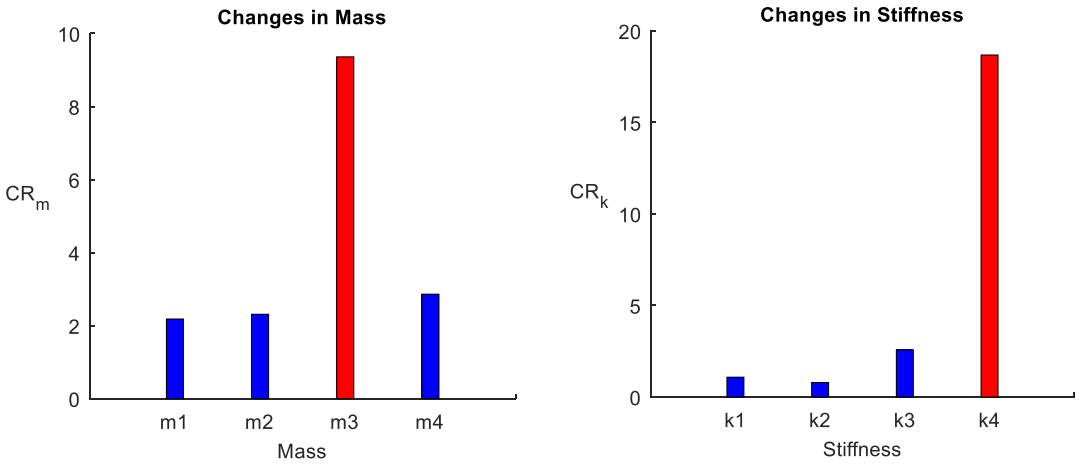

(a) (b)

Figure 5.22. FEMU for Mass and Stiffness Change Level and Location

There are some errors in other elements where there is no reduction of mass and stiffness. There are about the reduction of 2% in other elements that are the false estimations. Higher errors appear in the element closest to the damaged element. FEMU can reasonably update the stiffness and mass matrices as well as detect the location and level of changes in the matrices. Figure 5.22 shows that there are some errors in other elements. FEMU is a mathematic process to search for the approximate solution. When damage level of the particular element is small, the errors relatively tends to be small. However, the changes in other elements are relatively small compared to the damaged element. Even through the proposed method is applicable to identify and quantify the changes of elements, the contact is required to scale the modes.

5.2 Numerical Simulation for TcMS

The 4-story frame is used here to verify the proposed TcMS method. The temperature of structure can increase or decrease from the initial temperature measured

resulting in the change of responses. In Section 5.2.1, the temperature change of structure is the same regardless the locations. Ideally, the mass and stiffness of structure are changed uniformly due to the temperature change. In reality, the temperature change of structure is non-uniform. The varied change of temperature in mass and stiffness are considered in Section 5.2.2.

5.2.1 TcMS with Uniform Temperature Change over Structure

The scaled mode shape can be obtained from two sets of structural response with different temperature. The temperature and stiffness are correlated. The increase of temperature leads to reduce the stiffness, while the reduction of temperature tends to increase the stiffness of the structure. When the temperature changes were assumed to be uniform over the entire structure, the effects of varied temperature are studied with the range of ± 10 ℃ as shown in Table 5.11. A total of 8 cases is considered in this study except for the baseline ($\Delta T = 0$℃).

Table 5.11. Scenarios of Temperature Change Uniformly over Structure

Temperature Change (ΔT)								
-10 ℃	-7 ℃	-5 ℃	-2 ℃	0 ℃	2 ℃	5 ℃	7 ℃	10 ℃

Displacements of the structure with temperature changes are generated from FEA model subjected to a free vibration with the addition of 5% noise on the response. SSI is used to extract frequencies and mode shapes. Frequencies with 8 scenarios are shown in Figure 5.22 and Table 5.12.

Table 5.12. Frequencies of Structure with Uniform Temperature Change

	Frequencies with ΔT								
ΔT	-10 ℃	-7 ℃	-5 ℃	-2 ℃	0 ℃	2 ℃	5 ℃	7 ℃	10 ℃
1	8.95	8.95	8.95	8.94	8.94	8.94	8.93	8.93	8.92
2	25.07	25.06	25.05	25.04	2 5.03	25.03	25.01	25.00	24.99
3	39.95	39.93	39.92	39.90	39.89	39.87	39.86	39.84	39.82
4	48.83	48.80	48.79	48.77	48.75	48.73	48.71	48.69	48.67

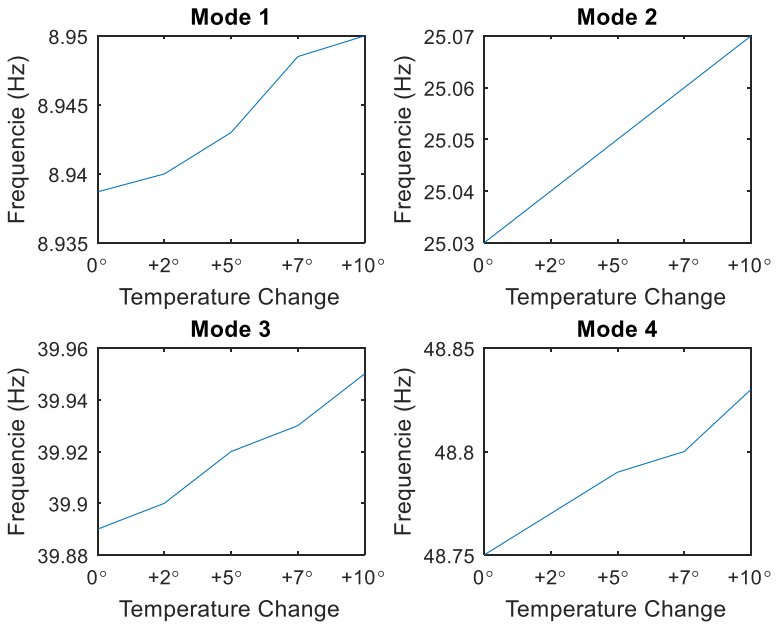

(a) Frequency Changes with Temperature Decrease

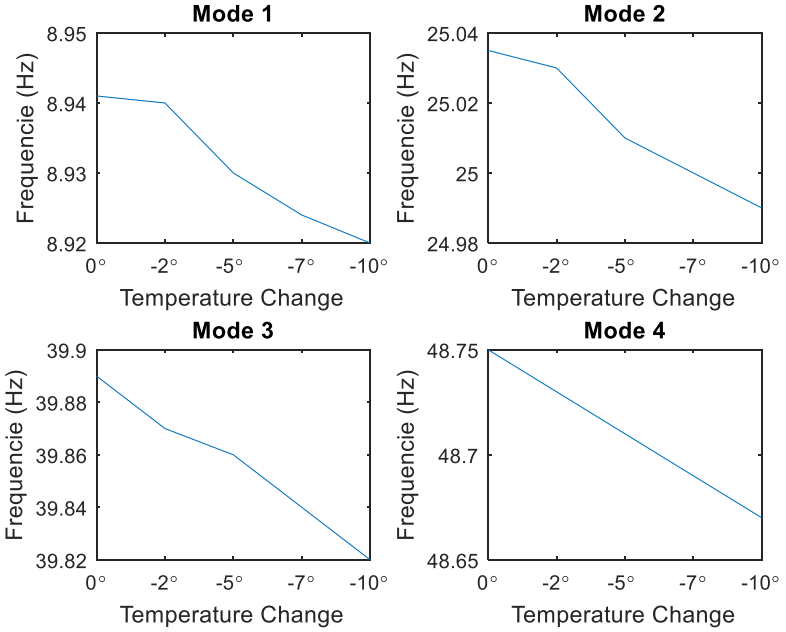

(b) Frequency Changes with Temperature Increase

Figure 5.23. Frequency Changes with Varied Temperatures

Table 5.12 and Figure 5.23 show frequency increase or decrease due to temperature change. As expected, the change of temperature has minimal changes in frequency. Larger

changes in frequencies are shown in higher modes. However, it is less than 0.2%. With frequencies and mode shapes extracted from SSI, Eq. 4.17 is used to obtain the scaled mode shapes. The unscaled mode shape scaled mode shapes of 8 scenarios are shown in Figure 5.24.

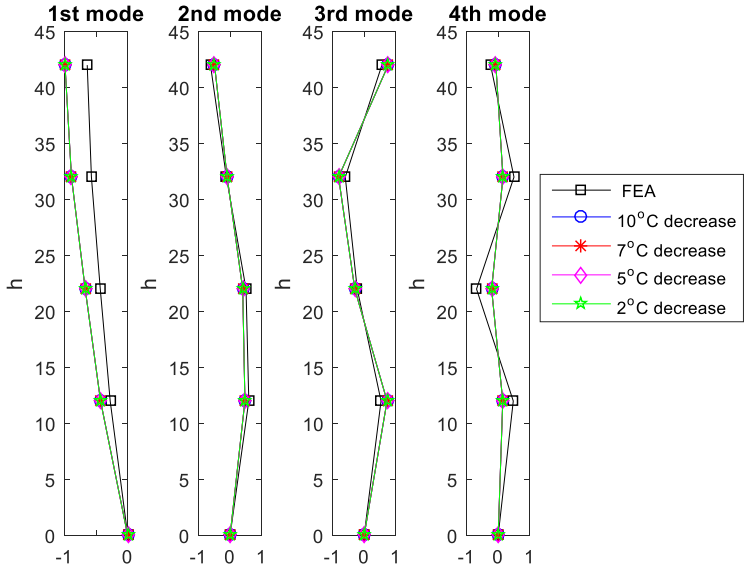

(a) Unscaled

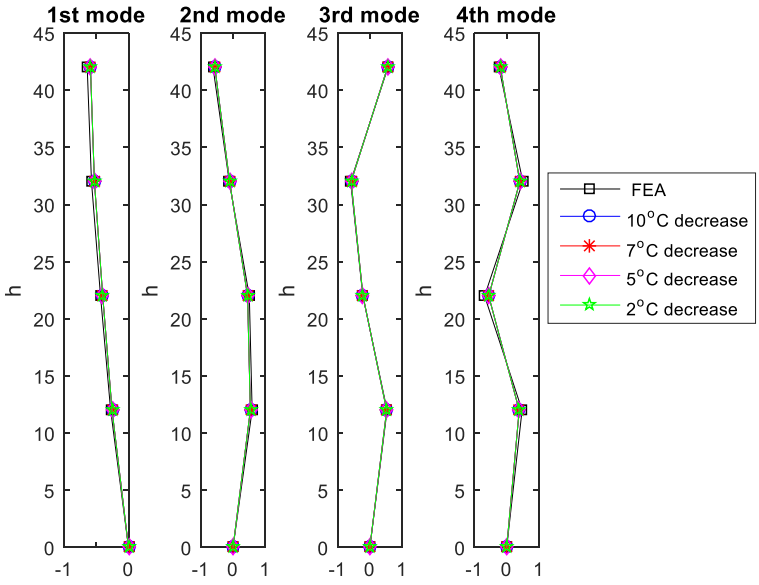

(b) Scaled

Figure 5.24. Modal Scaling using TcMS with Temperature Decrease

The same achievement has been received with increasing temperature in structure. Modal scaling results using temperature increase are shown in Figure 5.25.

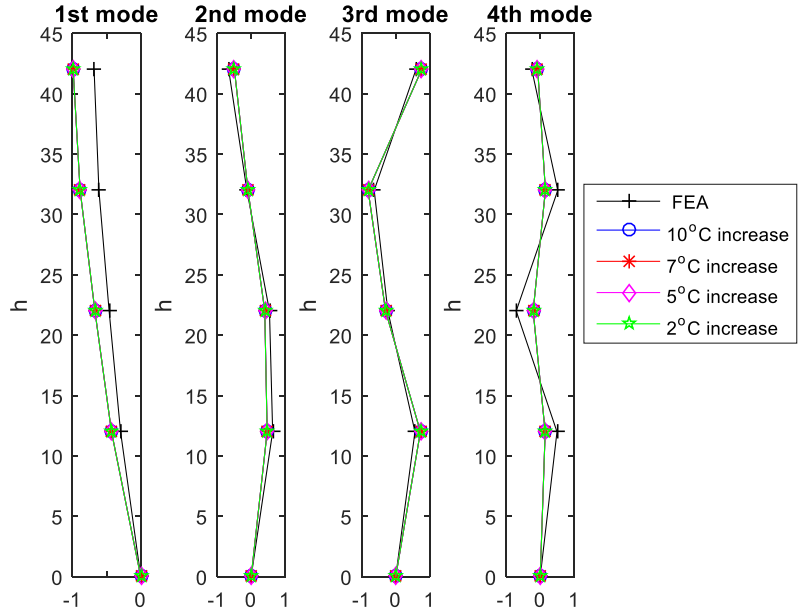

(a)

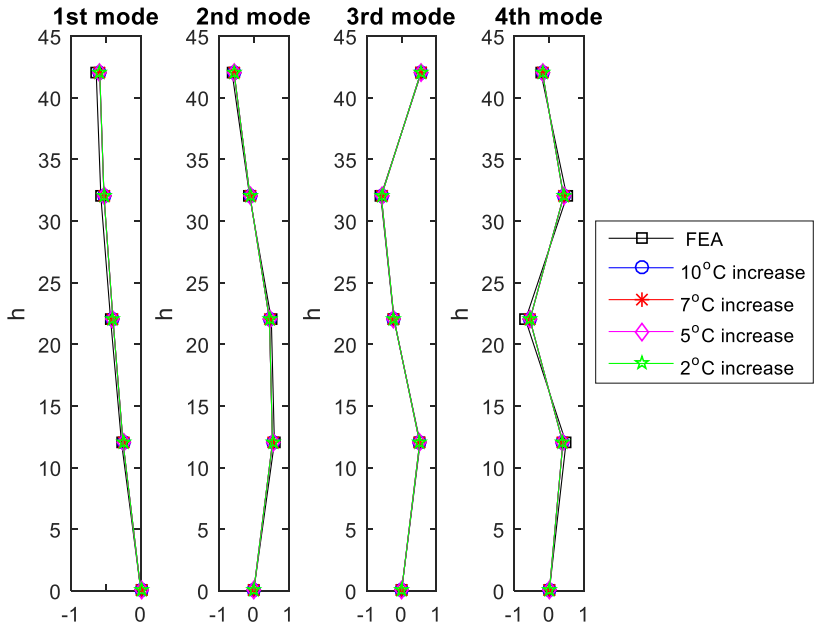

(b)

Figure 5.25. Modal Scaling using TcMS with Temperature Increase

Figures 5.24 and 5.25 indicate TcMS method can scale mode shape efficiently with all the temperature change of ± 10 ℃ from the baseline.

5.2.2 TcMS with Non-Uniform Temperature Change over Structure

TcMS has been proven to be an efficient modal scaling method when the temperature change is uniform over the structures. To mimic the real situation of non-uniform temperature distribution in the element, TcMS is applied in a single case. Random temperature over structure is shown in Table 5.13 and the temperature change over structure is shown in Figure 5.26.

Table 5.13. Non-uniform Temperature Change Distribution

In Consistent Temperature Change				
Element Number	1	2	3	4
ΔT	+10 ℃	+2 ℃	+5 ℃	+7 ℃

And the temperature change over structure is shown in Figure 5.23.

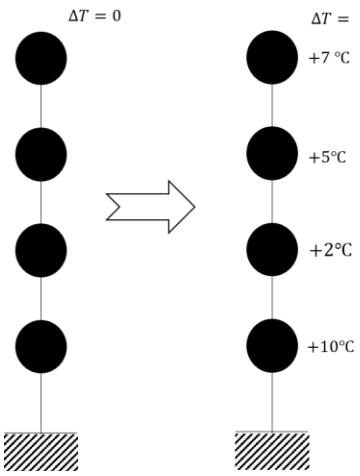

Figure 5.26. Non-uniform Temperature Change over Structure

The frequency changes due to non-uniform temperature changes over structure are shown in Table 5.14. Generally, the frequencies are not significantly changed.

Table 5.14. Model Frequencies Under Non-Uniform Temperature Change

	Frequencies (Hz)	
Modes	Baseline ($\Delta T = 0$)	Non-uniform Temperature Change
1	8.94	8.93
2	25.03	25.00
3	39.89	39.85
4	48.75	48.71

Table 5.14 shows frequency change due to non-uniform temperature change over the structure. The mode shapes extracted from SSI are scaled with non-uniform temperature changes. The results of model scaling using TcMS are shown in Figure 5.27.

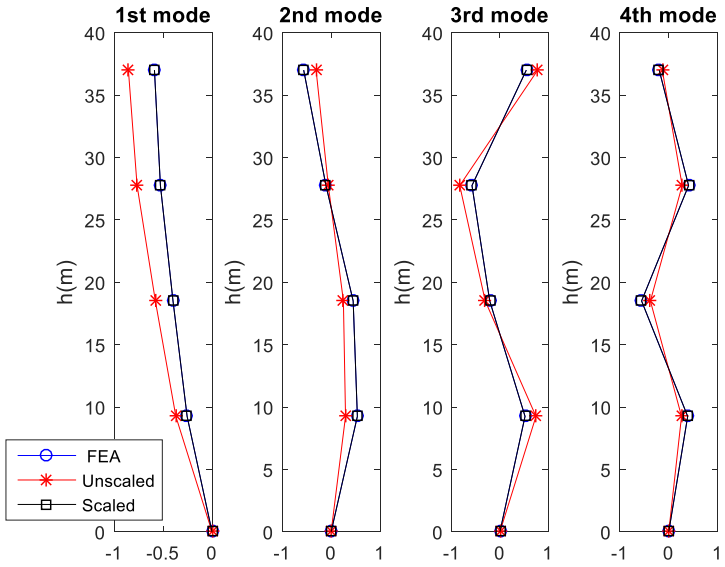

Figure 5.27. Modal Scaling using Non-Uniform Temperature

Figure 5.27 indicates that mode shapes extracted from OMA method can be efficiently scaled using TcMS using non-uniform temperature change.

5.3 Numerical Simulation (Case 2)

In this section, a numerical simulation is presented for the validation of the proposed damage detection method on truss structure. To scale the mode shape, the temperature change modal scaling method is used.

A simply supported steel truss is used as shown in Figure 5.28. A total of 6 nodes is used to construct 9 elements of a steel bridge.

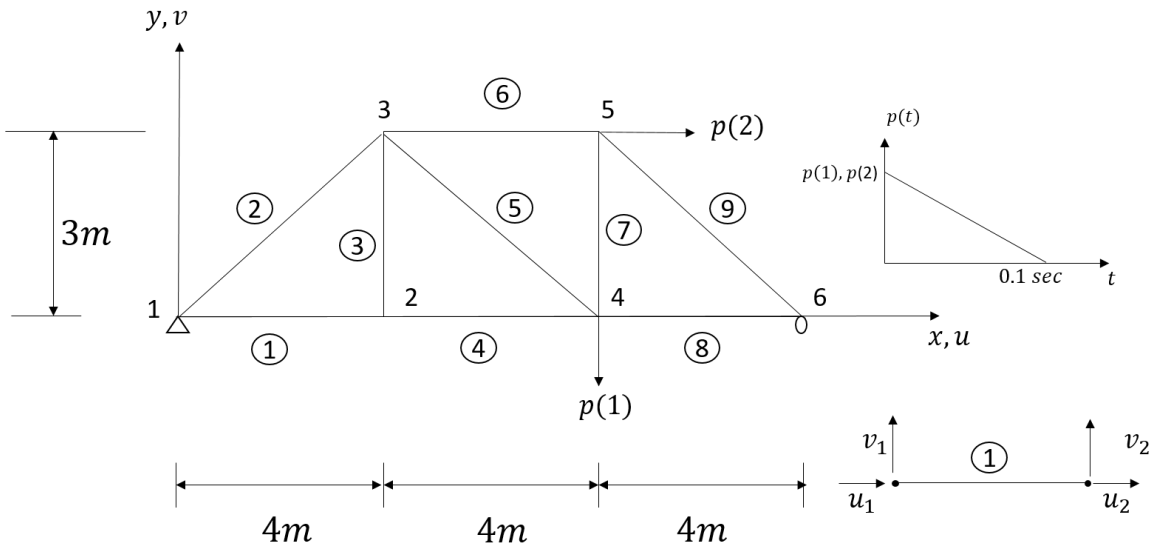

Figure 5.28. Numerical Simulation Example

Each element is assumed to be the bar element. Therefore, the total degrees of freedom of this structure is 12. The element stiffness of the bar element is as follows,

$$k = \frac{AE}{L}\begin{bmatrix} 1 & 0 & -1 & 0 \\ 0 & 0 & 0 & 0 \\ -1 & 0 & 1 & 0 \\ 0 & 0 & 0 & 0 \end{bmatrix} \tag{5.7}$$

And the element mass of the bar element is estimated as

$$m = \frac{\rho L}{6}\begin{bmatrix} 2 & 0 & 1 & 0 \\ 0 & 2 & 0 & 1 \\ 1 & 0 & 2 & 0 \\ 0 & 1 & 0 & 2 \end{bmatrix} \tag{5.8}$$

The damping matrix is assumed to be as follows,

$$\boldsymbol{C} = \alpha \boldsymbol{M} + \beta \boldsymbol{K} \tag{5.9}$$

where $\alpha = 0$, $\beta = 0.005$ are assumed to be defined here.

The properties of each element are listed in Table 5.15.

Table 5.15. Properties of Numerical Model (Case 2)

Properties	Cross Section area (m^2)	Elastic Modulus (GPa)	Density (kg/m^3)
Value	0.00025	200	7850

A vertical force, $p(1) = 1200\,N$ and a horizontal force, $p(2) = 400\,N$ are applied to the nodes 4 and 5 as shown in Figure 5.28. Nodes 1 and 6 are restrained to move vertical deflection. Only nodes 2, 3, 4, and 5 are not restrained to move vertically. Figure 5.29 shows the vertical displacement of each node in the vertical direction.

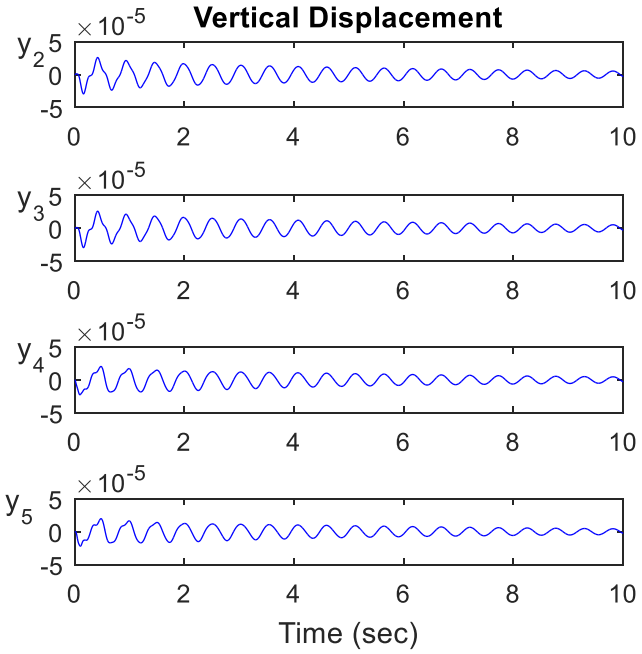

Figure 5.29. Vertical Displacement of Truss Nodes (unit: m.)

Nodes 2, 3, 4, 5, and 6 are not restrained to translate in the horizontal direction. Figure 5.30 shows the horizontal displacement of those nodes.

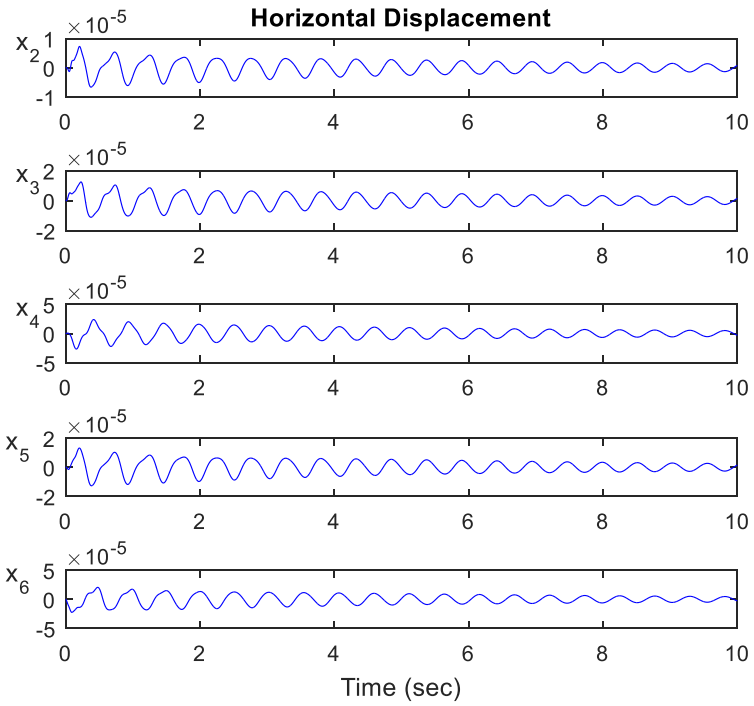

Figure 5.30. Horizontal Displacement of Truss Nodes (unit: m.)

5.3.1 Dynamic Characteristic Extraction using SSI

A total of 9 frequencies and mode shapes can be extracted from SSI using the horizontal and vertical displacements. The frequencies extracted from SSI are compared with them from FEA estimates (see Table 5.16).

Table 5.16. Frequencies of Truss (rad/sec)

Modes	FEA	SSI
1	12.04	12.07
2	23.40	23.41
3	36.99	37.00
4	62.17	62.17
5	81.67	81.84
6	105.11	105.13
7	109.01	109.02
8	115.50	115.52
9	140.11	140.13

The frequencies extracted from SSI are almost identical to those of FEA estimation. Mode shapes are also extracted from SSI and the MAC value of each mode corresponding to modes from the FEA estimation are listed in Table 5.17.

Table 5.17. MAC value of Mode Shape Extracted from SSI

	MAC value at each mode								
Modes	1	2	3	4	5	6	7	8	9
Value	1	1	1	1	0.9985	1	1	1	1

Table 5.17 shows that the MAC value between SSI extracted mode shapes and FEA estimation are 1 except for 5th mode. This indicates that the mode shape from SSI is accurately extracted from only displacements.

5.3.2 Modal Scaling using TcMS

The mode shapes obtained from OMA are unscaled. A temperature change of 5 ℃ is used to obtain the scaled mode shapes. All the nine modes of unscaled mode shapes are shown in Figure 5.31.

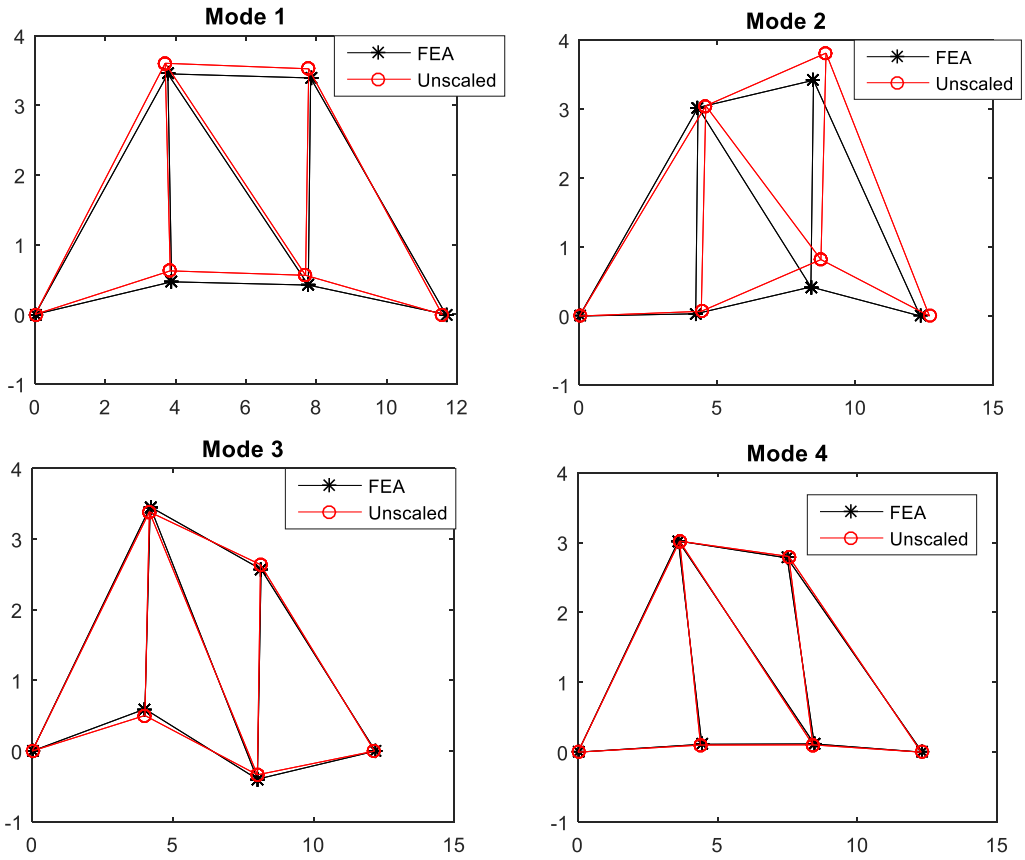

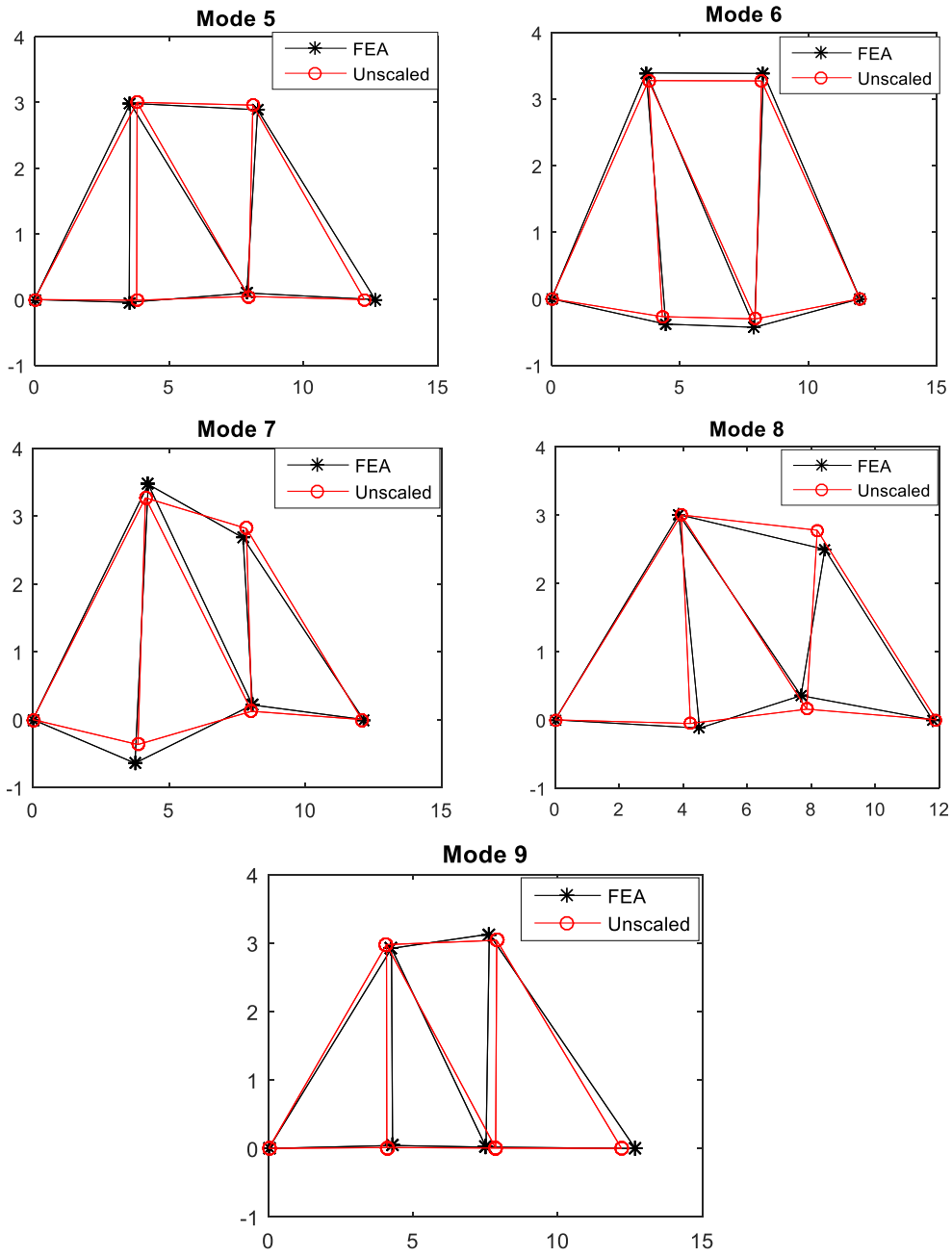

Figure 5.31. Unscaled Mode Shapes of Truss

Even through the MAC value shows high corresponding between the SSI extracted mode shapes and those of the FEA estimation, the mode shapes are unscaled and cannot

be used for the FEMU. Figure 5.32 shows the scaled mode shapes after 5 ℃ TcMS and those of FEA estimation.

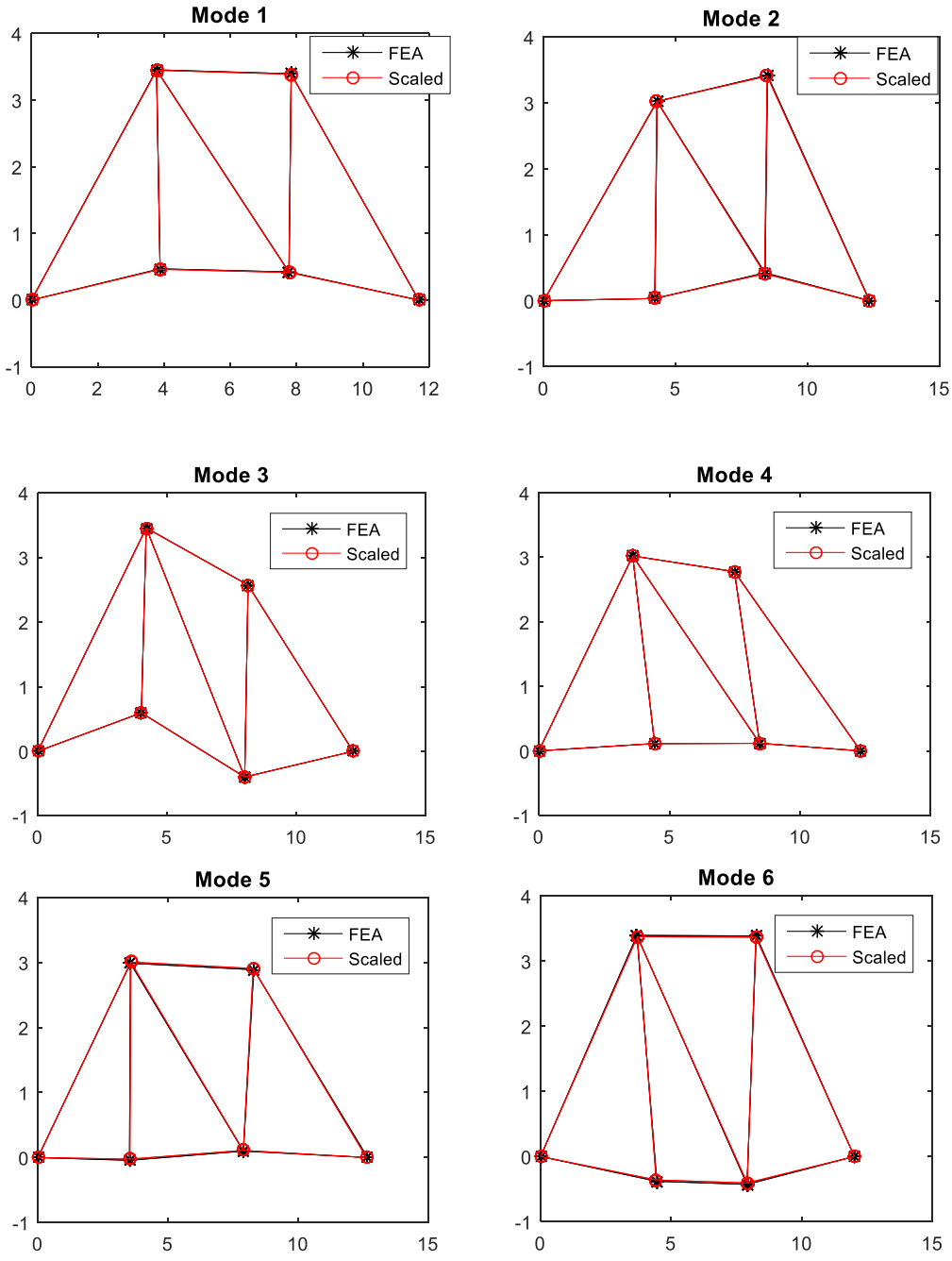

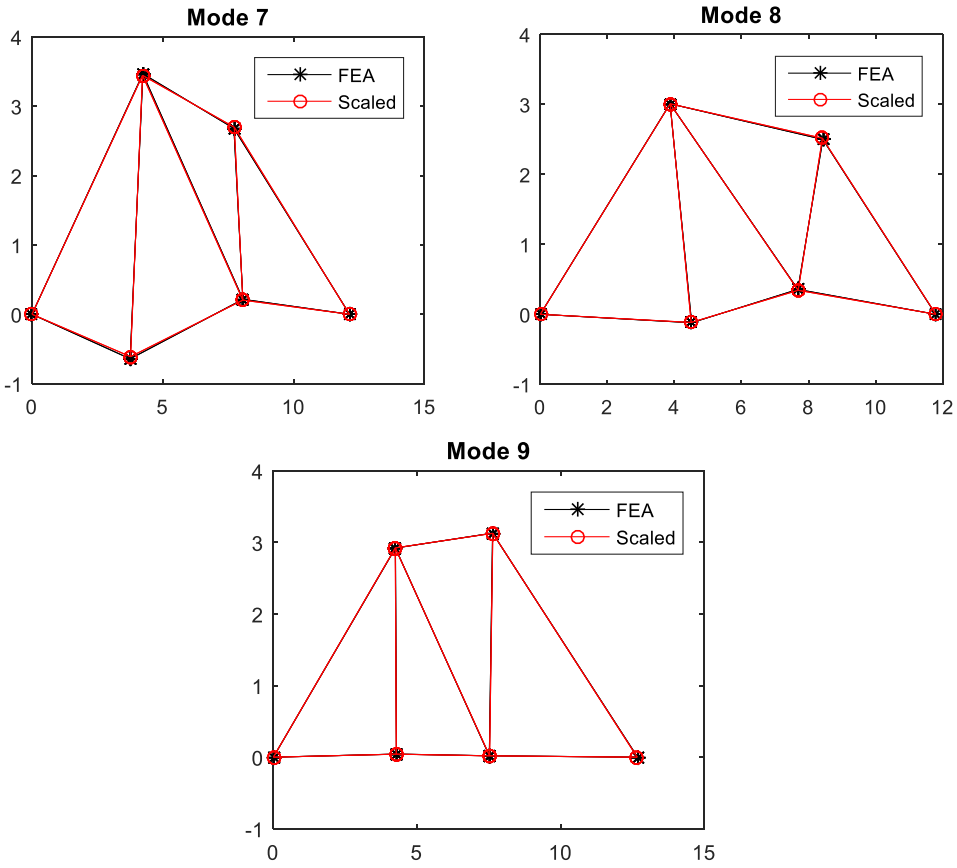

Figure 5.32. Unscaled Mode Shapes of Truss

Clearly, the scaled mode shapes are almost identical with those from FEA estimation. The scaled mode shapes then are used in FEMU for the estimation of mass and stiffness matrices.

5.3.3 Detection of Damage Locations and Severities

To validate the capability of the proposed method, mass and stiffness losses are introduced in elements. In element 3, the reduction of mass and stiffness are assumed to be 5 and 7% of the undamaged condition. Simultaneously, the mass reduction is assumed to be 10% of the undamaged condition in element 6 and the stiffness reduction is assumed to be 20% of the undamaged condition in element 8.

Table 5.18. Damage Simulation Matrix

Damage Simulation				
Element	m_3	m_6	k_3	k_8
Reduction	5%	10%	7%	20%

Displacements of the damaged structure are acquired from FEA with changed mass and stiffness matrices. Figure 5.33 shows vertical displacement and horizontal displacements of node 2.

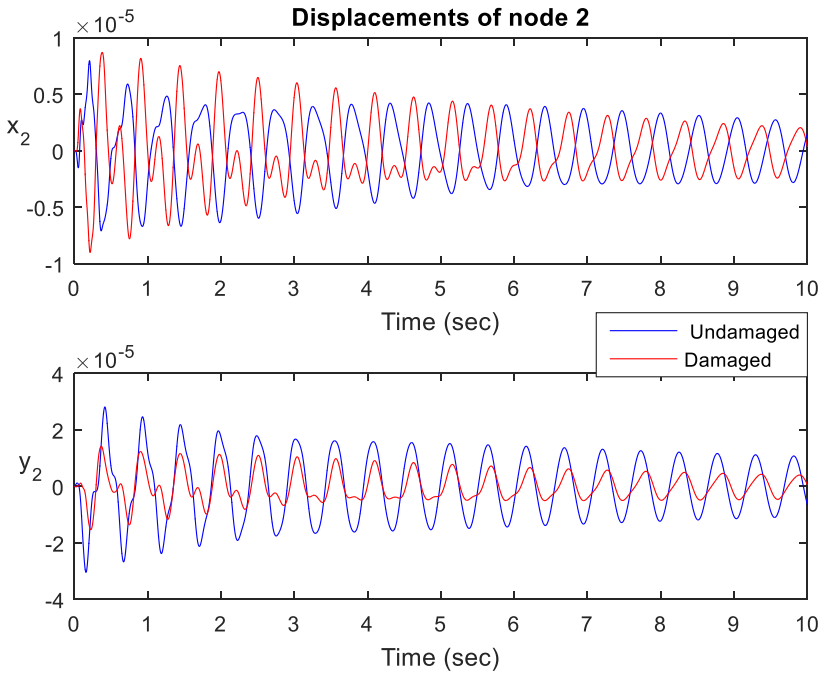

Figure 5.33. Displacement of Undamaged and Damaged Structure (Unit:m.)

SSI is used to extract the frequencies and mode shapes. The frequencies of the damaged structure are listed in Table 5.19.

Table 5.19. Frequencies of Damaged Truss Extracted from SSI (rad/sec)

Modes	Undamaged Structure	Damaged Structure
1	12.07	12.00
2	23.41	23.59
3	37.00	36.79
4	62.17	62.73
5	81.84	78.98
6	105.13	104.38
7	109.02	108.15
8	115.52	116.54
9	140.13	135.54

The frequencies of the truss of damaged condition reduces frequencies of healthy condition (the baseline) in all the modes. The percentage of change in frequencies caused by damage is calculated from Eq. 5.10 and shown in Figure 5.34.

$$\Delta\omega\% = \frac{\left|\omega_{undamaged} - \omega_{damaged}\right|}{\omega_{undamaged}} * 100\% \tag{5.10}$$

where $\omega_{undamaged}$ is the frequency of undamaged structure and $\omega_{damaged}$ is the frequency of damaged structure. Figure 5.34 shown the frequencies change due to damages.

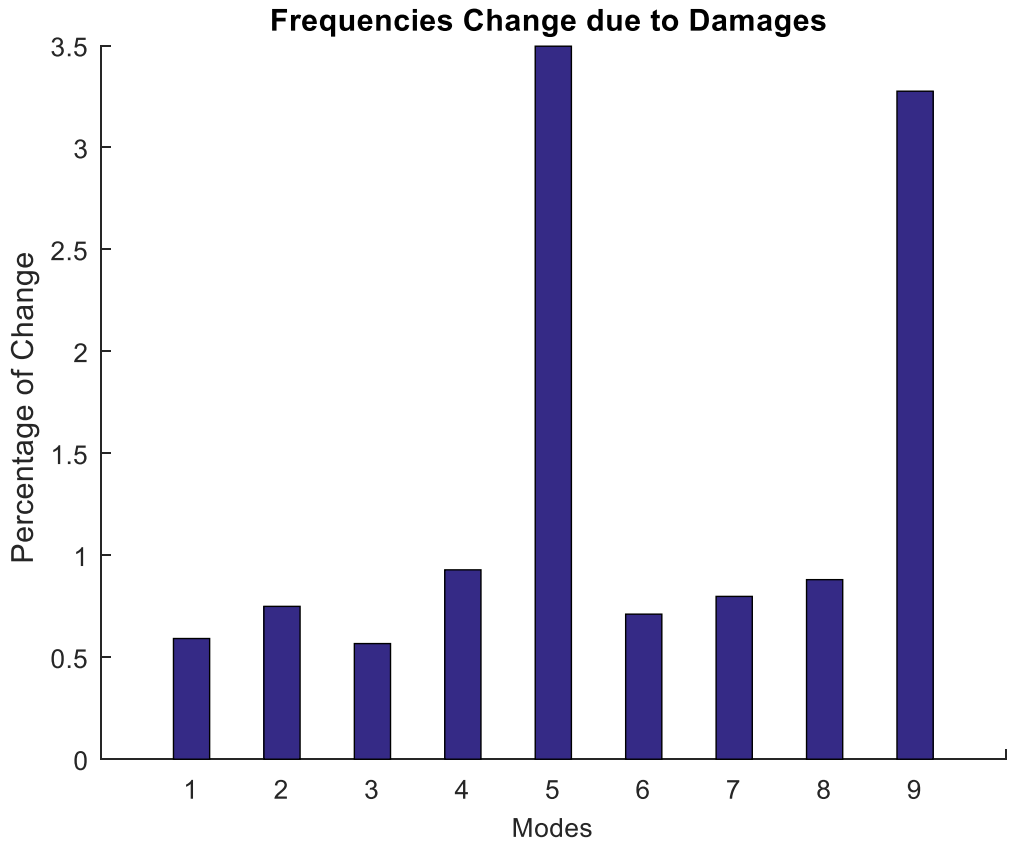

Figure 5.34. Frequencies Change Due to Damages

Figure 5.34 shows the change in frequencies ranging from 0.5% to 3.5% when the damages of in the structure exist. It should be noted that the maximum mass loss was 10% and maximum stiffness loss was 20% of the selected element. When the levels of damage are varied, the changes of frequency are varied. However, frequencies changes cannot identify the locations of damage. Mode shapes are also extracted from SSI and the MAC value between the damaged structure and the undamaged structure as shown in Table 5.20.

Table 5.20. MAC Value Between Damaged Structure and Baseline (Non-damage)

MAC value at each mode									
Modes	1	2	3	4	5	6	7	8	9
Value	0.9996	0.9996	0.9983	0.9851	0.9827	0.8435	0.8636	0.9967	0.9907

MAC value shows obvious differences between mode shapes at mode 6 and 7. Figure 5.35 shows mode shapes of damaged structure and the baseline (non-damage).

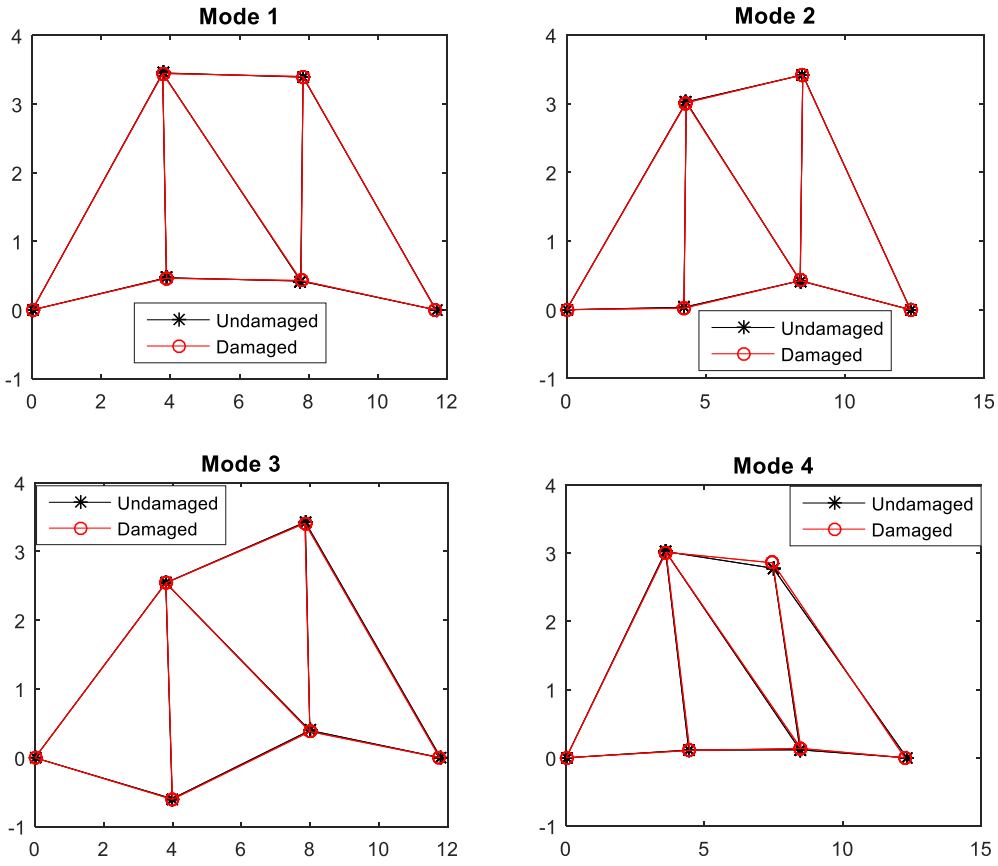

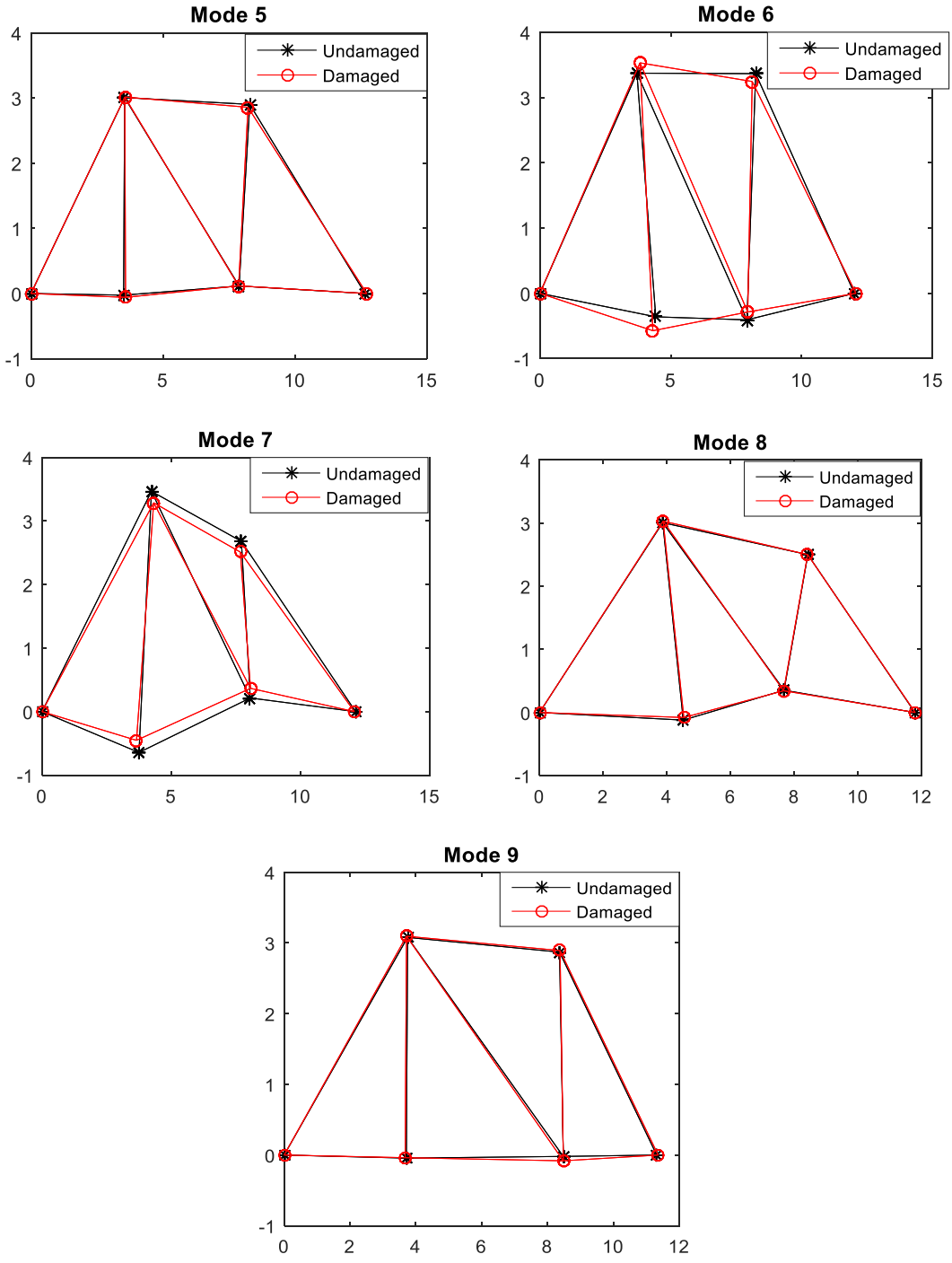

Figure 5.35. Damaged Truss Mode Shapes Compared with Baseline

The discrepancy between two sets of mode shapes can be used to achieve a Level 1 damage detection to confirm the existence of damages in the structure. However, the locations and severities of damages cannot be identified from the MAC value. FEMU is used to detect the locations of damages and their reduction rate of mass and stiffness (See Table 5.21).

Table 5.21. FEMU results for Damaged Truss Members

Damage Location and its Reduction of Mass (or Stiffness)				
Element (m, k)	m_3	m_6	k_3	k_8
In model	5 %	10 %	7 %	20 %
FEMU	5.69 %	10.28 %	7.34 %	21.8 %

Generally, the prediction accuracy is within 2% of both mass and stiffness of damaged elements.

Figure 5.36 shows the prediction of mass and stiffness reduction for the simulated damage scenario.

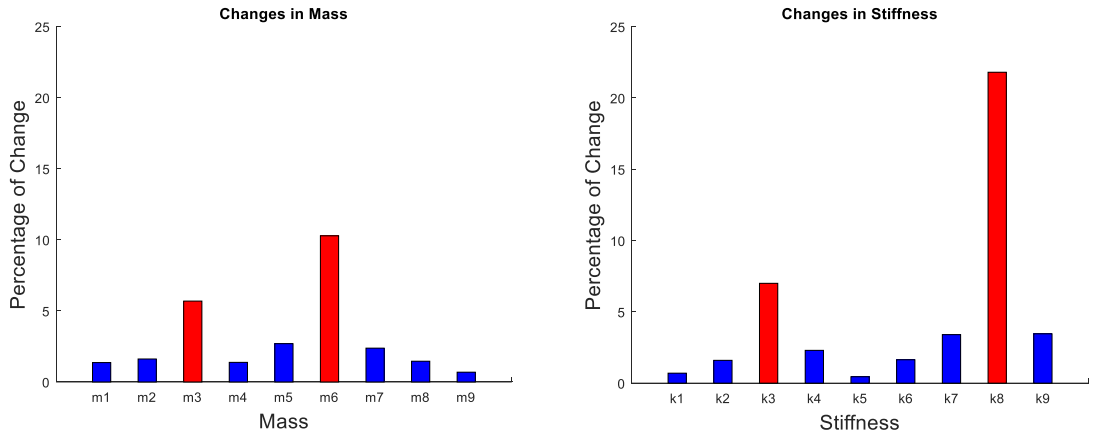

(a) (b)

Figure 5.36. FEMU for Mass and Stiffness Change of Each Element: (a) Mass, (b) Stiffness

Using FEMU, the change of mass and stiffness in the structure due to damage can be detected with their locations and severities. However, undamaged members are also identified as damaged member within 2.5% (mass) and 4% (stiffness). The FEMU is able to identify the elements for the priority of damage evaluation. When there are significant damages, the estimation is fairly accurate. FEMU can reasonably update the stiffness and mass matrices as well as detect the location and the level of changes in the system matrices of the truss structure.

5.4 Conclusions

Following conclusions can be drawn in this Chapter:

(1) SSI can accurately extract frequencies of the structure using only the response of the structure under different types of loading with or without dampings.

(2) When there is no noise in the simulation process, the proposed system identification method can identify the system matrices using responses (displacements) under different types of excitation within less than 1% error.

(3) The increases of noise reduce the accuracy of estimates of frequencies, mode shapes, and system matrices. Errors of the identification under disturbance less than 75% white noise are still acceptable for the application of proposed algorithm.

(4) The values of MAC extracted from SSI are close to 1 that indicates a high corresponding relationship between the true mode shape and mode shapes extracted from SSI.

(5) The McMS method efficiently scales the mode shapes from unscaled mode shapes from SSI.

(6) The TcMS method can efficiently scale the mode shapes with both uniform and non-uniform temperature change.

(7) FEMU can reasonably update the mass and stiffness matrices of both cantilever beam and a truss structure to detect the changes of the system matrices.

Results indicate that theoretically the proposed damage detection algorithms can rationally detect the changes of mass and stiffness due to the presence of damages. The locations and severities of damages can be identified and estimated by the change in system matrices from the baseline.

CHAPTER 6

EXPERIMENTAL VALIDATION

Numerical simulation chapter shows that the proposed method can accurately identify the system and detect damage. To evaluate the performance of the proposed algorithm using displacements acquired from non-contact based optical sensor as the only input, laboratory program was designed using a cantilever beam. The test program and results are discussed.

6.1 Experimental Program

A cantilever beam system is used to validate the proposed algorithm using vibration response captured by the non-contact based optical sensor. The experimental program is designed to test 1) the effect of contact based sensor on structural dynamic characteristics, 2) the optimal change of mass for modal scaling, and 3) the capability of proposed method for damage detection.

6.1.1 Experimental Set-up

A steel member is used in this test. The section properties and geometry are shown in Table 6.1

Table 6.1. Properties and Geometrics of the Steel Member

Length (mm)	Width (mm)	Thickness (mm)	Density (kg/m^3)	Young's modulus (GPa)
939.8	50.8	6.35	7850	200

Both high-speed camera and accelerometers are used to obtain the displacement and acceleration for the beam vibration. Figure 6.1 shows the test set-up.

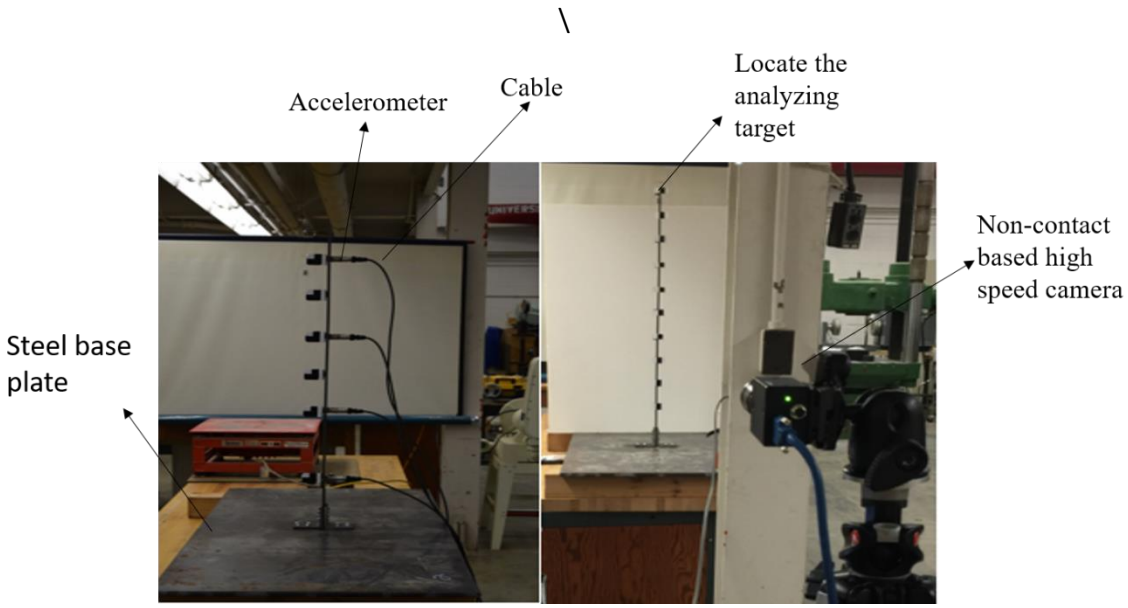

(a) (b)

Figure 6.1. Test Set-up

The experimental program was performed at the structural/material laboratory of Civil and Environmental Engineering department. The steel member is fixed on the steel base plate using four bolts and nuts with 'L' shape angle to construct a cantilever beam. In Figure 6.1 (a), accelerometers are attached to the beam, the horizontal displacements of the beam vibration is captured by the high-speed. In Figure 6.1 (b) the marks for targeting location to capture the motion of movement is attached and the weight of them can be neglected.

6.1.2 Sensor System Components

Accelerometer system components are listed below:

- National Instrument 9234 with a 9178 USB interface;
- IMI 603C01 accelerometer: (frequency range: 0.5 to 10000 Hz);
- PCB 080A93 mounting pad;
- PCB 080A120 mounting magnates;
- PCB 052BR010AC multi conductor cable;
- LabVIEW software.

The LabVIEW software can store the measurement of accelerometers on the computer. Later, the displacement is calculated from the integration of acceleration.

Non-contact based high-speed camera components are listed below. The commercially available system (RDI Technologies) including software and hardware are provided by Dr. Jeffrey Hay.

- FLIR Grasshopper 3 GS3-U3-23S6M-C with a Sony IMX174 mono sensor: Resolution: 1920 × 1200;
- USB3 cable;
- RDI BridgeView software;
- Microsoft Surface Book.

The system and principle are developed by the Ph.D. work of Dr. Hay under the supervision of Dr. Kielkopf. More information can be found in the dissertation of Dr. Hay (Hay 2011). The system is already patented in 2014 (Kielkopf and Hay 2014). That was used to measure the vibration of bridges to extract dynamic characteristics (Hay et al. 2012). After measuring the distance from the lens of the camera to the target using Laser Distance Measure (Bosch product if $\pm 1/16''$ accuracy), the value can be used to adjust the displacements of a target object in recorded images to extract the actual displacement in inches.

6.2 Experimental Program

This section provides the experimental program of this study. Four test programs are explained consecutively. Section 6.3 presents corresponding results.

6.2.1 Response from Two Sensor System

Four channels of accelerometers are used to acquire the acceleration at the sampling rate of 2000 Hz. At the same time, the displacement of each node (i.e. target) is acquired with the high-speed camera at the sampling rate of 520 Hz and the duration of data acquisition are both 10 seconds. When the beam is under free vibration, the displacement of the third node from bottom obtained from the optical sensor and the integration of acceleration acquired from the accelerometer were measured as shown in Figure 6.2.

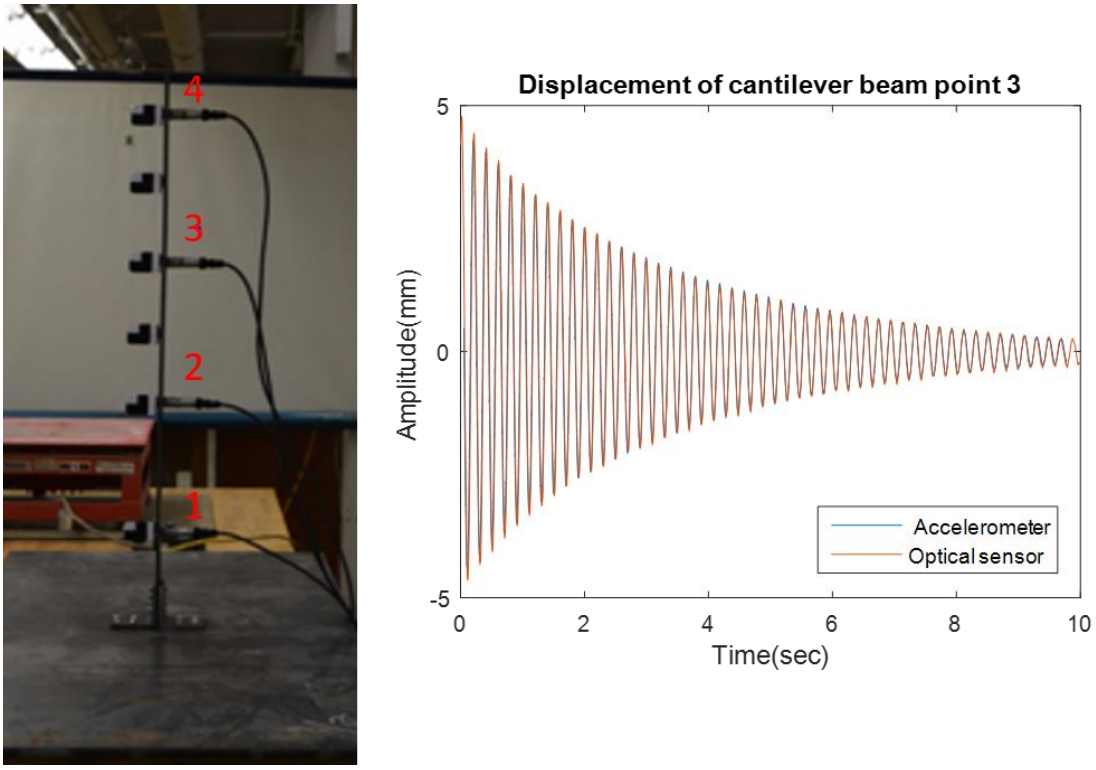

Figure 6.2. Comparison Between Optical Sensor and Accelerometers

The displacement double integrated from acceleration and displacement directly measured from RDI system show almost identical in the measurement of frequency, amplitude, and damping. The optical sensor then will be primarily used as the data acquisition method in this study.

6.2.2 The Effect of Contact Based Sensor on Dynamic Characteristics

The influence from accelerometers' self-weight and the additional stiffness from the cables are analyzed by comparing the dynamic characteristics extracted from three experimental set-ups with the results calculated from FEA. Three set-ups are: 1) the cantilever beam without any contact based sensors, 2) the cantilever beam with the added

mass of accelerometers' self-weights, and 3) the cantilever beam with the added mass and stiffness provided by the self-weights of the sensors and cables. Random impacts were applied to the beam at random locations to simulate the random ambient vibration. The three set-ups are listed in Table 6.2.

Table 6.2. Test Matrix for Effect of Contact Based Sensor

Set-up I	Set-up II	Set-up III
No attachment	With accelerometers, and no cables	With accelerometers and cables

The displacement of each scenario is acquired by the optical sensor are shown in Figure 6.3.

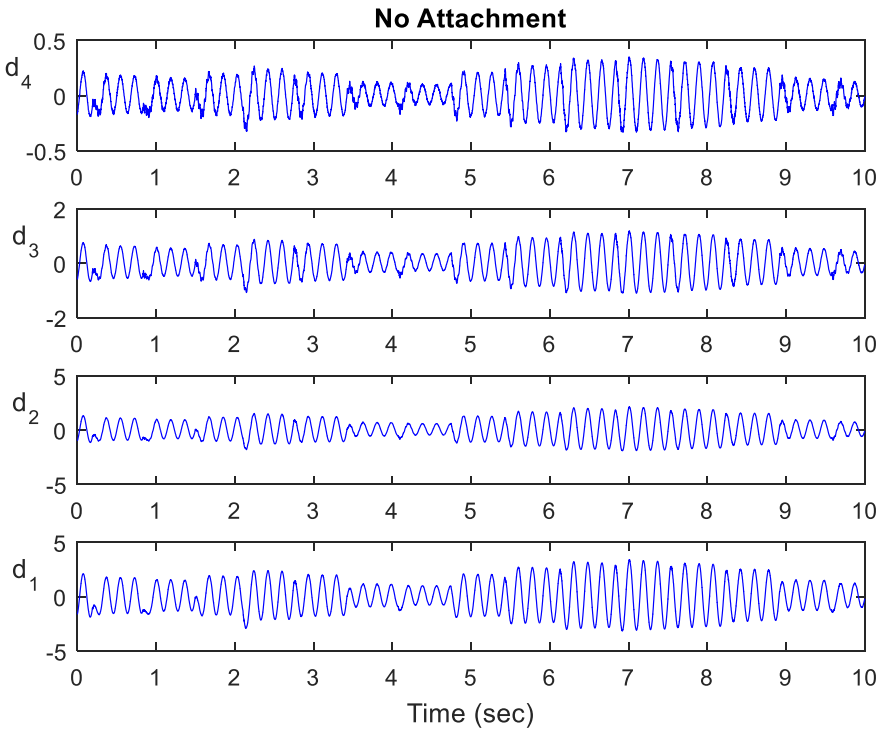

(a)

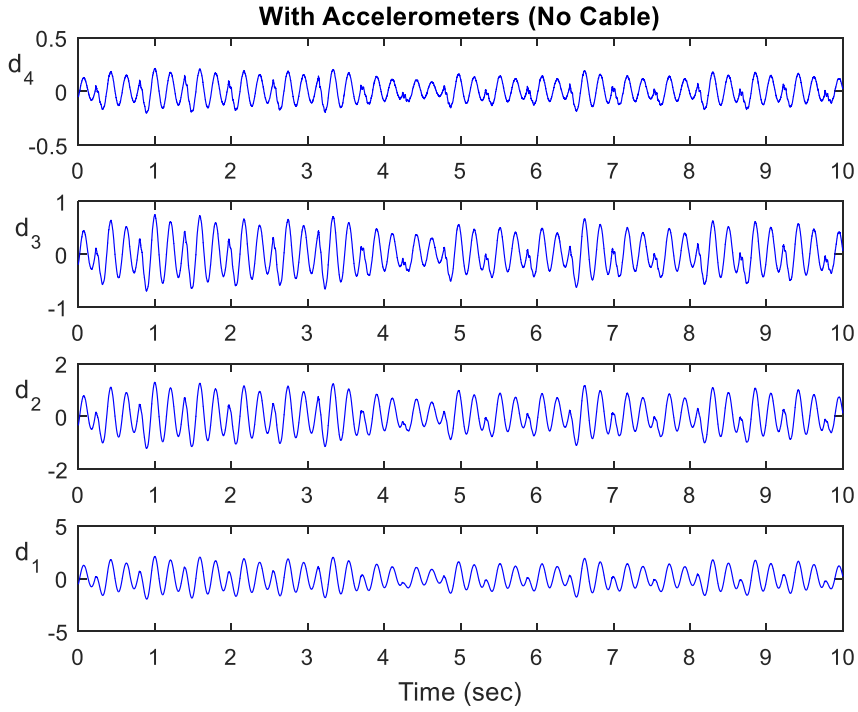

(b)

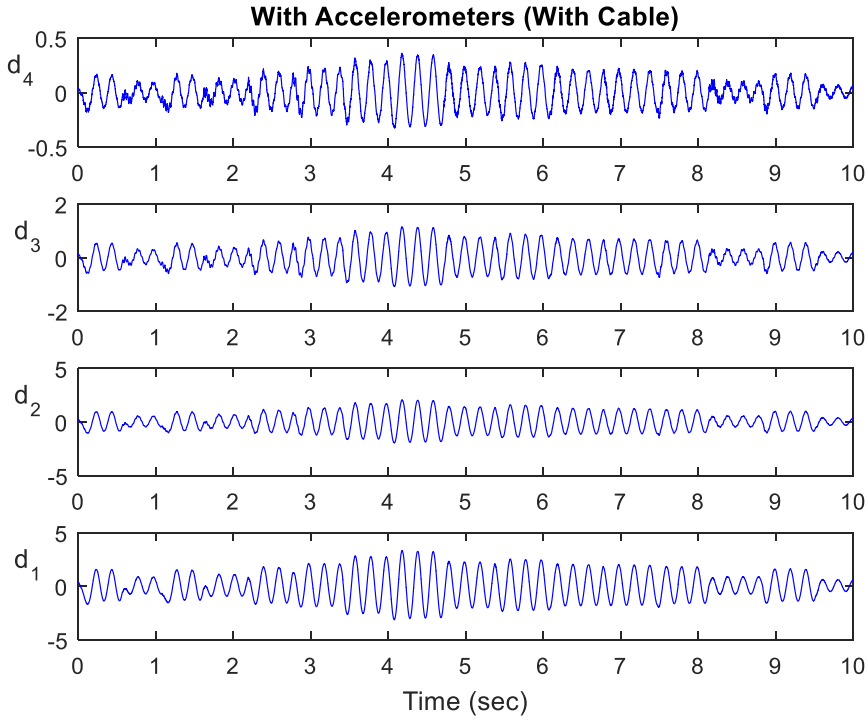

(c)

Figure 6.3. Displacements of Beam with/without Accelerometers and/or Cables: (Unit: mm) (a)Test Set-up I, (b) Test Set-up II, (c) Test Set-up III

Measured displacements are used in SSI to extract the dynamic characteristics. During each data acquisition process, the impacts were randomly applied during each test as shown in Figure 6.3. Therefore, responses are different every time. The results of analysis are presented in the Section 6.3.1.

6.2.3 Application of McMS Method

Only unscaled mode shapes are obtained from OMA method (i.e., SSI). However, to conduct a high level of SHM, scaled mode shapes are required. In the proposed method, the unscaled mode shapes willyield in incorrect updating of mass and stiffness and the scaled mode shapes must be obtained. McMS was used in this experimental test for obtaining the scaled mode shapes. Different levels of mass were added on each beam element to identify the appropriate change of mass. A total of 6 beam elements is used. The amount of mass was considered with 3.5%, 7% and 10.5% of the element mass and placed on beam as shown in Figure 6.4.

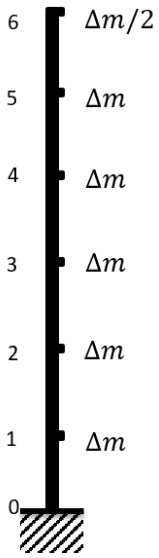

Figure 6.4. Mass Change of Beam

And the amounts of mass change at each point of the beam are listed in Table 6.3.

Table 6.3. Amount of Mass Change at Each Point of Beam

Point No.	1	2	3	4	5	6
$\Delta m\ (g) - 3.5\%$	13.78	13.78	13.78	13.78	13.78	6.89
$\Delta m\ (g) - 7\%$	27.55	27.55	27.55	27.55	27.55	13.78
$\Delta m\ (g) - 10.5\%$	41.32	41.32	41.32	41.32	41.32	20.66

Note: Points No. is shown in Figure 6.4. (0~6).

The frequencies and mode shapes of each mass change model are analyzed and the scaled mode shapes of the beam with different amount of mass change are compared. The results are presented in the Section 6.3.2.

6.2.4 Damage Assessment

Different damages are designed and applied in the beam including boundary condition change and structure damages such as holes and cut-down (herein, crack). Table 6.4 shows the damage scenarios with their assigned Test I.D. A total of six damage scenarios have different damage types, locations, and severities.

Table 6.4. Descriptions of Damage Scenarios

Damage Types	Test I.D.	Damage Location	Damage Description
Boundary Condition Change (B)	I.B	Boundary	Two bolts are removed
	II.B	Boundary	Three bolts are removed
Structural Damages (S)	I.S	Element 1	One $\frac{11}{32}$" hole
		Element 2	One $\frac{7}{8}$" crack
	II.S	Element 1	One $\frac{11}{32}$" hole
		Element 2	One $\frac{7}{8}$" crack
		Element 3	One $\frac{11}{32}$" hole
		Element 4	One $\frac{11}{32}$" hole
Structural and Boundary Damage (BS)	I.BS	I.B + II.S	

In The test I.D., the letter of B and S stand for the damage types. The letter of I or II stand for the severity of damage level. The letter of II indicates a higher level of damage than I. Each damage type is explained in the following section.

6.2.4.1 Boundary Condition Change Damage

For the analysis of boundary condition, different bolts and nut connected to the beam are removed. The objective of this test is to identify boundary condition change such as joint damages. Two levels of boundary condition change are generated by the removal

of No.1 and No.2 bolts (Test I.D.= I.B) and the removal of No.1, 2, and 3 bolts (Test I.D = II.B). The base connection and the bolts are illustrated in Figure 6.5.

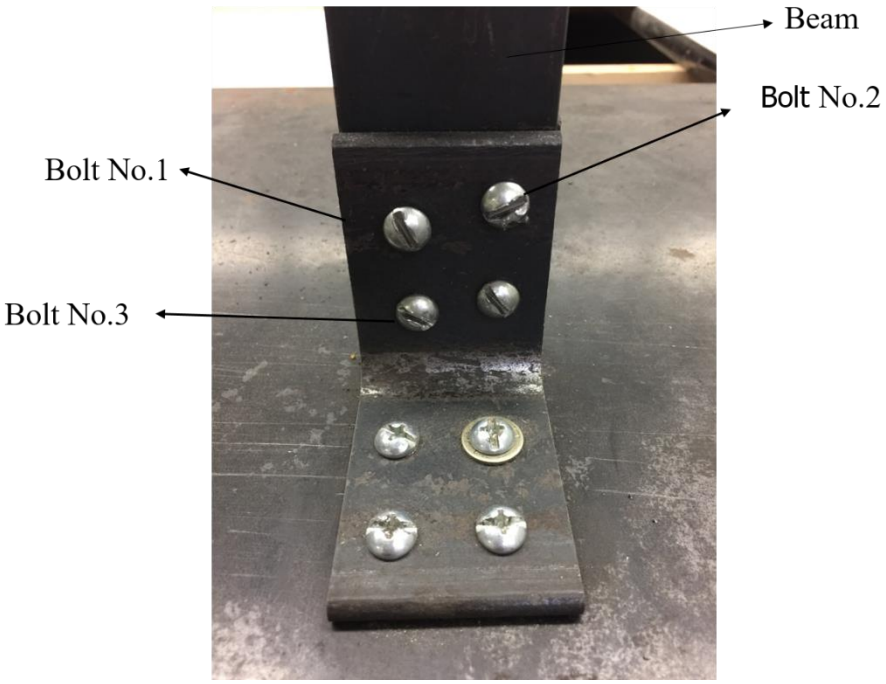

Figure 6.5. Joint between Beam and Base Plate

Five displacements of the beam (see Point Nos: 1~6 in Figure 6.4) under random excitation is acquired by the optical sensor and are shown in Figure 6.6 (a) [Test I.D.=I.B] and (b) [Test I.D. = II.B].

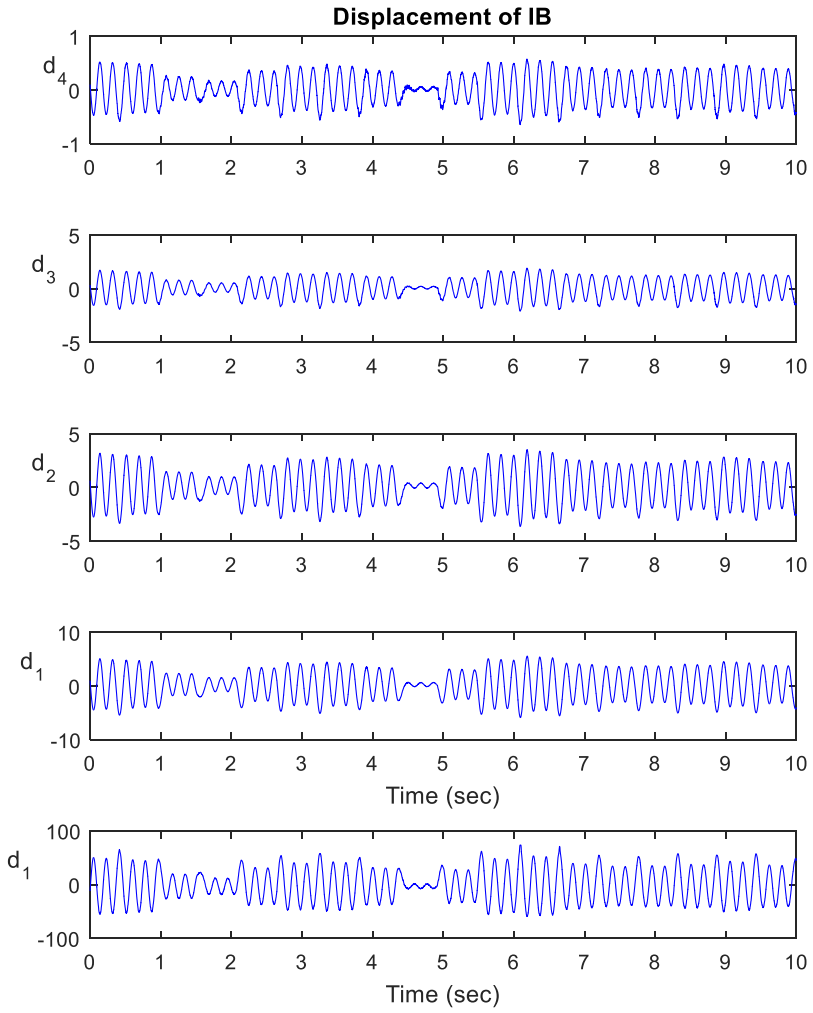

(a)

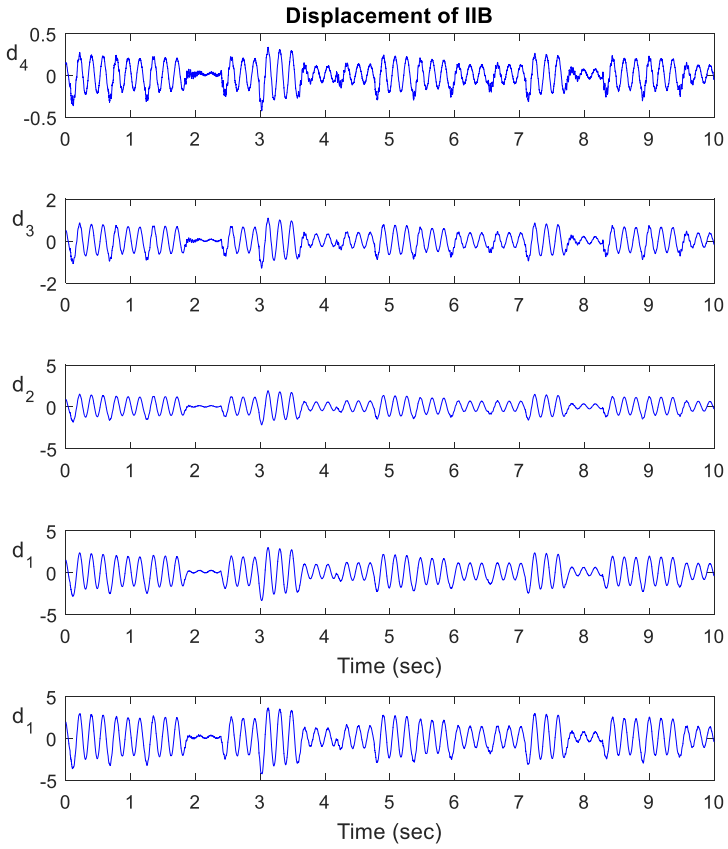

(b)

Figure 6.6. Displacement of Boundary Condition Change (Unit: mm)

(a) I.B, (b) II.B

Displacements d_i are used as the input for proposed damage detection method. The results are presented in the Section 6.3.3.1.

6.2.4.2 Structural Damage

The objective of this test program is to identify any structural damages such as holes and cracks. Using a four-element beam model, three levels of damage condition, IS, IIS and IBS are generated by drilling holes and cutting down to create cracks. Different

scenarios are shown in Figure 6.7. The damage levels are consecutively increased using the same beam.

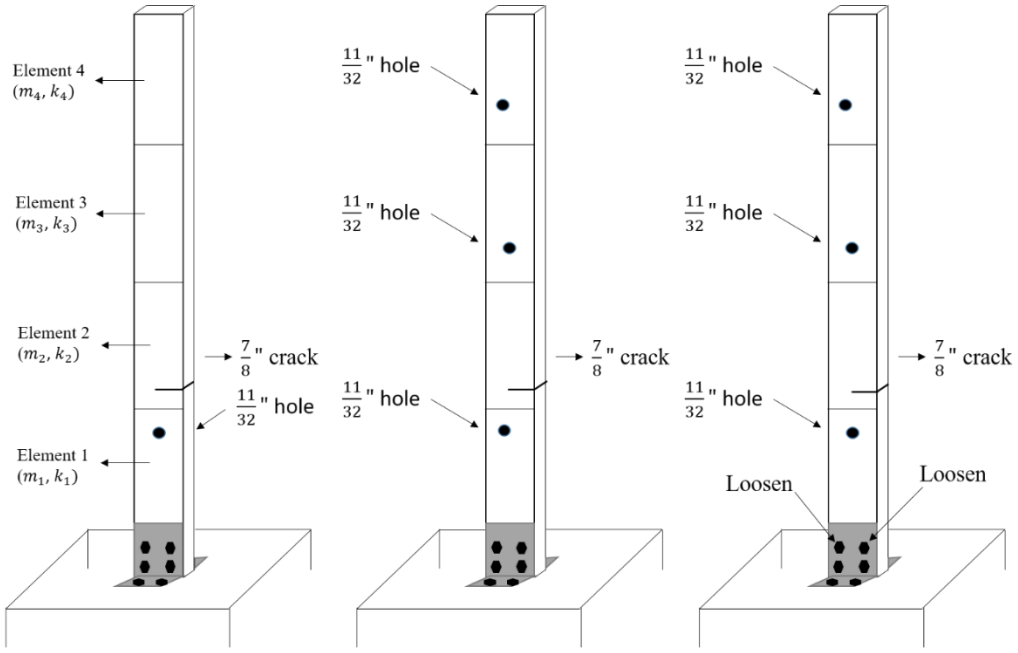

(a) (b) (c)

Figure 6.7. Illustration of Structural Damages: (a) I.S, (b) II.S, and (c) I.BS

Without boundary condition change, damage scenarios I.S and II.S will experience mass and stiffness changes due to holes and crack. The expected mass and stiffness change are shown in Table 6.5. The mass change due to damage is about 5%~6%.

Table 6.5. Mass Change of Each Element (I.S and II.S)

	Mass Change in Each Element			
Damage	m_1	m_2	m_3	m_4
I.S	5.02%	5.91%	0%	0%
II.S	5.02%	5.91%	5.02%	5.02%

A total of five displacements d_i, of the beam under the random excitation is acquired by the optical sensor and are shown in Figure 6.8 (a) [Test I.D.=I.S], (b) [Test I.D.=II.S] and (c) [Test I.D.=I.BS].

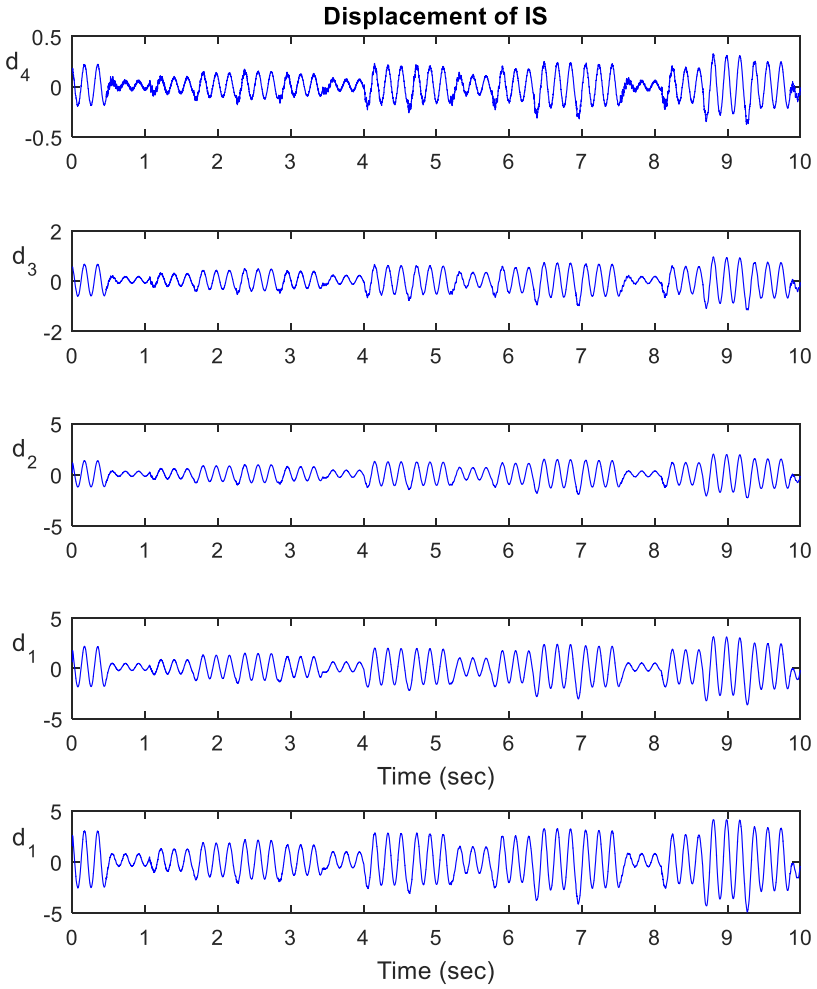

(a)

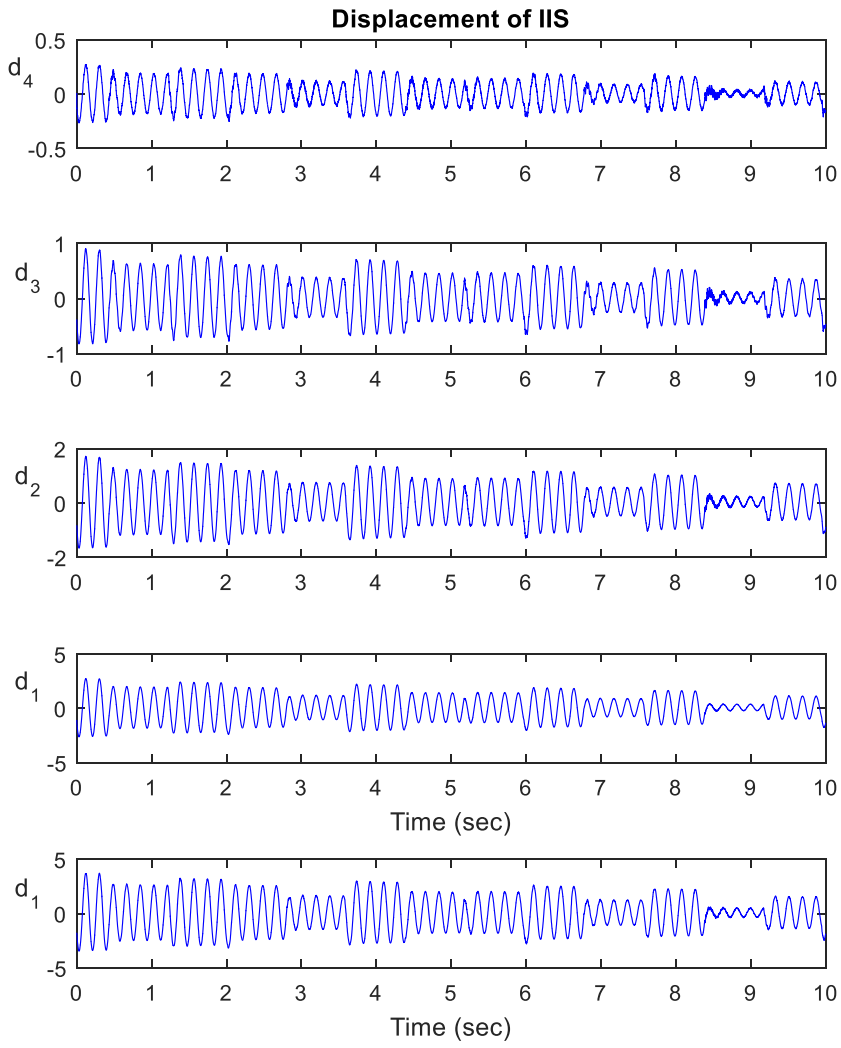

(b)

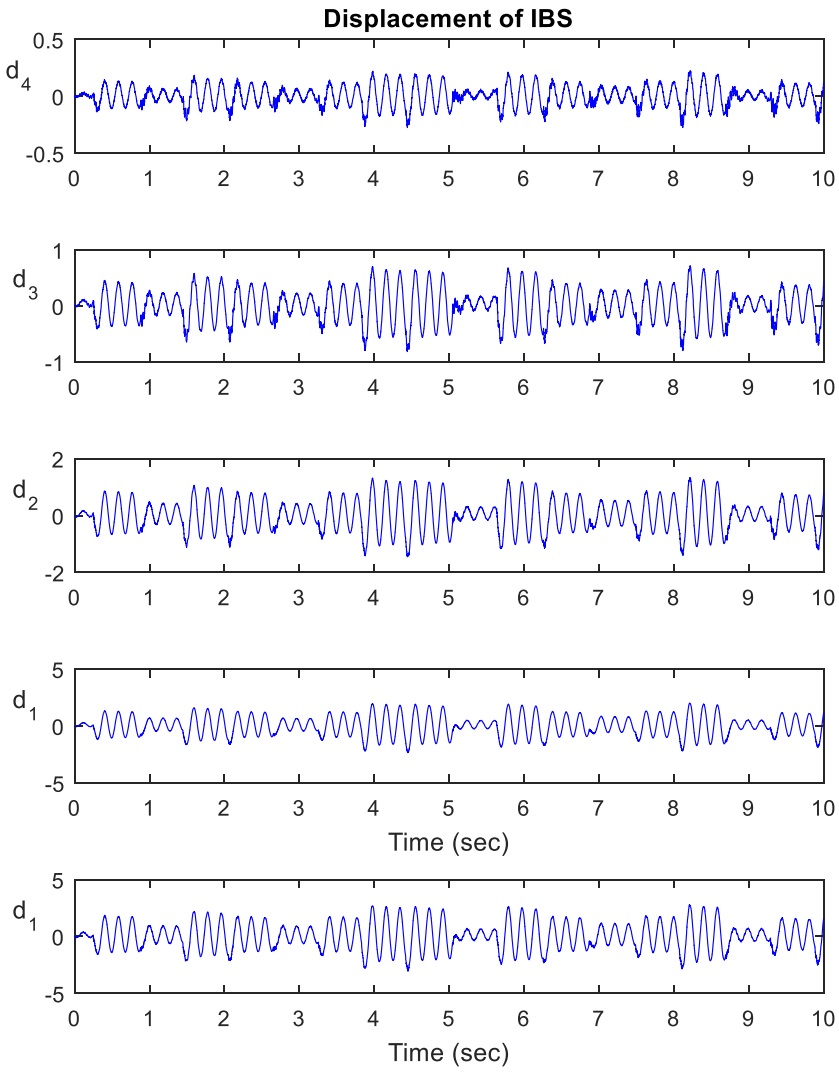

(c)

Figure 6.8. Displacement of Structural Damages: (Unit: mm)
(a) I.S, (b) II.S, (c) I.BS

The excitation is random and unmeasurable. Displacements from Figure 6.8 are used as the input for proposed damage detection method. The results are presented in the Section 6.3.3.2.

6.3 Experimental Results

In the following section, the results of the test program are presented. Figure 6.9 shows a typical frequency and singular value of power spectral density (PSD) relation, each of the pick stands for the frequency of corresponding modes.

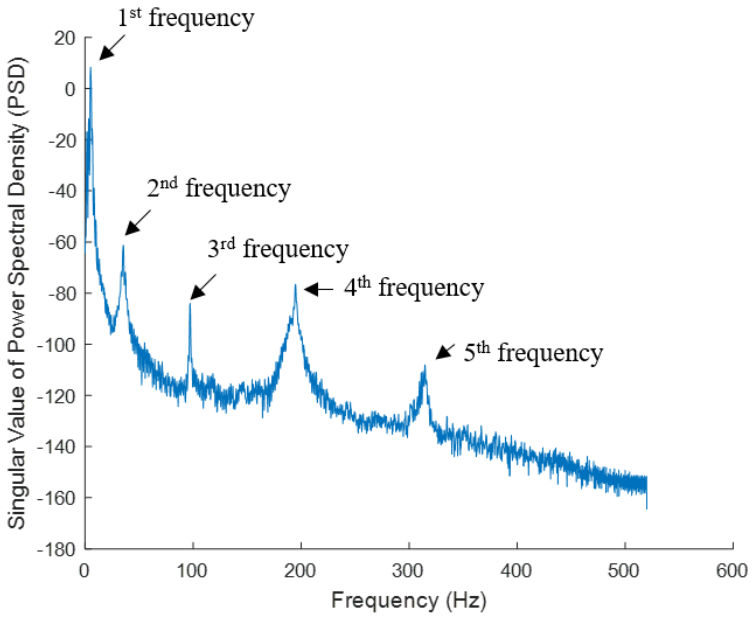

Figure 6.9. Frequency and Singular Value of PSD

The number of modes that can be extracted from SSI depends on the number of points to measure displacements and the sampling frequencies. The detected frequencies need to be in the range of the sampling frequencies. Five modes of frequencies are clearly shown in Figure 6.9. With the application of SSI, the correlated mode shapes can be extracted as well.

6.3.1 Effects of Contact Based Sensor on Dynamic Characteristics

Frequencies of the beam with test set-ups I, II, and III and shown in Table 6.6 compared with the FEA estimation.

Table 6.6. Frequencies of Beam with/without Accelerometers and Cables

Modes	FEA	Set-up I (No attachment)	Set-up II (With accelerometers, and no cables)	Set-up III (With accelerometers and cable)
1	5.69	5.59	5.33	5.09
2	35.68	36.05	33.01	31.48
3	99.91	99.53	87.85	67.79
4	195.80	194.50	167.70	158.90
5	323.68	319.20	290.70	265.10

Note: Discerptions of these set-ups are presented in Table 6.2.

Frequencies generally decrease when adding accelerometers' self-weight and the stiffness of cable from contact based sensor system. Higher modes show higher reduction of frequencies. For example, the fundamental frequencies are varied from 5.59 to 5.09 while the fifth frequency decrease from 319.20 to 265.10 when adding the additional mass and stiffness. The reduction of frequencies is also shown in Figure 6.10.

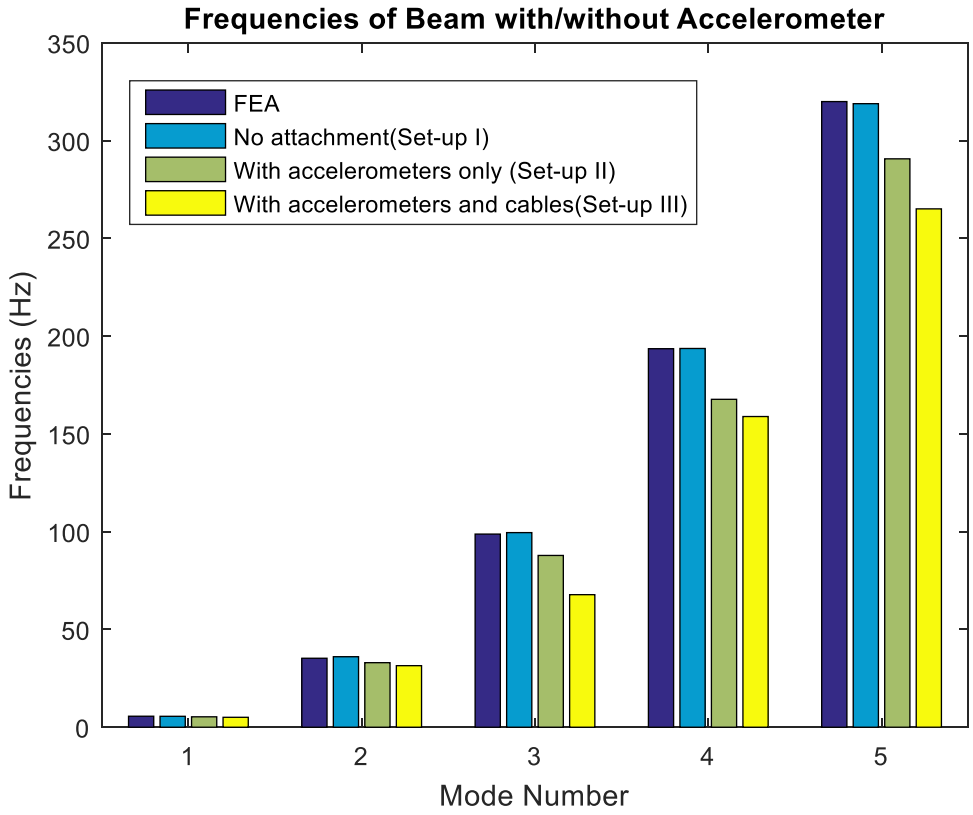

Figure 6.10. Frequencies of Beam with/without Accelerometer

The change of frequencies caused by sensor attachment can be calculated from Eq. 6.1.

$$CR_{\omega i} = \frac{\omega_{i_1} - \omega_{i_2}}{\omega_{i_1}} \tag{6.1}$$

where $CR_{\omega i}$ is the change ratio of ith frequency caused by the existence of accelerometer and/or cable, ω_{i_1} is the frequency of structural without any attachment, and ω_{i_2} is the frequencies of structure the with attachment of sensors and/or cables. The frequencies change ratio of each set-up are shown in Figure 6.11.

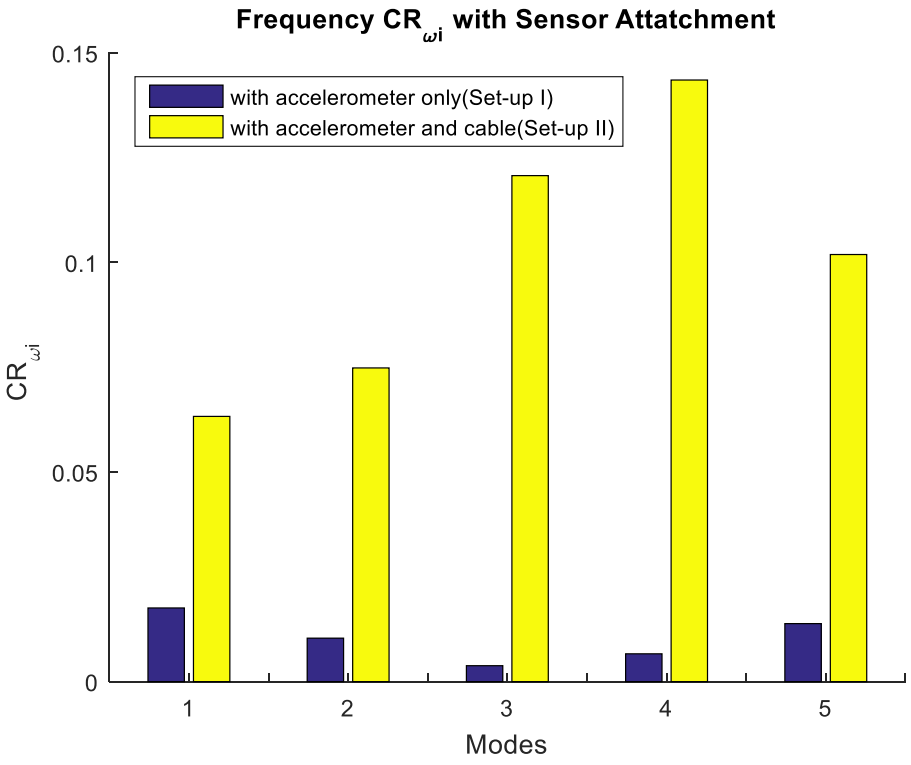

Figure 6.11. Frequencies Change Ratio, $CR_{\omega i}$ due to Contact Based Sensor

As seen in Figure 6.11, there is the maximum of 15% changes due to the attachment of sensor and its cable. There are significant changes due to the addition of cable. This indicates that non-contact based sensor and DAQ system are desired, especially, for small scale structures. In this study, the mass of accelerometer is equivalent to about 40% of an element.

Mode shapes are also extracted from SSI with different set-ups. MAC value of each mode shape correlated with theoretical mode shapes estimated using FEA are shown in Table 6.7 and the mode shapes are shown in Figure 6.12.

Table 6.7. MAC value of Beam with/without Accelerometer and Cables

Modes	Set-up I (No attachment)	Set-up II (With accelerometers and no cables)	Set-up III (With accelerometers and cable)
1	0.9999	0.9998	0.9995
2	0.9990	0.9960	0.9866
3	0.9967	0.9571	0.9424
4	0.9941	0.9512	0.9222

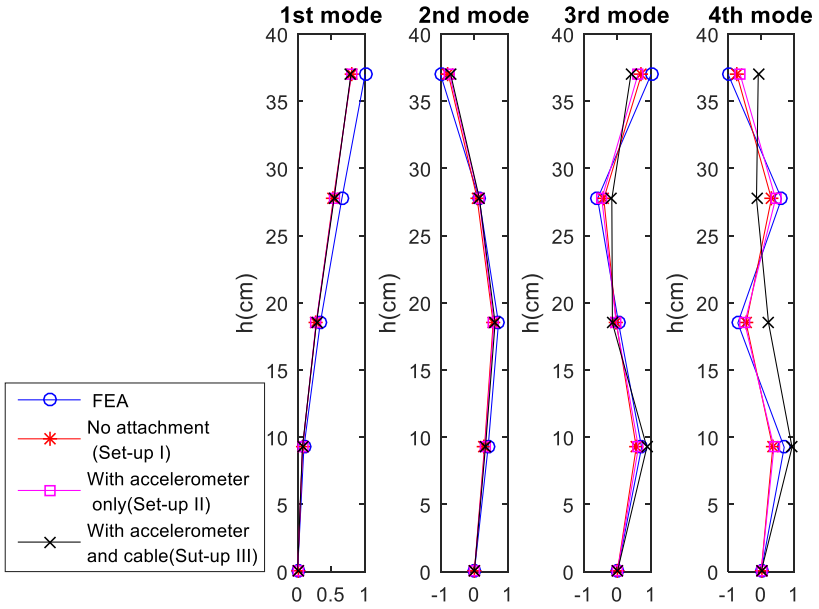

Figure 6.12. Mode Shapes of Beam with/without Accelerometers and Cables

MAC values of mode shapes with no attachment are higher than 0.98. The addition of contact based sensors reduced the MAC value. When both accelerometers and cables are attached to the beam, the MAC value decreases significantly in higher modes (i.e. 3rd and 4th mode) that are lower than the acceptable value of 0.95. This indicates that the results of the beam without the addition of mass and stiffness from sensor system are close

to the FEA results. And the additional mass and stiffness reduced the correlation between the extracted mode shapes and the FEA results.

6.3.2 Effect of Mass in McMS Method

Different levels of mass can affect the accuracy of modal scaling. Therefore, the appropriate levels of mass change should be identified. Table 6.8 listed the MAC values with FEA mode shapes of the original beam (no mass added).

Table 6.8. MAC Value of McMS Method

Modes	MAC value of Different McMS			
	No mass added	3.5% McMS	7% McMS	10.5% McMS
1	0.9999	0.9998	0.9996	0.9998
2	0.9990	0.9981	0.9973	0.9985
3	0.9967	0.9908	0.9911	0.9926
4	0.9941	0.9589	0.9562	0.9487

Table 6.8 shows a high correlation between experimentally extracted mode shapes and scaled mode shape calculated from FEA. MAC value is higher than 0.95 except for the case of 10.5% McMS. MAC value of 4th modes decreased lower than 0.95, This indicates that McMS method using 10.5% of the element mass is not acceptable.

Even through MAC values show a high correlation between varied mass McMS method and the FEA estimation, it does not mean the mode shapes are scaled. The plot of the unscaled mode shapes still shows the high discrepancy. Figure 6.13 shows unscaled mode shapes and scaled mode shapes using different McMS methods.

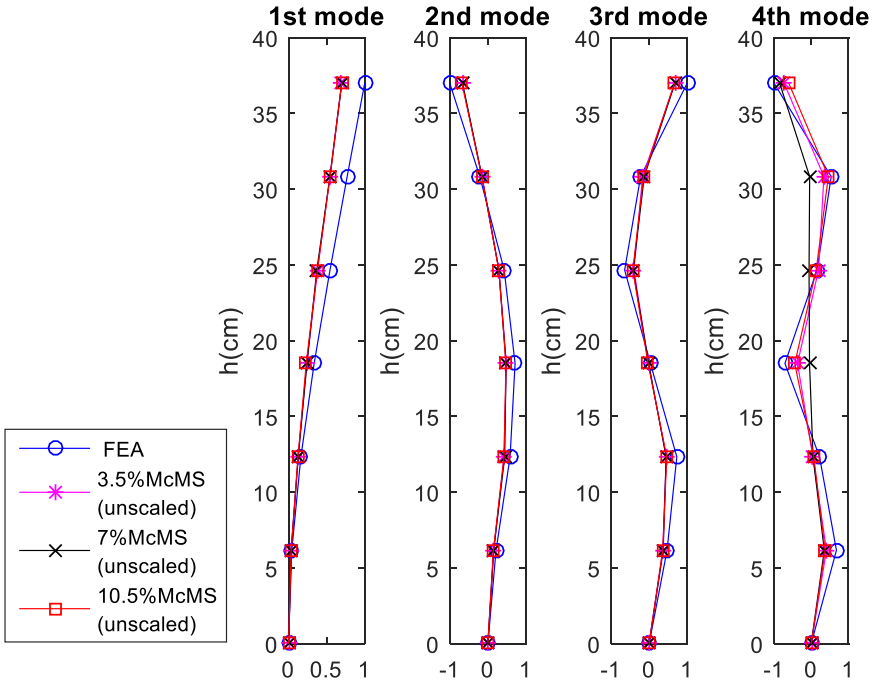

(a)

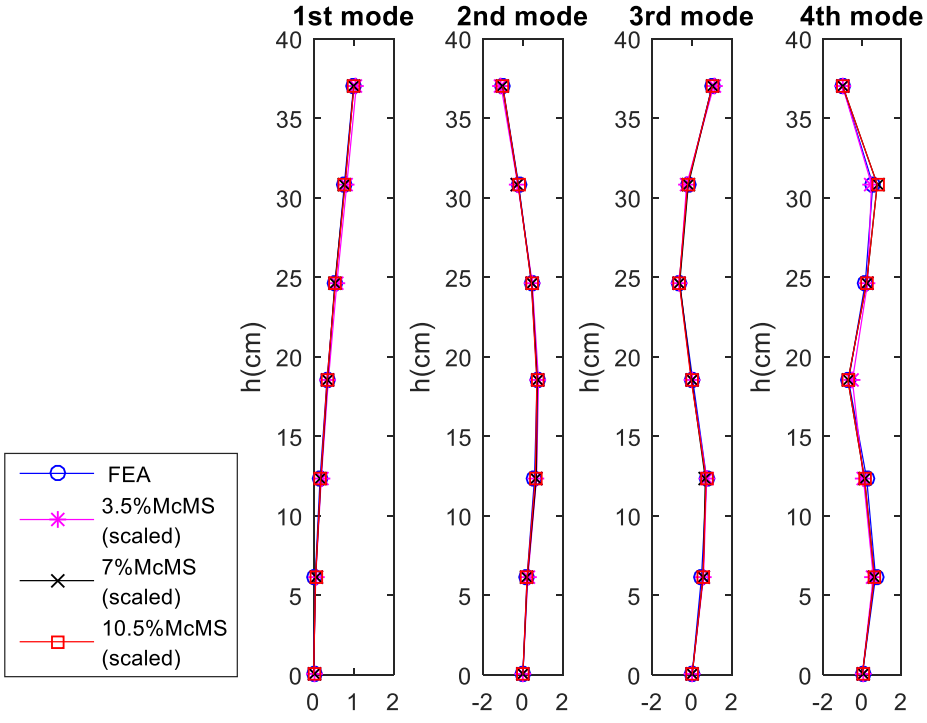

(b)

Figure 6.13. Mode Shapes of Different McMS Method

(a) Unscaled mode shapes, (b) Scaled mode shapes

McMS method scaled mode shapes for the ranges of mass from 3.5% to 10.5% of element mass. From MAC value and scaled mode shapes, the element mass of 10.5% is still a reasonable value for McMS method. In the following section of damage detection, 3.5% McMS was used.

6.3.3 Damage Assessment

Using scaled mode shape and frequencies, FEMU can be used to update the mass and stiffness of the cantilever beam. By analysing the changes in mass and stiffness matrices, locations and levels of damages in structure can be assessed.

6.3.3.1 Detection of Boundary Condition Change

The SSI is used to extract the dynamic characteristics from the displacements. Table 6.9 shows frequencies of each damage scenario of boundary condition change, compared with the frequencies of no damage structure (herein. Ref. as the baseline).

Table 6.9. Frequencies with Boundary Condition Chang

Test I.D.	Frequencies of Each Mode (Hz)				
	1	2	3	4	5
Ref.	5.59	36.05	99.53	194.50	319.20
I.B	5.33	35.80	99.02	193.98	316.11
II.B	5.08	34.28	98.01	190.40	313.3

With removing bolts at the boundary, frequencies generally decrease as the damage levels increase. The frequencies in lower modes change significantly, compared to higher modes. Mode shapes of each scenario are also extracted from the SSI. Using 3.5% McMS method, the scaled modes are found from 1st mode to 5th modes (see Figure 6.14). A total of twelve points is used to extract the frequencies and mode shapes.

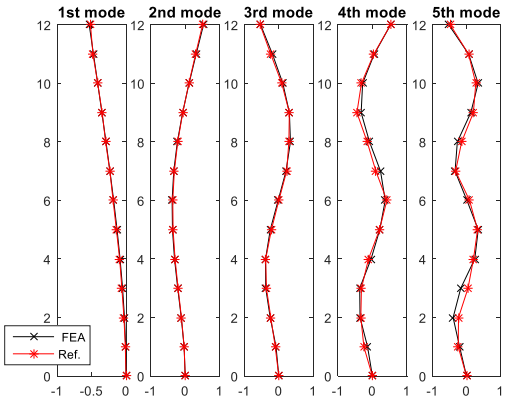

(a) FEA and Baseline (Ref.)

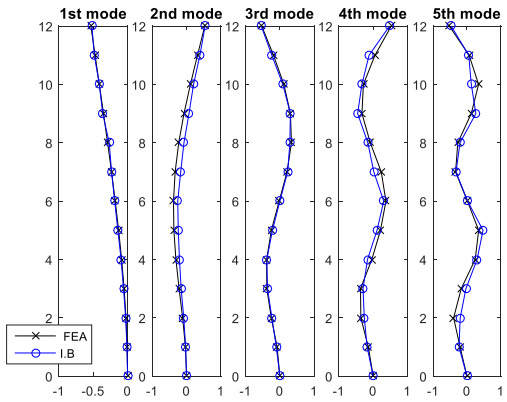

(b) FEA and I.B

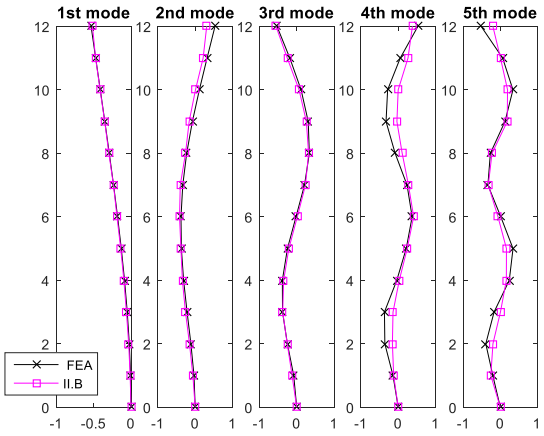

(c) FEA and II.B

Figure 6.14. Mode Shapes of FEA, I.B, II.B and Ref.

Figure 6.14 shows that the mode shapes of non-damaged structures are close to FEA mode shapes. The small discrepancy between them mostly are negligible and this

might be attributed to defects of the beam and other factors. Therefore, the measured mode shapes of the baseline represent the condition of the non-damaged beam. The MAC value between Ref. and I.B (or II.B) are listed in Table 6.10.

Table 6.10. MAC Value between Ref. and I.B, II.B.

Test I.D.	MAC Value at Each Mode				
	1	2	3	4	5
I.B	0.9989	0.9687	0.9889	0.8263	0.7955
II.B	0.9988	0.9581	0.9928	0.6376	0.5909

MAC value decreases as the mode increases. This is consistent with the observation from Figure 6.14. MAC value of mode 1, 2, and 3 is not sensitive to determine the existence of damages regarding boundary condition change. However, MAC value of mode 4 and 5 can detect the existence of damage. The MAC value of 4th mode is lower than 0.85 for I.B and 0.65 for II.B, respectively. In addition, the MAC value of 5th mode decreases further as the damage level increases. For example, the MAC value of II.B (0.59) is lower than I.B (0.796). The information is insufficient for assessing the location and severity of damage. Therefore, FEMU is applied to update mass and stiffness matrices of the beam.

Mass and stiffness of baseline (Ref.) and damaged case (I.B and II.B) are updated. Figure 6.15 shows the mass change from the mass of the baseline. When updating mass and stiffens matrices, the beam is assumed to be 4 elements.

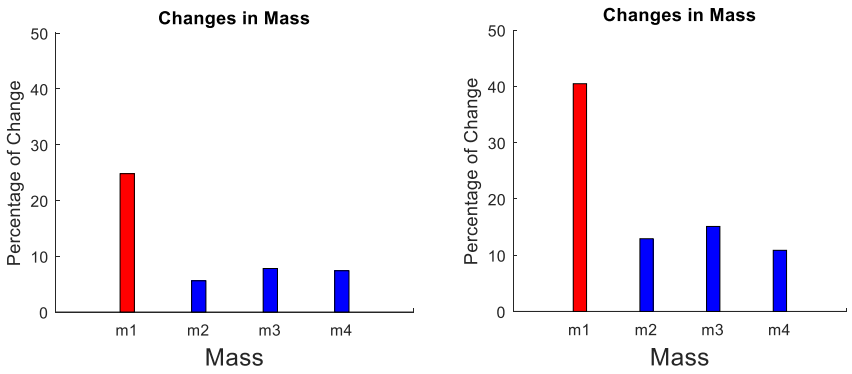

(a) (b)

Figure 6.15. Mass Changes of 4 elements
(a) I.B (loosen 2 bolts), (b) II.B (loosen 3 bolts)

Figure 6.15 shows that the mass of the first element is closest to the boundary has significant mass change, compared with other elements. The increase of mass is attributed to length change resulting from loosening bolts. It can be observed that mass change enlarged from I.B case (25%) to II.B case (40%). Therefore, the participation of mass increased due to the increase of damage level. Other elements (2, 3, and 4) have the similar level of changes of mass (about 8% in I.B and about 12% in II.B).

Stiffness changes due to boundary change are also found in Figure 6.16.

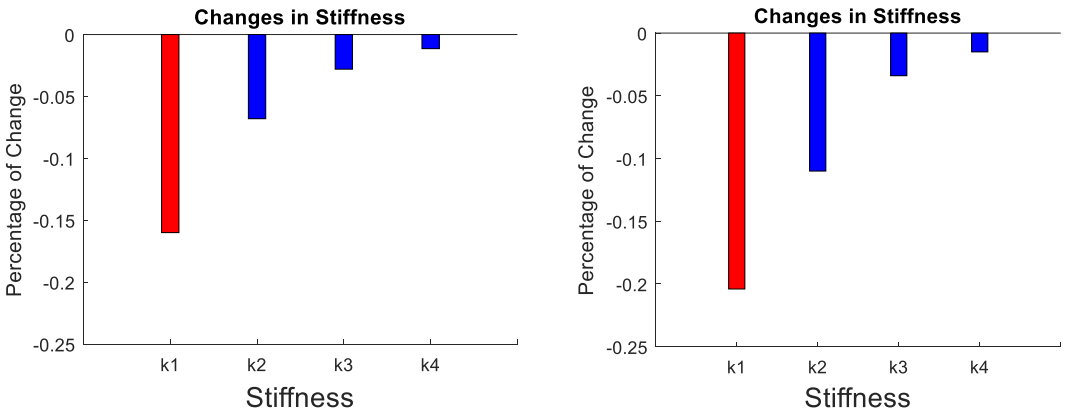

(a) (b)

Figure 6.16. Stiffness Changes pf 4 elements
(a) I.B (loosen 2 bolts), (b) II.B (loosen 3 bolts)

Figure 6.16 shows the reduction of stiffness when boundary conditions changed. The reduction of stiffness of II.B case is higher than that of I.B case. The change ratio of stiffness is less than 0.5%. However, change rates of the stiffness change are smaller than those of mass change. Even through the change rates are relatively small, the stiffness change of the first element is greater than other elements. The element 2 is also affected by the change of boundary conditions. The reduction of stiffness gradually decreases from element 1 to element 4. The location of damages is identified from mass change and stiffness change. Figures 6.15 and 6.16 show that the damage of boundary condition (I.B and II.B) leads to increase the mass in element 1 of more than 25% and decrease stiffness of less than 0.5%. The result indicates that the proposed damage detection method can detect the damage due to the change of boundary condition (such as loosen bolts).

6.3.3.2 Detection of Structural Damages and Combined Boundary Condition Change and Structural Damages

Frequencies of the beam with each damage scenario are listed in Table 6.11.

Table 6.11. Frequencies with Structural Damage with/without Boundary Condition Change

Test I.D.	Frequencies of Each Mode (Hz)				
	1	2	3	4	5
Ref.	5.59	36.05	99.53	194.50	319.20
I.S	5.08	36.82	98.26	193.22	316.62
II.S	5.59	35.29	98.00	192.71	316.88
I.BS	5.08	35.55	97.25	192.97	314.59

When the damage occurred in structure, frequencies change accordingly. However, there is the reduction of frequencies in most modes due to the damages. There is no fundamental frequency change in the damage case of I.S. Also, there is one case of the increase of frequency in the 2nd mode for the I.S case. The 3.5% McMS scaled mode shapes are shown in Figure 6.17.

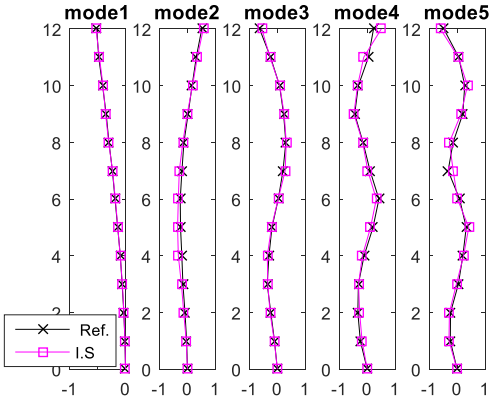

(a) Ref. and I.S

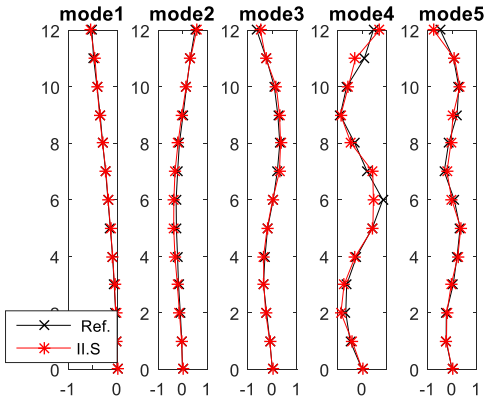

(b) Ref. and II.S

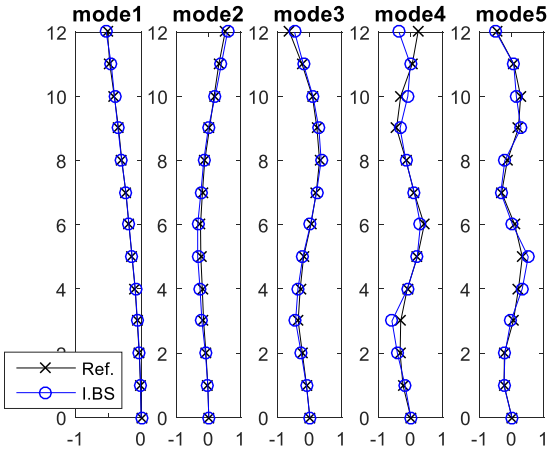

(c) Ref. and I.BS

Figure 6.17. Mode Shapes of Ref., I.S, II.S and I.BS

Figure 6.17 shows that the lower mode shapes (modes 1-3) of different damage scenarios are close to mode shapes of health condition (Ref.). As the modes increases, there is the reduction of the corresponding between mode shapes of damaged structure and undamaged structure (see Figure 6.17 mode 4 and 5). The MAC value between the baseline and different scenarios of damages are listed in Table 6.12.

Table 6.12. MAC Value between Ref. and I.S, II.S, I.BS

Test I.D.	MAC Value of Each Mode				
	1	2	3	4	5
I.S	0.9979	0.9669	0.9806	0.6589	0.7455
II.S	0.9975	0.9240	0.9823	0.8820	0.7756
I.BS	0.99836	0.9421	0.9893	0.7700	0.8527

MAC value decreases significantly as the mode increases. Especially, the fourth and fifth modes have substantially lower MAC values than other damage cases. In the cases of modes 1 through 3, the value of MAC is higher than 0.90. This is consistent with the observation from Figure 6.17. MAC values are insufficient information for assessing the location and severity of damages. FEMU is applied to update mass and stiffness matrices of the beam with different damage scenarios.

The mass change value due to damages are compared with actual mass losses is shown in Table 6.13.

Table 6.13. Comparison Mass Losses between FEMU and Actual Estimation

Mass Losses of Test I.D.								
Test I.D.	I.S				II.S			
Element	m_1	m_2	m_3	m_4	m_1	m_2	m_3	m_4
Actual Loss	0.502%	0.591%	0%	0%	0.502%	0.591%	0.502%	0.502%
FEMU	0.559%	0.641%	0.04%	0.023%	0.625%	0.646%	0.628%	0.584%

The mass losses in the element due to holes are about 0.5% that is about 0.1~0.15% lower than the estimated values of FEMU. Similarly, mass losses in the element due to cracks are about 0.6% and it is also lower than the estimation.

Mass and stiffness matrices of the baseline and I.S case are updated and the changes between them are shown in Figure 6.18.

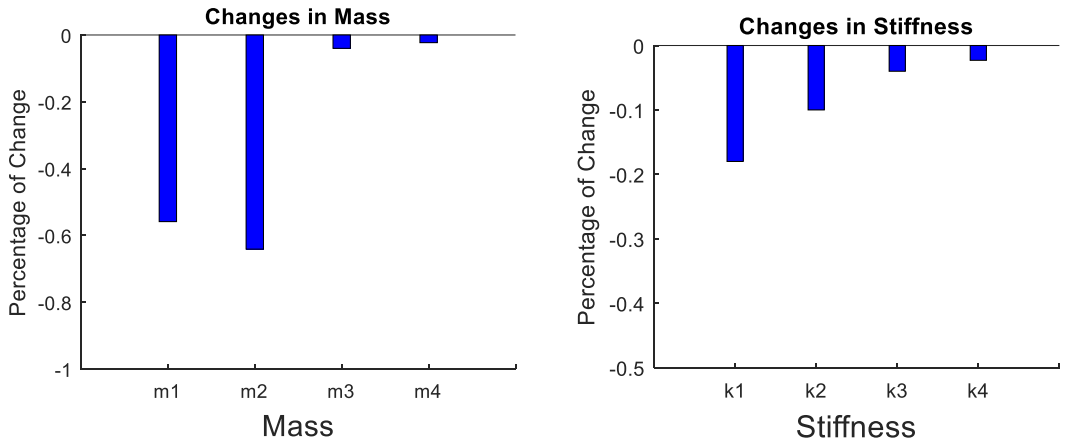

(a) I.S

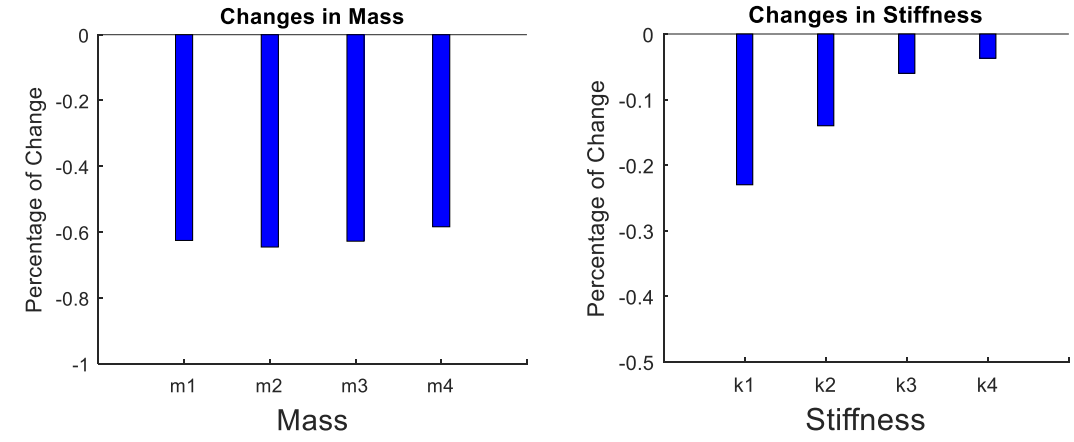

(b) II.S

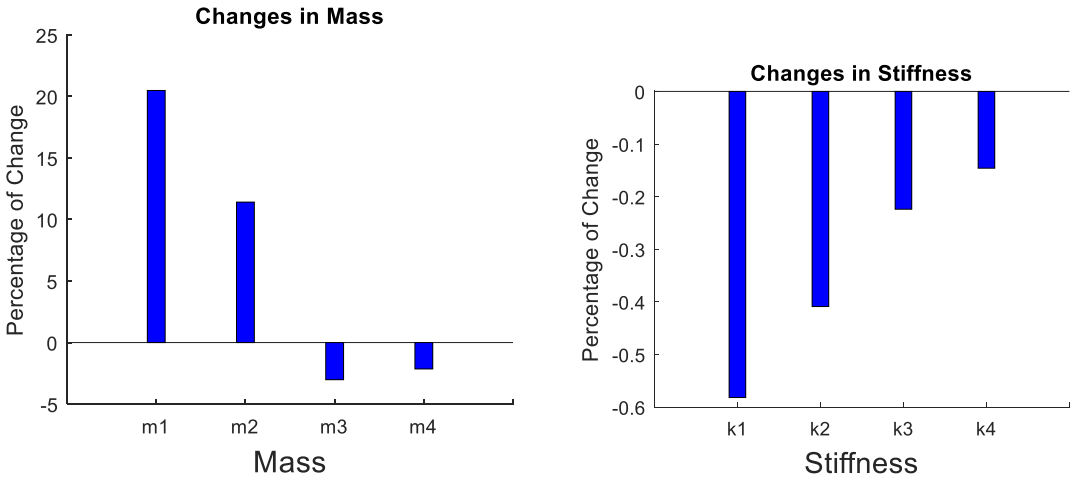

(c) I.BS

Figure 6.18. Mass and Stiffness Change of Structural Damage with/without Boundary Condition Change: (a) I.S, (b) II.S, (C) I.BS

Figure 6.18 (a) shows that the existence of a hole in element 1 leads to decrease in mass and stiffness in the element 1 (m1 and k1 in Figure 6.18 (a)). The stiffness of element 2 (k2 in Figure 6.18 (a)) has about 2 times higher change in percentage than that of element 3 due to the crack in element 2 which is close to element 1. Figure 6.18 (b) shows the reduction of mass and stiffness due to the existence of the holes and cracks in the beam. The change of mass in elements 1 through 4 have about 6%. Stiffness change is relatively high in elements 1 and 2 due to crack and a hole, compared to the change of elements 3 and 4.

Generally, the existence of a crack in element 2 leads to decrease the stiffness in elements 1 and 2. However, the magnitude of percentage changes is different in the same damage types of elements 1 and 3 in I.S and II.S cases. In the previous section, loosen bolts caused a significant increase in mass and a minimal decrease in stiffness (generally, less than 0.2%), while holes or cracks reduced both mass and stiffness. The dominant reduction is observed in mass and the similar level of reduction of stiffness which is similar to the I.B and II.B cases. Generally, stiffness change is sensitive to the existence of crack, while mass change is sensitive to holes. Both matrices can be used for damage detection.

Damage and boundary conduction change might happen at the same time (II.S+I.B), Figure 6.18 (c) shows the mass and stiffness change of I.BS case. It shows that the mass of elements 1 and 2 increases due to the boundary condition change. However, the damages of element 1 (hole) can reduce the increase of mass. As seen in Figure 6.15 (a) the mass change of element 1 is +25% (I.B). The I.S case showed the 4% reduction of mass (see Figure 6.18 (c)). The elements 3 and 4 shows the reduction of mass due to holes. Fig 6.18 (c) shows higher stiffness change compared to other damage cases. When comparing the change of stiffness in I.BS case with that of II.S and I.B, individually, the total of stiffness change seems to be the total reduction of II.S and I.B. For example, element 1 of I.BS case has significant reduction of stiffness compared to k1 in II.S case.

6.4 Summary

(1) Frequencies decrease as the damage level of boundary condition damage level increases. Mode shapes have lower corresponding between I.B and II.B cases and health condition, especially in higher modes.

(2) When boundary condition changes, the mass of the element closest to boundary has significant increases due to the increase of the effective length of the element. The stiffness of the structure has the minimal reduction of less than 0.6%. Even through the magnitude of stiffness change is small, the changes can still detect the location of the damage.

(3) Mass matrices are sensitive to damage types such as holes on the structure, while stiffness is more sensitive to damage such as cracks. Holes in structure do not change stiffness, significantly. Both matrices need to be estimated to detect damages and assess their locations and levels.

(4) The location and level of damage can be detected with the magnitude of mass and/or stiffness change from FEMU. When multiple damage scenario occures in the structure, the amount of mass and/or stiffness change in each element needs to be evaluated. Generally, the mass reduction estimated from FEMU is close to the actual mass reduction. However, there are slight overestimation of algorithm results, compared to the actual reduction of mass due to damages.

CHAPTER 7

SUMMARY, CONCLUSIONS AND RECOMMENDATIONS

This dissertation has proposed and validated an innovative structural damage detection method and a non-contacted based modal scaling method. This research has shown a potential application of the non-contact based sensor into the system identification and damage assessment of the structure. Both simulation and experimental program are conducted. The following summary and conclusions are presented followed by future recommendations.

7.1 Summary

This research is motivated by the need to improve the efficiency and reduce the costs for structural health monitoring. The works of this dissertation:

(1) proposed and validated a structural damage assessment algorithm using displacements as only input and system matrices as damage indicator.

Acceleration of structure under vibration has been the most popular input for dynamic characteristics extraction using either OMA or EMA. However, the installation, location and available number of sensors have limitations in the response acquisition

process. With the development of motion detection techniques, displacements of structure can be detected without interrupting the operation of structures. To use these advantages in data acquisition, the corresponding algorithms needs to be adopted and analyzed. The adopted SSI algorithm use displacements of structure acquired from ambient excitation as the only input to extract dynamic characteristics.

Dynamic characteristics such as frequencies and mode shapes have been used as an indicator for damage detection. However, they are insufficient to detect the location and its severity of damages. To achieve a higher level SHM, mass and stiffness are proposed to be used as the damage indicator. Direct FEMU methods are used to obtain the system matrices (mass and stiffness) from displacements of structural vibration. The mode shapes extracted from SSI should be scaled before updating system matrices. Mass change scaling method (McMS) is used to obtain the scaled mode shapes for updating.

The proposed integration of methods is validated by a numerical simulation with four-story frame structure model. The effect of different loading type and noise in the vibration response is analyzed. Different scenarios of damage is simulated in the numerical model and the capability of proposed damage detection method is validated. An experimental test on a cantilever beam is conducted. Displacements of the cantilever beam acquired from non-contact based optical sensor are used as the input for damage detection method. Different amounts of mass are added to obtain scaled mode shapes. The applicability of different ratio of mass to element mass is evaluated. Different damage scenarios are designed and damages are applied in the beam, the capability of the proposed method in detecting damage is evaluated through the experimental program.

(2) proposed a non-contacted based modal scaling method using temperature change for revising the potential of non-contacted based operational SHM.

The proposed integrated algorithm with adopting three algorithms in the first stage is verified to be a rational method to assess damages with their locations and severities. However, McMS method still requires the contact to modify the mass of structures. To achieve non-contact SHM of the entire process, a model scaling method based on temperature change is proposed in the dissertation: Temperature change Modal Scaling (TcMS)

Numerical simulation of the four-story steel frame model is used to validate the proposed modal scaling method. Different temperature change is conducted in the simulation. The effect of the magnitude of temperature change is analyzed through the simulation. Both uniform and non-uniform temperature change are used in the numerical validation.

The proposed TcMS method seems to replace the McMS in the proposed algorithm integration, and the damage detection method can be non-contact based through the entire process. A numerical model of the nine-member truss is used to verify this integration. TcMS method uses the fact that temperature change would lead to change in structural dynamic characteristics for scaling. In the future, the experimental validation is required to prove the applicability of TcMS method.

7.2 Conclusions

Numerical simulations and experimental program are conducted in this study and following conclusions are drawn:

(1) Loading type doesn't significantly affect the accuracy of SSI regarding the extracting of frequencies and damping ratios. However, the mode shapes extracted from SSI of the structure under short time span of air blast leads to increase some discrepancy. This indicates that under some circumstance such as explosion, the proposed method may not be applicable.

(2) Higher noise added on the response causes higher adverse impacts on the accuracy of SSI results. When noise level is lower than 100% of the maximum amplitude of response added on the input, frequencies extracted have an error of less than 1%. When increasing the noise level up to 125%, the frequency errors also increased, especially, at the higher modes. The conclusion can be drawn that SSI can accurately extract the dynamic characteristics in the noise lever of lower than 75%.

(3) Proposed TcMS demonstrates the applicability of mode shape scaling within the ranges of $\pm 10℃$ changes of structures. It is also validated using scenarios of both uniform and non-uniform temperature change distribution over the structure.

(4) FEMU can accurately update the system matrices and detect the damage in both numerical simulation and experimental validation. The proposed combination of two direct updating method has improved the accuracy by reducing the error.

The change of stiffness and/or mass caused by damages can be identified using FEMU with their locations and levels of change.

(5) The dynamic characteristics of the structure are affected by contact based sensors and their cables. The experimental test program and results show the significant reduction of frequencies when accelerometers and their cables are attached to the beam. The effects also shown in mode shapes. The dynamic characteristics obtained from the non-contact based sensor are very close to FEA estimation of the cantilever beam.

(6) McMS can successfully scale the mode shapes of the cantilever beam with a mass change ranging from 3% to 10% of the element mass. However, when the mass change exceeds 10%, the accuracy of mode shapes scaling decreases.

(7) Boundary condition change causes the reduction of frequencies and MAC value. And structural damages such as holes and cut-downs (cracks) change frequencies and MAC values, accordingly. The proposed method is experimentally verified to identify the locations and severities of damages in the beam.

(8) The experimental program and results show that the mass reduction due to holes and crack estimated by the proposed method is close to actual mass reduction. However, there are the overestimation of 0.1~0.15% in the damaged elements that have 0.5% of mass reduction. Also, there aer estimations of slight damages ($\leq 0.1\%$) in undamaged elements.

7.3 Recommendations

There are several areas or directions of future study, which we could further enhance the work presented in this dissertation.

(1) The dynamic characteristics extraction method can be improved for the structure under loading types such as air blast. And other loading types can be analyzed as well.

(2) Stiffness prediction is needed and the error control of non-damaged element needs to be developed.

(3) The stiffness thermal coefficient of materials other than steel should be estimated. The most civil structures are constructed using the combination of different construction materials. Therefore, the validation of this method is needed in further simulation and experimental program. In this manner, the TcMS method can be applied to more structure types.

(4) Environmental effects such as moisture and wind can be considered in damage assessment to increase the accuracy and robustness of the proposed algorithm..

(5) The proposed damage detection method needs to be validated using additional types of structures in simulation, experimental and field testing programs.

REFERENCES

Aenlle, M., and Brincker, R. (2013). "Modal scaling in operational modal analysis using a finite element model." *International Journal of Mechanical Sciences*, 76, 86-101.

Ågårdh, L. (1991). "Modal analyses of two concrete bridges in Sweden." *Structural Engineering International*, 1(4), 35-39.

Akaike, H. (1975). "Markovian representation of stochastic processes by canonical variables." *SIAM Journal on Control*, 13(1), 162-173.

Alampalli, S., Fu, G., and Aziz, I. A. "Modal analysis as a bridge inspection tool." *Proc., Proceedings of The International Modal Analysis Conference*, SEM Society for Experimental Mechanics Inc. , 1358-1358.

Alvin, K. (1997). "Finite element model update via Bayesian estimation and minimization of dynamic residuals." *AIAA Journal*, 35(5), 879-886.

Alvin, K., Robertson, A., Reich, G., and Park, K. (2003). "Structural system identification: from reality to models." *Computers & Structures*, 81(12), 1149-1176.

Antunes, P., Travanca, R., Rodrigues, H., Melo, J., Jara, J., Varum, H., and André, P. (2012). "Dynamic structural health monitoring of slender structures using optical sensors." *Sensors*, 12(5), 6629-6644.

ASCE (2017). "ASCE Infrastructure Report Card." http://www.infrastructurereportcard.org/cat-item/roads/

Au, S.-K. (2011). "Fast Bayesian FFT method for ambient modal identification with separated modes." *Journal of Engineering Mechanics*, 137(3), 214-226.

Baruch, M. (1978). "Optimization procedure to correct stiffness and flexibility matrices using vibration tests." *AIAA Journal*, 16(11), 1208-1210.

Berman, A., and Nagy, E. (1983). "Improvement of a large analytical model using test data." *AIAA Jjournal*, 21(8), 1168-1173.

Berman, A., and Nagy, E. J. (1983). "Improvement of a Large Analytical Model Using Test Data." *AIAA Journal*, 21(8), 1168-1173.

Bernal, D. (2004). "Modal scaling from known mass perturbations." *Journal of Engineering Mechanics*, 130(9), 1083-1088.

Blevins, R. D., and Plunkett, R. (1980). "Formulas for natural frequency and mode shape." *Journal of Applied Mechanics*, 47, 461.

Boonyapinyo, V., and Janesupasaeree, T. (2010). "Data-driven stochastic subspace identification of flutter derivatives of bridge decks." *Journal of Wind Engineering and Industrial Aerodynamics*, 98(12), 784-799.

Bradford, S. C., Clinton, J. F., Favela, J., and Heaton, T. (2004). "Results of Millikan Library forced vibration testing." *Forced Vibration Testing.* California Institute of Technology. (Unpublished), http://resolver.caltech.edu/CaltechEERL:EERL-2004-03

Brincker, R., and Andersen, P. "A Way of Getting Scaled Mode Shapes in Output Only Modal Analyis." *Proc., of the International Modal Analysis Conference (IMAC) XXI, paper 141*, Citeseer,141.

Brincker, R., Andersen, P., Møller, N., and Herlufsen, H. "Output only modal testing of a car body subject to engine excitation." *Proc. of the 18th International Modal Analysis Conference, San Antonio, Texas*.

Brincker, R., Rodrigues, J., Andersen, P., and Aps, S. V. S. (2004). "Scaling the mode shapes of a building model by mass changes." *Proceeding of the 22nd IMAC*, 119-126

Brincker, R., Ventura, C., and Andersen, P. "Why output-only modal testing is a desirable tool for a wide range of practical applications." *Proc. of the International Modal Analysis Conference (IMAC) XXI, paper*.

Brockenbrough, R. L., and Merritt, F. S. (1999). *Structural steel designer's handbook*, McGraw-Hill New York.

Brownjohn, J., Magalhaes, F., Caetano, E., and Cunha, A. (2010). "Ambient vibration re-testing and operational modal analysis of the Humber Bridge." *Engineering Structures*, 32(8), 2003-2018.

Buckner, B. D., Markov, V., Lai, L.-C., and Earthman, J. C. (2008). "Laser-scanning structural health monitoring with wireless sensor motes." *Optical Engineering*, 47(5), 054402-054409.

Caesar, B., and Peter, J. (1987). "Direct update of dynamic mathematical models from modal test data." *AIAA Journal*, 25(11), 1494-1499.

Caicedo, J. M., Dyke, S. J., and Johnson, E. A. (2004). "Natural excitation technique and eigensystem realization algorithm for phase I of the IASC-ASCE benchmark problem: Simulated data." *Journal of Engineering Mechanics*, 130(1), 49-60.

Cao, M., Sha, G., Gao, Y., and Ostachowicz, W. (2016). "Structural Damage Identification Using Damping: A Compendium of Uses and Features." *Smart Materials and Structures*. 1361-665X.

Capecchi, D., and Vestroni, F. (1999). "Monitoring of structural systems by using frequency data." *Earthquake engineering & structural dynamics*, 28(5), 447-461.

Carvalho, J., Datta, B. N., Gupta, A., and Lagadapati, M. (2007). "A direct method for model updating with incomplete measured data and without spurious modes." *Mechanical Systems and Signal Processing*, 21(7), 2715-2731.

Cha, Y.-J., Chen, J. G., and Buyukozturk, O. (2015). "motion magnification based damage detection using high speed video." *the 10th International Workshop on Structural Health Monitoring*. 1-3.

Chang, C.-M., and Loh, C.-H. (2015). "Improved Stochastic Subspace System Identification for Structural Health Monitoring." *Journal of Physics: Conference Series*, 628(1), 12010.

Chang, P. C., Flatau, A., and Liu, S. (2003). "Review paper: Health Monitoring of Civil Infrastructure." *Structural health monitoring*, 2(3), 257-267.

Chase, S. B., and Laman, J. A. (2000). "Dynamics and field testing of bridges." *Transportation in the New Millennium: State of The Art and Duture Directions*.

Chen, J. G., Wadhwa, N., Cha, Y.-J., Durand, F., Freeman, W. T., and Buyukozturk, O. (2014). "Structural modal identification through high speed camera video: Motion magnification." *Topics in Modal Analysis I, Volume 7*, Springer, 191-197.

Chen, J. G., Wadhwa, N., Cha, Y.-J., Durand, F., Freeman, W. T., and Buyukozturk, O. (2015). "Modal identification of simple structures with high-speed video using motion magnification." *Journal of Sound and Vibration*, 345, 58-71.

Cobb, R. G., and Liebst, B. S. (1997). "Sensor placement and structural damage identification from minimal sensor information." *AIAA Journal*, 35(2), 369-374.

Cobb, R. G., and Liebst, B. S. (1997). "Structural damage identification using assigned partial eigenstructure." *AIAA Journal*, 35(1), 152-158.

Coppotelli, G. (2009). "On the estimate of the FRFs from operational data." *Mechanical Systems and Signal Processing*, 23(2), 288-299.

Cury, A., Cremona, C., and Dumoulin, J. (2012). "Long-term monitoring of a PSC box girder bridge: Operational modal analysis, data normalization and structural modification assessment." *Mechanical Systems and Signal Processing*, 30(33), 13-37.

Devriendt, C., Magalhães, F., Weijtjens, W., De Sitter, G., Cunha, Á., and Guillaume, P. (2014). "Structural health monitoring of offshore wind turbines using automated operational modal analysis." *Structural Health Monitoring*, 13(6), 644-659.

Doebling, S. W., Farrar, C. R., and Prime, M. B. (1998). "A summary review of vibration-based damage identification methods." *Shock and Vibration Digest*, 30(2), 91-105.

Doebling, S. W., Farrar, C. R., Prime, M. B., and Shevitz, D. W. (1996). "Damage identification and health monitoring of structural and mechanical systems from changes in their vibration characteristics: a literature review."

Dorvash, S. (2013). "Structural Health Monitoring and Application of Wireless Sensor Networks." Dissertation, *Lehigh University*

Elsner, J. B., and Tsonis, A. A. (2013). *Singular spectrum analysis: a new tool in time series analysis*, Springer Science & Business Media.

Ewins, D. J. (2000). *Modal testing : theory, practice, and application*, Research Studies Press, Baldock, Hertfordshire, England, vol(15).

Fan, J., Zhang, Z., and Hua, H. (2007). "Data processing in subspace identification and modal parameter identification of an arch bridge." *Mechanical Systems and Signal Processing*, 21(4), 1674-1689.

Fang, S.-E., Perera, R., and De Roeck, G. (2008). "Damage identification of a reinforced concrete frame by finite element model updating using damage parameterization." *Journal of Sound and Vibration*, 313(3), 544-559.

Farrar, C., and James III, G. (1997). "System identification from ambient vibration measurements on a bridge." *Journal of Sound and Vibration*, 205(1), 1-18.

Farrar, C. R., and Cone, K. M. (1994). "Vibration testing of the I-40 bridge before and after the introduction of damage." Los Alamos National Lab., NM (United States).

Farrar, C. R., Doebling, S. W., Cornwell, P. J., and Straser, E. G. "Variability of modal parameters measured on the Alamosa Canyon Bridge." *Proc., The International Society for Optical Engineering*, SPIE 257-263.

Farrar, C. R., Doebling, S. W., and Nix, D. A. (2001). "Vibration–based structural damage identification." *Philosophical Transactions of the Royal Society of London A: Mathematical, Physical and Engineering Sciences*, 359(1778), 131-149.

Farrar, C. R., and Worden, K. (2007). "An introduction to structural health monitoring." *Philosophical Transactions of the Royal Society of London A: Mathematical, Physical and Engineering Sciences*, 365(1851), 303-315.

Fox, C. "The location of defects in structures: a comparison of the use of natural frequency and mode shape data." *Proc., International Modal Analysis Conference*, SEM 522-522.

Friswell, M., and Mottershead, J. E. (1995). *Finite element model updating in structural dynamics*, Springer Science & Business Media.

Friswell, M., and Penny, J. "Is damage location using vibration measurements practical?" *Proceedings of EUROMECH 365 international workshop: DAMAS*.

Friswell, M. I., and Mottershead, J. E. (1995). *Finite element model updating in structural dynamics*, Kluwer Academic Publishers, Dordrecht; Boston, vol.(38).

Fritzen, C.-P., Jennewein, D., and Kiefer, T. (1998). "Damage detection based on model updating methods." *Mechanical Systems and Signal Processing*, 12(1), 163-186.

Gentile, C., and Bernardini, G. (2008). "Output-only modal identification of a reinforced concrete bridge from radar-based measurements." *NDT & E International*, 41(7), 544-553.

Gentile, C., and Gallino, N. (2008). "Ambient vibration testing and structural evaluation of an historic suspension footbridge." *Advances in Engineering Software*, 39(4), 356-366.

Ghasemi, H., Canizares, C., and Moshref, A. (2006). "Oscillatory stability limit prediction using stochastic subspace identification." *IEEE Transactions on Power Systems*, 21(2), 736-745.

Gontier, C. (2005). "Energetic classifying of vibration modes in subspace stochastic modal analysis." *Mechanical Systems and Signal Processing*, 19(1), 1-19.

Grosse, C. U., and Krüger, M. "Wireless acoustic emission sensor networks for structural health monitoring in civil engineering." *Proc. European Conf. on Non-Destructive Testing (ECNDT), DGZfP BB-103-CD*, Citeseer.

Grouve, W., Warnet, L., De Boer, A., Akkerman, R., and Vlekken, J. (2008). "Delamination detection with fibre Bragg gratings based on dynamic behaviour." *Composites Science and Technology*, 68(12), 2418-2424.

Halling, M. W., Muhammad, I., and Womack, K. C. (2001). "Dynamic field testing for condition assessment of bridge bents." *Journal of Structural Engineering*, 127(2), 161-167.

Hanson, D. (2006). "Operational modal analysis and model updating with a cyclostationary input." The University of New South Wales Australia.

Hay, J. R. (2011). "High Dynamic Range Imaging for The Detection of Motion." PhD Dissertation, University of Louisville.

Hay, J. R., Kielkopf, J. F., and Clark, F. O. (2012). "Non-contact stand-off optical sensing of cable vibrations for monitoring structural health of the William H. Harsha Bridge." *15th International Conference on Experimental Mechanics*, ICEM, Porto, Portugal, VOL.3019.

Hearn, G., and Testa, R. B. (1991). "Modal analysis for damage detection in structures." *Journal of Structural Engineering*, 117(10), 3042-3063.

Hermans, L., and Van der Auweraer, H. (1999). "Modal testing and analysis of structures under operational conditions: industrial applications." *Mechanical Systems and Signal Processing*, 13(2), 193-216.

Holt, R., and Hartmann, J. (2008). "Adequacy of the U10&L11 Gusset Plate Design for the Minnesota Bridge No. 9340."National Transportation Safety Board.

James III, G. H., Carne, T. G., and Lauffer, J. P. (1993). "The natural excitation technique (NExT) for modal parameter extraction from operating wind turbines." Sandia National Labs., Albuquerque, NM (United States).

Jang, J.-H., Yeo, I., Shin, S., and Chang, S.-P. (2002). "Experimental investigation of system-identification-based damage assessment on structures." *Journal of Structural Engineering*, 128(5), 673-682.

Kawchuk, G. N., Decker, C., Dolan, R., and Carey, J. (2009). "Structural health monitoring to detect the presence, location and magnitude of structural damage in cadaveric porcine spines." *Journal of Biomechanics*, 42(2), 109-115.

Khatibi, M., Ashory, M., and Malekjafarian, A. "Scaling of mode shapes using mass-stiffness change method." *Proc., Proceedings of the International Operational Modal Analysis Conference (IOMAC). Copenhagen, Denmark*, 699-706.

Khatibi, M., Ashory, M., Malekjafarian, A., and Brincker, R. (2012). "Mass–stiffness change method for scaling of operational mode shapes." *Mechanical Systems and Signal Processing*, 26, 34-59.

Kielkopf, J. F., and Hay, J. (2014). "System and Method for Precision Measurement of Position, Motion and Resonances." Google Patents, April 8 Patent No. 8693735.

Kiesel, S., Peters, K., Hassan, T., and Kowalsky, M. (2007). "Behaviour of intrinsic polymer optical fibre sensor for large-strain applications." *Measurement Science and Technology*, 18(10), 3144.

Kirkegaard, P. H., and Rytter, A. (1995). "Vibrational Based Inspection of A Steel Mast." Proc. of the 12th International Modal Analysis, Vol. 2251 p. 1602

Lam, H., Ko, J., and Wong, C. (1998). "Localization of damaged structural connections based on experimental modal and sensitivity analysis." *Journal of Sound and Vibration*, 210(1), 91-115.

Lam, H. F., Katafygiotis, L. S., and Mickleborough, N. C. (2004). "Application of a statistical model updating approach on phase I of the IASC-ASCE structural health monitoring benchmark study." *Journal of engineering mechanics*, 130(1), 34-48.

Li, Z. (2011). "Subspace identification for structural health monitoring."

Liu, C., Olund, J., Cardini, A., D'Attilio, P., Feldblum, E., and DeWolf, J. (2008). "Structural health monitoring of bridges in the State of Connecticut." *Earthquake Engineering and Engineering Vibration*, 7(4), 427-437.

Liu, P.-L. (1995). "Identification and damage detection of trusses using modal data." *Journal of Structural Engineering*, 121(4), 599-608.

López-Aenlle, M., Brincker, R., Pelayo, F., and Canteli, A. F. (2012). "On exact and approximated formulations for scaling-mode shapes in operational modal analysis by mass and stiffness change." *Journal of Sound and Vibration*, 331(3), 622-637.

López-Higuera, J. M. (2002). *Handbook of optical fibre sensing technology*, Wiley.

López Aenlle, M., Brincker, R., and Fernández Canteli, A. C. (2005). "Some methods to determine scaled mode shapes in natural input modal analysis." *International Modal Analysis Conference* SEM, Orlando, FL.

López Aenlle, M., Brincker, R., Fernández Canteli, A. C., and Villa García, L. M. (2005). "Scaling factor estimation by the mass change method."Proc. of International Operational Modal Analysis Conference, 2005

Magalhães, F., Cunha, Á., and Caetano, E. (2009). "Online automatic identification of the modal parameters of a long span arch bridge." *Mechanical Systems and Signal Processing*, 23(2), 316-329.

Mahmoud, M., Abe, M., and Fujino, Y. "Analysis of suspension bridge by ambient vibration measurement using time domain method and its application to health monitoring." *Proceedings of the International Modal Analysis Conference-IMAC*, 504-510.

Mascarenas, D. D. L., Flynn, E. B., Todd, M. D., Overly, T. G., Farinholt, K. M., Park, G., and Farrar, C. R. (2010). "Development of capacitance-based and impedance-based wireless sensors and sensor nodes for structural health monitoring applications." *Journal of Sound and Vibration*, 329(12), 2410-2420.

Mayes, R. L. (1992). "Error localization using mode shapes-an application to a two link robot arm." *The International Modal Analysis Conference*, SEM, San Diego, CA.

MC90, C. (1993). "Design of Concrete Structures. CEB-FIP Model Code 1990." Thomas Telford.

Mirza, M. S., Ferdjani, O., Hadj-Arab, A., Joucdar, K., Khaled, A., and Razaqpur, A. (1990). "An experimental study of static and dynamic responses of prestressed concrete box irder bridges." *Canadian Journal of Civil Engineering*, 17(3), 481-493.

Mita, A. "Emerging needs in Japan for health monitoring technologies in civil and building structures." *Proc. Second International Workshop on Structural Health Monitoring*, 56-67.

Monkman, G., and Connolly, C. (2005). "High-speed cameras and laser doppler vibrometers." *Sensor Review*, 25(2), 100-104.

Moss, R., and Matthews, S. (1995). "In-service structural monitoring. a state of the art review." *Structural Engineer*, 73(2), 265.

Naeim, F. (1989). *The seismic design handbook*, Springer Science & Business Media.

Ojeda, A. P. (2012). "MATLAB implementation of an operational modal analysis technique for vibration-based structural health monitoring." Massachusetts Institute of Technology.

Olsson, D. M., and Nelson, L. S. (1975). "The Nelder-Mead simplex procedure for function minimization." *Technometrics*, 17(1), 45-51.

Ooijevaar, T., Loendersloot, R., Warnet, L., De Boer, A., and Akkerman, R. (2010). "Vibration based Structural Health Monitoring of a composite T-beam." *Composite Structures*, 92(9), 2007-2015.

Overschee, P. v., and Moor, B. L. R. d. (1996). *Subspace identification for linear systems : theory, implementation, applications*, Kluwer Academic Publishers, Boston, p. 14-17.

Parloo, E., Guillaume, P., Anthonis, J., Heylen, W., and Swevers, J. (2003). "Modelling of sprayer boom dynamics by means of maximum likelihood identification techniques, part 1: a comparison of input-output and output-only modal testing." *Biosystems Engineering*, 85(2), 163-171.

Parloo, E., Verboven, P., Guillaume, P., and Van Overmeire, M. (2002). "Autonomous structural health monitoring—Part II: Vibration-based in-operation damage assessment." *Mechanical Systems and Signal Processing*, 16(4), 659-675.

Pastor, M., Binda, M., and Harčarik, T. (2012). "Modal Assurance Criterion." *Procedia Engineering*, 48(1), 543-548.

Patil, D. P., and Maiti, S. K. (2005). "Experimental verification of a method of detection of multiple cracks in beams based on frequency measurements." *Journal of Sound and Vibration*, 281(1–2), 439-451.

Peeters, B., and De Roeck, G. (2001). "One-year monitoring of the Z 24-Bridge: environmental effects versus damage events." *Earthquake Engineering & Structural Dynamics*, 30(2), 149-171.

Pintelon, R., Guillaume, P., Rolain, Y., Schoukens, J., and Van Hamme, H. (1994). "Parametric identification of transfer functions in the frequency domain-a survey." *IEEE Transactions on Automatic Control*, 39(11), 2245-2260.

Pothisiri, T., and Hjelmstad, K. (2003). "Structural damage detection and assessment from modal response." *Journal of Engineering Mechanics*, 129(2), 135-145.

Qin, S., Kang, J., and Wang, Q. (2016). "Operational modal analysis based on subspace algorithm with animproved stabilization diagram method." *Shock and Vibration*, 2016.

Rainieri, C., and Fabbrocino, G. (2014). "Operational modal analysis of civil engineering structures." Springer, p.156

Ramos, L. F., Aguilar, R., and Lourenço, P. B. (2011). "Operational modal analysis of historical constructions using commercial wireless platforms." *Structural Health Monitoring*, 10(5), 511-521.

Reynders, E., Pintelon, R., and De Roeck, G. (2008). "Uncertainty bounds on modal parameters obtained from stochastic subspace identification." *Mechanical Systems and Signal Processing*, 22(4), 948-969.

Reynders, E., Teughels, A., and De Roeck, G. (2010). "Finite element model updating and structural damage identification using OMAX data." *Mechanical Systems and Signal Processing*, 24(5), 1306-1323.

Ruotolo, R., and Surace, C. (1999). "Using SVD to detect damage in structures with different operational conditions." *Journal of Sound and Vibration*, 226(3), 425-439.

Rytter, A. (1993). "Vibration based inspection of civil engineering structures." Ph.D. Dissertation, Aalborg University, p.08.

Salane, H., and Baldwin Jr, J. (1990). "Identification of modal properties of bridges." *Journal of Structural Engineering*, 116(7), 2008-2021.

Salawu, O. (1997). "Detection of structural damage through changes in frequency: a review." *Engineering structures*, 19(9), 718-723.

Shih, C., Tsuei, Y., Allemang, R., and Brown, D. (1988). "Complex mode indication function and its applications to spatial domain parameter estimation." *Mechanical systems and Signal Processing*, 2(4), 367-377.

Sikorsky, C., Stubbs, N., Park, S., Choi, S., and Bolton, R. "Measuring bridge performance using modal parameter based non-destructive damage detection." *SPIE proceedings series*, Society of Photo-Optical Instrumentation Engineers, 1223-1229.

Siringoringo, D. M., and Fujino, Y. (2008). "System identification of suspension bridge from ambient vibration response." *Engineering Structures*, 30(2), 462-477.

Smyth, A., and Wu, M. (2007). "Multi-rate Kalman filtering for the data fusion of displacement and acceleration response measurements in dynamic system monitoring." *Mechanical Systems and Signal Processing*, 21(2), 706-723.

Sohn, H. (2007). "Effects of environmental and operational variability on structural health monitoring." *Philosophical Transactions of the Royal Society of London A: Mathematical, Physical and Engineering Sciences*, 365(1851), 539-560.

Sohn, H., Farrar, C. R., Hemez, F. M., Shunk, D. D., Stinemates, D. W., Nadler, B. R., and Czarnecki, J. J. (2003). "A review of structural health monitoring literature: 1996–2001." *Los Alamos National Laboratory*.

Sohn, H., Worden, K., and Farrar, C. R. (2002). "Statistical damage classification under changing environmental and operational conditions." *Journal of Intelligent Material Systems and Structures*, 13(9), 561-574.

Sommer, A., and Thoft-Christensen, P. (1990). "Inspection and maintenance of marine steel structures. State-of-the-art."

Stachura, S. (2007). "Northern End of I-35W Bridge Is Now Focus of Probe." *Minnesota Public Ratio* Minnesota.

Teughels, A., and De Roeck, G. (2005). "Damage detection and parameter identification by finite element model updating." *Archives of Computational Methods in Engineering*, 12(2), 123-164.

Wadhwa, N., Rubinstein, M., Durand, F., and Freeman, W. T. (2013). "Phase-based video motion processing." *ACM Transactions on Graphics (TOG)*, 32(4), 80.

Wahab, M. A. (2001). "Effect of modal curvatures on damage detection using model updating." *Mechanical Systems and Signal Processing*, 15(2), 439-445.

Washer, G. (2001). "Reliability of visual inspection for highway bridges." *USDOT, FHWA*, 1.

Wood, M. G. (1992). "Damage analysis of bridge structures using vibrational techniques." University of Aston in Birmingham.

Xia, Y., Chen, B., Weng, S., Ni, Y.-Q., and Xu, Y.-L. (2012). "Temperature effect on vibration properties of civil structures: a literature review and case studies." *Journal of Civil Structural Health Monitoring*, 2(1), 29-46.

Xia, Y., Hao, H., Brownjohn, J. M., and Xia, P. Q. (2002). "Damage identification of structures with uncertain frequency and mode shape data." *Earthquake Engineering & Structural Dynamics*, 31(5), 1053-1066.

Yan, W.-J., and Ren, W.-X. (2012). "Use of continuous-wavelet transmissibility for structural operational modal analysis." *Journal of Structural Engineering*, 139(9), 1444-1456.

Yang, L., Kim, Y. H., Hay, J. R., and Kielkopf, J.(2017). "Non-Contact Based Structural Damage Detection Using Stochastic Subspace Identification and a FEM Updating Method." *Proc., Structures Congress 2017*, 483-494.

Zhang, G., Tang, B., and Tang, G. (2012). "An improved stochastic subspace identification for operational modal analysis." *Measurement*, 45(5), 1246-1256.

Zhang, L., and Brincker, R. (2005). "An overview of operational modal analysis: major development and issues." Proceedings of the 1st International Operational Modal Analysis Conference, April 26-27, 2005, Copenhagen, Denmark

Zhang, Q., Chang, C., and Chang, T. (2000). "Finite element model updating for structures with parametric constraints." *Earthquake Engineering & Structural Dynamics*, 29(7), 927-944.

Zimmerman, D. C., and Kaouk, M. (1992). "Eigenstructure assignment approach for structural damage detection." *AIAA Journal*, 30(7), 1848-1855.

Zimmerman, D. C., and Kaouk, M. (1994). "Structural damage detection using a minimum rank update theory." Transations, *American Society of Mechanical Enigneers, Journal of Vibration and Acoustics,* 116, 222-222.

APPENDIX

Nomenclature

φ_{m1}	Measured mode at t_1
φ_{m2}	Measured mode at t_2
y_k	Measured output
x_k	State vector
$y(t)$	Measured output over time
$\boldsymbol{M}$	Mass matrix
$\boldsymbol{D}$	Damping matrix
$\boldsymbol{K}$	Stiffness matrix
$f(t)$	The loading vector
$x(t)$	State space vector
$\boldsymbol{A}$,$\boldsymbol{B}$, $\boldsymbol{C}$	System matrices
f_k	Unknown input
w_k	Input noise
v_k	Output noise
$n_{y,k}$	Output measurement noise
$\boldsymbol{Q}$, $\boldsymbol{R}$, $\boldsymbol{S}$	covariance and cross-covariance matrices
$\boldsymbol{Y}$	Block Hankel matrix
$\boldsymbol{Y_{i\|j}}$	Row i to row j of Block Hankel matrix
$\boldsymbol{\Gamma_i}$	Observability matrix
$\boldsymbol{\mathcal{O}_i}$	Projection matrix
$\boldsymbol{\widehat{X}_i}$	State matrix
$\underline{\boldsymbol{\Gamma_i}}$	Γ_i without the last l rows
δ_{pq}	Kronecker delta

E(.)	expected value operator
ρ_W, ρ_v	Kalman filter residuals
$[m]$	Mass matrix
$[k]$	Stiffness matrix
$[\Delta m]$	Mass change matrix
$[\Delta k]$	Stiffness change matrix
ΔT	Temperature change
$\{\phi\}$	Scaled mode shape
$\{\phi_0\}$	Scaled mode shape before modification
$\{\phi_1\}$	Scaled mode shapes after mass modification
$\{\phi_2\}$	Scaled mode shapes after stiffness modification
$\{\phi_3\}$	Scaled mode shapes after mass-stiffness modification
$\{\phi_4\}$	Scaled mode shapes after temperature modification
$\{\psi\}$,	Unscaled mode shape
$\{\psi_0\}$	Unmodified mode shape (unscaled)
$\{\psi_1\}$	Mass added modified mode shape (unscaled)
$\{\psi_2\}$	Stiffness added modified mode shape (unscaled)
$\{\psi_3\}$	Mass-Stiffness added modified mode shape (unscaled)
$\{\psi_4\}$	Temperature changed modified mode shape (unscaled)
ω_0	Natural frequency
ω_1	Frequency after mass modification
ω_2	Frequency after stiffness modification
ω_3	Frequency after mass-stiffness modification
ω_4	Frequency after temperature modification
α	Scaling factor
α_1	Scaling factor of MCMS
α_2	Scaling factor of SCMS
α_3	Scaling factor of MSCMS
α_4	Scaling factor of TCMS
J_i	Objective function

λ_n	Dimensionless parameter
l	Beam length
μ	Mass per unit length
E	Elastic modulus
I	Moment of inertia
δ	Increase in the corresponding parameters
θ_T	Thermal coefficient of material
θ_E	Thermal coefficient of modulus
θ_m	Thermal coefficient of mass
θ_k	Thermal coefficient of stiffness
$\boldsymbol{M_u}$	Updated mass matrix
$\boldsymbol{K_u}$	Updated stiffness matrix
J	Objective function
V_e	Eigenvector form measurement
L_e	Eigenvalue from measurement
V_{eu}	Updated eigenvector
t	Time
p	Force
ω_{i_FEA}	Frequency of ith mode calculated form FEA
ω_{i_SSI}	Frequency of ith mode extracted form SSI
ξ_{i_FEA}	Damping ratio of ith mode calculated form FEA
ξ_{i_SSI}	Damping ratio of ith mode extracted form SSI
$\overline{\Delta T}$	Average temperature change along structure
ΔT_i	temperature change at ith element
n	Number of element analyzed
$DR_{\omega i}$	Difference ratio of frequencies
$DR_{\xi i}$	Difference ratio of damping
$CR_{\omega i}$	Change ratio of ith frequency

CURRICULUM VITAE

Li Yang

Email: li.yang.2@louisville.edu

EDUCATION

B.S. in Materials Science & Engineering (2009)

Southeast University – Nanjing, China

Outstanding Thesis Award

M.S. in Materials Science (2012)

Nanjing Hydraulic Research Institute – Nanjing, China

Zhang Guangdou Science and Technology Education Fund Scholarship

Ph.D. in Civil & Environmental Engineering (2017)

University of Louisville– Louisville, KY

Fellowship Award

EXPERIENCES

Graduate Research Assistant, University of Louisville

8/2012-5/2017

Assistant Civil Engineer, Nanjing Hydraulic Research Institute

9/2009-5/2012

Project Manager Assistant, Nanjing Traffic Department

5/2010-9/2010

Material Analyst, State Key Laboratory of High Performance Civil Engineering Materials

5/2009-9/2009

CERTIFICATIONS

EIT certificated

Greenroads certificated

PROFESSIONAL ACTIVITIES

Member of American Society of Civil Engineering (ASCE) since 2012

Member of Society of Women Engineers (SWE) since 2014

PUBLICATION

Yang, L., Kim, Y.H. "Modal Scaling Based on Temperature Change". *In preparation*.

Yang, L., Kim, Y.H., Hay, J., and Kielkopf, J. "Experimental Study of Stochastic Subspace Identification and FEM Updating for SHM Using Response Captured by High-Speed Camera". *In preparation*.

Yang, L., Kim, Y.H., Hay, J., and Kielkopf, J. (2017), "Non-Contact Based Structural Damage Detection using Stochastic Subspace Identification and FEM Updating Method: Model Validation". *Structural Congress, Denver, CO. April.*

Yang, L., Kim, Y.H., (2016). "Analytical Study of Structural Damage Detection Using Stochastic Subspace Identification and Finite Element Model Updating". *Engineering Mechanics Institute Conference, Nashville, TN, April. 460.*

Hu, Z., Wei, H., Shan, G., and **Yang, L**., (2013) "Causes and Prevention of Cracks in Large Channel Concrete". *South to North water transfers and water science & technology, (B02), 74-77.*

Hu, Z., **Yang, L**., and Liu, H., (2013) "Durability of concrete with recycled aggregates". *China Concrete and Cement Products, (3), 1-5.*

Yang, L. (2012). "pumping concrete research overview". *China Science & Technology, 552-553*